# Advances in Computer Science

# Research in Computing Science

## Series Editorial Board



***Research in Computing Science*** es una publicación trimestral, de circulación internacional, editada por el Centro de Investigación en Computación del IPN, para dar a conocer los avances de investigación científica y desarrollo tecnológico de la comunidad científica internacional. **Volumen 118,** noviembre 2016. Tiraje: 500 ejemplares. *Certificado de Reserva de Derechos al Uso Exclusivo del Título* No. : 04-2005-121611550100-102, expedido por el Instituto Nacional de Derecho de Autor. *Certificado de Licitud de Título* No. 12897, *Certificado de licitud de Contenido* No. 10470, expedidos por la Comisión Calificadora de Publicaciones y Revistas Ilustradas. El contenido de los artículos es responsabilidad exclusiva de sus respectivos autores. Queda prohibida la reproducción total o parcial, por cualquier medio, sin el permiso expreso del editor, excepto para uso personal o de estudio haciendo cita explícita en la primera página de cada documento. Impreso en la Ciudad de México, en los Talleres Gráficos del IPN – Dirección de Publicaciones, Tres Guerras 27, Centro Histórico, México, D.F. Distribuida por el Centro de Investigación en Computación, Av. Juan de Dios Bátiz S/N, Esq. Av. Miguel Othón de Mendizábal, Col. Nueva Industrial Vallejo, C.P. 07738, México, D.F. Tel. 57 29 60 00, ext. 56571.

**Editor responsable:** *Grigori Sidorov, RFC SIGR651028L69*

**Research in Computing Science** is published by the Center for Computing Research of IPN. **Volume 118**, November 2016. Printing 500.  Printed in Mexico City, in the IPN Graphic Workshop – Publication Office.

# Advances in Computer Science

**Navonil Majumder**
**Yazaed Zaid Guadarrama Rendón (eds.)**


Instituto Politécnico Nacional, Centro de Investigación en Computación
México 2016

**ISSN: 1870-4069**



Instituto Politécnico Nacional (IPN)
Centro de Investigación en Computación (CIC)
Av. Juan de Dios Bátiz s/n esq. M. Othón de Mendizábal
Unidad Profesional "Adolfo López Mateos", Zacatenco
07738, México D.F., México

http://www.rcs.cic.ipn.mx
http://www.ipn.mx
http://www.cic.ipn.mx



Indexed in LATINDEX, DBLP and Periodica

Printing: 500

Printed in Mexico

ISSN 1870-4069

# Editorial

The purpose of this volume is to showcase the most recent advancements in the selected areas of Computer Science. The works included in this volume were carefully curated by the editors, through blind review process, on the basis of originality and technical quality. This issue of the journal *Research in Computing Science* will be useful for the researches and the students working in various areas of Computer Science, as well as for all the readers interested in the enrichment of their knowledge in this field.

All the submitted papers were reviewed by at least two independent members of the editorial board. In general, the acceptance rate was 55.56%. This volume contains revised and corrected versions of the 15 accepted papers.

We would like to express our gratitude towards all the people who contributed to this volume. Firstly, the authors of the papers for their technical excellence, which guaranteed the quality of this publication. We also want to thank the members of the editorial board for their hard work in evaluation and selection of the best papers among the many submissions that we received. We sincerely express our gratitude to the *Sociedad Mexicana de Inteligencia Artificial* (SMIA) for their collaboration in the preparation of this publication. Also, we want to give special recognition to *Centro de Investigación en Computation* of *Instituto Politecnico Nacional* (CIC-IPN) for their support in the publication of this volume. The submission, review, and selection process were facilitated for free by the *EasyChair*, www.EasyChair.org.

*Navonil Majumder*
*Yazaed Zaid Guadarrama Rendón*
Guest Editors

November 2016

ISSN 1870-4069

# Table of Contents

Page

ISSN 1870-4069

# Discovering Relationships among Personal and Academic Factors with Academic Performance using Association Rules

Silvia Beatriz González Brambila, Josué Figueroa González

Universidad Autónoma Metropolitana, Ciudad de México, Mexico

{sgb, jfgo}@correo.azc.uam.mx

**Abstract.** Educational environment produces a lot of information related with many aspects, besides the traditional system, the growth of online educative systems and the called e-learning, have increased the amount of data available for its analysis. Data Mining offers different techniques for processing information in order to discover patterns that can be used for obtaining knowledge which helps improving or taking decisions about certain topics. This work presents the concepts related with, and the use of the called Educational Data Mining, specifically the technique of Association Rules, for obtaining relationships among the academic and personal factors with academic performance.

**Keywords:** Academic performance factors, association rules, educational data mining, knowledge discover, mining scholarship data.

## 1 Introduction

Educational environment produces a lot of information that can help in the improvement of many aspects related with education if it is analyzed and processed in a right way. Data Mining allows analyzing big volumes of information searching for interesting patterns that allow making decisions and solving problems. Data Mining techniques have been applied frequently to commerce and customer preferences situations, however in the last decade, these techniques have been applied to an educative environment creating the called Educational Data Mining (EDM) [10].

There are many definitions about what EDM is, but in a general way, it can be understood as the development of techniques and processes that allow discovering knowledge from data generated in an educational environment [8]. EDM uses the same techniques that Data Mining, in general, these techniques are: classification, clustering, regression and association rules. All of these techniques use different algorithms like decision trees, neural networks, k-nearest neighbor, Bayesian classifiers and others, for processing information and which are used depending the desired goal.

Applying these techniques to the information produced in an educational environment, allows to discover knowledge, which can improve many aspects related with education, like: courses planning, students performance during their studies or even in a single course or exam or identifying risk factors which can cause a student drop up its studies or fail in approving a certain course.

One of the problems that worry the most in an educative system is the academic performance; this one can be affected by a lot of aspects, like personal, academic or even labor ones, so it could be difficult to identify the most important events or situations that can affect the academic performance of students. Considering this, the goal of this paper is to present the use of EDM, reviewing and applying their main stages, in order to identify the relationship among different personal and academic events or situations, and discovering how they affect the performance of medium high level students.

The paper is structured as follows: Section 2 presents the necessary concepts for understanding and performing the process for obtaining knowledge using Association Rules. Section 3 presents related works. Section 4 presents the development of the knowledge obtaining process following the Knowledge Discovery in Databases (KDD) steps [4]. Finally, conclusions are presented in Section 5.

## 2 Obtaining Knowledge using Association Rules

The formal process of KDD is composed by several steps , although the amount of stages may vary, four steps can be identified: obtaining information, cleaning information, data mining and interpretation.

### 2.1 Association Rules

Association Rules are used to discover the relationships among a set of items, rules are related by to measures: support and confidence. In a formal way, an association rule is defined as: Let I = $\{I_1, I_2, \ldots, I_m\}$ a set of attributes known as items and let T a set of transactions $\{t_1, t_2, \ldots, t_n\}$ represented as t[k] = 1 if t is related with $I_k$ and t[k] = 0 if not [1]. Let X be a set of some elements of I, a transaction satisfies X if for all the elements $I_k$ in X, t[k] = 1. An association rule is an implication represented by X $\Rightarrow$ $I_{ij}$ where X is a set of some elements in I and $I_j$ is an element of I which is not present in X [1]. The most common algorithms for obtaining association rules are: Apriori, Equivalence Class Transformation (ECLAT) and Frequent Pattern (FP-algorithm). Apriori algorithm is based on identifying the frequent items in an individual way from the data set, and extend them to larger sets of items but only if they appear frequently in the set [2].

### 2.2 Measuring the Importance of a Rule

When the association rules are generated, it is common that a huge quantity of them appear, however, not all the rules are enough significant for taking a

decision. There are a lot of rules which are not important and can be discarded. For this reason, some concepts can be used for measuring the importance of a rule [11]. These techniques include: support, confidence, conviction, lift, leverage, coverage, correlation and odds ratio, being the most commonly used support, confidence and lift. Support of a set of elements X represents de percentage of transactions which contains X in a group of transactions D and is defined as

$$support(X) = \frac{|X|}{|D|}. \tag{1}$$

Confidence for an association X $\Rightarrow$ Y is the grade of the amount which contains X as antecedent and Y as a consequence. X can represent an item or a set of items, and it can be defined as

$$confidence(X \Rightarrow Y) = \frac{support(X \cup Y)}{support(X)}. \tag{2}$$

Lift indicates the occurrence frequency of X and Y respects an expected value and is defined as

$$lift(X \Rightarrow Y) = \frac{support(X \Rightarrow Y)}{support(X) * support(Y)}. \tag{3}$$

When value of lift is = 1, it means that the relationship between observed and expected values could be a random consequence. If lift is > than 1, it represents that exists a strong relationship between an antecedent and a consequence, in this case, X and Y are complements. If lift is < than 1, it means that there is not a strong relationship and X and Y can be classified as substitutes. Note that the value for lift for X $\Rightarrow$ Y it is not necessary the same for Y $\Rightarrow$ X.

## 3 Related Works

The amount of works about EDM has grown in the last decade and are applied to different topics [9]. The application of EDM includes traditional system, e-learning, learning systems, courses development, students performance and others. The most common use of EDM is related with student performance using classification techniques, it is applied for classifying or predicting the behavior or results for students in courses or exams, however, many works that use generation rules as main topic also can be found.

The generation of association rules can be found in topics like identifying patterns for students which can have learning problems or identifying a relationship among some common mistakes solving certain kind of exercises [7].

In [5] are presented the generation of rules for finding the relationship among three kinds of common mistakes at the moment of solving a problem. In [3] some Data Mining techniques are applied to a set of data gathered from a university, association rules are used for identifying the relationship among variables shared by students which obtain the best notes in a course.

In [6], the main goal was to analyze different ways of measuring the efficiency of some association rules about the results obtained for some students which uses or not the material given by a professor in an on-line educative system.

## 4 Generating Rules and Obtaining Knowledge

In order to obtain the association rules related with the academic performance, were considered the steps of the KDD process.

### 4.1 Obtaining Information

The data to be processed were obtained from the Medium High Level sub Secretary of Education [12]. The information was gathered from polls answered by youths. There were 13,014 students, but 4,779 were discarded because they did not start their middle high studies, so only 8,235 were considered to be processed. The poll had a lot of questions about personal, academic and labor factors, for this work, only were considered the personal and academic ones. An example of the data present in the poll can be reviewed in the Table 1.

**Table 1.** Sample of raw data obtained from the poll.

| $p45$ | $p46$ | $p47$ | $p48$ | $p50h$ | $p50m$ | $p51_1$ | $p51_2$ | $p51_3$ | $p52_1$ |
|---|---|---|---|---|---|---|---|---|---|
| 999 | 99.8 | 1 | 4 | -1 | 15 | 7 | 1 | 5 | 2 |

This sample represents the data stored and were difficult for processing and understanding, so, before generating the rules, a process for cleaning the data was necessary.

### 4.2 Data Cleaning Process

From all the variables (questions) included in the poll, only were considered the personal and academic ones. The data cleaning, or data cooking, process, included a transformation from continue values (numeric) to discrete values (categories) for some of the data. This, because it could be obtained better results using discrete values. For example, considering the academic factor "Travel time to school", it was converted from values that represented "less than 30 minutes", "from 30 minutes to 1 hour" or "more than 1 hour" to Low, Medium or Hight. "Last year average" was converted from continue values (8.5, 9.6) to discrete values and categories like High, Medium or Low. Some variables were discarded because most of the students did not have them, for example, the entrance exam score, which was not remembered by many students, or the final medium level score. At the end, were considered 11 and 10 academic variables.

Personal factors were: Relatives which student was living, family support with scholar problems, cigar consume, alcohol consumption, bullying, problems at home, lack of money, low self esteem, serious illness or decease of a relative, parents which finished medium high level and academic performance.

Academic factors were: Type of Medium level school, travel time to school, reason for school selection, class attendance average, last year average, scholarship, scholar personal support, understanding problems, problems related with school and academic performance.

Both groups had a variable related with Academic Performance, which was the interesting variable of the work.

### 4.3 Using Association Rules Algorithm for Data Mining

For generating the association rules, it was used the *Apriori* algorithm and for selecting the most representative rules, the lift value was considered. The processing was performed using R. Information was managed in its list presentation, where each row is a transaction and each column represents an item (variable). When one variable had more than one possible value, this was considered as another item. Associations had two parts, the left one or antecedent, and the right one or consequence, although were generated rules with many variables in both sides, only were considered for the interpretation step the ones with the variable related to academic performance in the right side as a consequence.

For clearing the results and helping the interpretation, for each variable, a letter (key) was assigned, the letters which appear in the rules for the academic factors and their possible values correspond to

- (A) Type of Medium level school: Private, Public, Both,
- (B) Travel time to school: Low, Medium, High,
- (C) Reason for choosing school: Academic, Economic, Personal, Assigned,
- (D) Class attendance average: Low, Medium, High,
- (E) Last year average: Low, Medium, High,
- (F) Scholarship: Yes, No,
- (G) Scholar personal support: Yes, No,
- (H) Understanding problems: Yes, No,
- (I) School related problems: Yes, No,
- (Z) Academic performance: Low, Medium, High.

Rules related with Low, Medium and High academic performance considering Academic factors are presented in Table 2, Table 3 and Table 4 respectively. The interpretation of the rules can be found in the Interpreting Rules sub section.

For Personal Factors, a set of letter and variable was also created, the key letter, variable and possible values were:

- (A) Relatives which student was living with: Alone, Direct, Couple, Other,
- (B) Family support for scholar problems: Parents, Brothers, Friends, Any,
- (C) Cigar consume: Low, Medium, High,

**Table 2.** Association rules considering academic factors for low academic performance.

| Rule | Confidence | Lift |
|---|---|---|
| {A=PUBLIC,B=LOW,C=PERSONAL,D=MEDIUM,E=LOW, F=NO,G=YES,I=NO} | 0.6769 | 4.0281 |
| {C=PERSONAL,E=LOW,F=NO,G=YES,H=YES} | 0.6721 | 3.9996 |
| {B=LOW,C=PERSONAL,E=LOW,H=YES} | 0.6666 | 3.9671 |

**Table 3.** Association rules considering academic factors for medium academic performance.

| Rule | Confidence | Lift |
|---|---|---|
| {B=HIGH,C=ACADEMIC,E=MEDIUM,F=NO,G=SI} | 0.6666 | 1.7168 |
| {B=HIGH,C=ACADEMIC,E=MEDIUM,F=NO,I=NO} | 0.6610 | 1.7022 |
| {B=MEDIUM,C=ACADEMIC,D=HIGH,E=MEDIUM, F=NO,G=NO,I=NO} | 0.65346 | 1.6828 |

**Table 4.** Association rules considering academic factors for high academic performance.

| Rule | Confidence | Lift |
|---|---|---|
| {A=PRIVATE,C=ACADEMIC,D=HIGH,E=HIGH, F=NO,G=YES,H=NO,I=NO} | 0.9393 | 2.1174 |
| {A=PRIVATE,C=ACADEMIC,D=HIGH,E=HIGH, F=NO,G=YES,H=NO} | 0.9342 | 2.1057 |
| {A=PRIVATE,B=MEDIUM,C=ACADEMIC, D=HIGH,E=HIGH} | 0.93023 | 2.0968 |

- (D) Alcohol consume: Low, Medium, High,
- (E) Bullying: Yes, No,
- (F) Problems in home: Yes, No,
- (G) Lack of money in home: Yes, No,
- (H) Low self esteem: Yes, No,
- (I) Serious illness or decease of a relative: Yes, No,
- (J) Parents which finished medium high level: Father, Mother, Both, Any,
- (Z) Academic performance: Low, Medium, High.

Rules related with Low, Medium and High academic performance considering Personal factors are presented in Table 5, Table 6, and Table 7 respectively.

The interpretation of these rules can be found in the "Interpreting Rules" sub section.

### 4.4 Obtaining Knowledge from Academic and Personal Rules

Interpreting the rules is quite simple, the left side can be interpreted as a set of actions which tends to a certain result. For example, consider the following

**Table 5.** Association rules considering personal factors for low academic performance.

| Rule | Confidence | Lift |
|---|---|---|
| {D=HIGH,F=YES,G=NO,J=ANY} | 1 | 5.9506 |
| {C=NO,D=LOW,F=YES,H=YES, J=ANY} | 0.8888 | 5.2894 |

**Table 6.** Association rules considering personal factors for medium academic performance.

| Rule | Confidence | Lift |
|---|---|---|
| {B=NO,C=HIGH,D=MEDIUM,E=NO,G=NO} | 1 | 2.5752 |
| {B=NO,C=HIGH,D=MEDIUM,G=NO,I=NO} | 1 | 2.5752 |
| {A=DIRECT,B=YES,C=NO,D=NO,F=YES, G=YES,H=YES,I=NO,J=ANY} | 0.90909 | 2.3411 |

**Table 7.** Association rules considering personal factors for high academic performance.

| Rule | Confidence | Lift |
|---|---|---|
| {D=NO,E=NO,F=YES,H=NO,I=YES,J=BOTH} | 0.8888 | 2.00363 |
| {D=HIGH,F=NO,J=FATHER} | 0.88888 | 2.00363 |

rule which is present in Table 7, indicating Personal factor related with High academic performance: {D=HIGH,F=NO,J=FATHER} $\rightarrow$ Z=HIGH. This can be interpreted as: High alcohol consume, not having problems in home and father finished medium high school, are related to having a High Academic Performance.

But this direct interpretation is not enough, for obtaining knowledge, the most representative rules were analyzed (with the highest value of lift) in order to find interesting patterns. For example, it was found that many (70%) of the rules with a lift value from 1.85 to 2.1 for Academic factors, have as private, the school where medium level was finished. Looking for this criteria in the rules for medium and high performance, was found that 78% of the rules related with low performance have as Public this value. Medium academic performance did not consider this factor.

Something similar occurs about the reason for choosing school, all the rules related with high academic performance which have this criteria, have as value Academic, meanwhile, several of the rules associated with low performance have as value Personal.

A relevant criteria is also the average attendance, which is related directly with the performance, high, medium, and low attendance average correspond to high, medium, and low academic performance.

From this, talking about Academic factors, the kind of school where the student studied medium level, it is a decisive factor, indicating that public schools

of this level may be having problems or not an enough academic level. Also, the fact that a student chooses a school due to personal factors should not be the best decision, promoting that the criteria for choosing a school be for its academic characteristics, should be a better option in the performance of students.

A similar analysis was performed for the Personal factors. Here, a rule indicates that the fact that any of the parents have finished medium high school, it is a factor related with low academic performance. From the rules obtained about this performance, all of them contains this value for the criteria. Something similar occurs with a medium performance, but with a high performance, all of the values for this criteria, when it appeared, have the value of Both, Father or Mother.

A factor, also present in low academic performance is having low self esteem, reviewing the rules, all the ones that have this criteria with a value of Yes correspond to a Low performance, meanwhile the value of No, it's present in the rules associated with high academic performance.

Some values are a little difficult to identify, for example, consider Alcohol consumption, which has values of High in all the rules, however, analyzing a bigger set of those ones, can be found that this value was present in more rules for low performance, and in less rules for medium and high performance, which have more rules with the value of Low or No consume.

From this analysis, it can be concluded that an important factor for having a good academic performance is not related with the student, but with the parents, promoting that adult people to finish at least this level, could improve the academic performance of their children. Also aspects like self esteem and the consumption of alcohol should be considered.

## 5 Conclusions

Educational Data Mining offers great opportunities for processing and obtaining knowledge from data generated in an educational environment. The amount and variety of information that can be analyzed is enormous and if it's right processed and interpreted, it can be a powerful tool for improving many of the aspects that occur in education. The goal of this work was to identify relationships among academic and personal aspects with academic performance, so the association rule technique was chosen, this is the first step for obtaining knowledge, choosing the correct technique of Data Mining, according the kind of problem to treat and the desired goal. About the whole process, KDD offers a set of formal steps that helps in the application of the EDM. Before analyzing and processing the information, it is important that a correct cleaning and pre-processing of the data is performed, considering the format of the original data, it was necessary to perform this process, where it's important to know the problem and environment, so the best criteria, transformations and categories can be specified, this contributes to obtaining better results, removing variables that are not significant and creating categories also helps in getting clearer associations. At the moment of interpreting the rules, it's necessary a certain

level of knowledge about the problem and concepts that are being analyzed. Using the lift property for measuring the importance of the rules, and taking the ones with the biggest value contribute to a clearer interpretation of those ones. But it is necessary to analyze several rules (with the highest value of lift) to identify the relationship between some criteria with the academic performance.

From the obtained rules, it is clear that factors like the studies level of the parents, alcohol consumption, self esteem and attendance average are related with the academic performance. This can be used for different institutions, not necessarily educative, for taking decisions or implementing politics that can improve the academic performance of students.

## References

1. Agrawal, R., Imielinski, T., Swami, A.: Mining association rules between sets of items in large databases. Acm sigmod record vol. 22, No. 2, pp. 207–216, ACM (1993)
2. Agrawal, R., Srikant, R.: Fast algorithms for mining association rules. In: 20th int. conf. Very large data bases, VLDB, pp. 487–499 (1994)
3. Baradwaj, B.K., Pal, S.: Mining educational data to analyze students' performance. ArXiv preprint arXiv:1201.3417 (2012)
4. Fayyad, U., Piatesky-Shapiro, G., Smyth, P.: The KDD Process for Extracting Useful Knowledge from Volumes of Data. Communications of the ACM. 11, pp. 27–34 (1996)
5. Merceron, A., Yacef, K.: Revisiting interestingness of strong symmetric association rules in educational data. In: Proc. of Int. Workshop on Applying Data Mining in e-Learning, pp. 3–12 (2007)
6. Merceron, A., Yacef, K.: Interestingness measures for association rules in educational data. In: Educational Data Mining (2008)
7. Merceron A., Yacef K.: Measuring correlation of strong symmetric association rules in educational data. In: Romero C, Ventura S, Pechenizkiy M, Baker RSJd, eds. Handbook of Educational Data Mining, pp. 245–256. CRC Press (2010)
8. Rajadhyax, N., Shirwaikar, R.: Data Mining on Educational Domain. International Journal of Advanced Studies in Computers, Science and Engineering, 1(1), pp. 1 (2012)
9. Romero, C., Ventura, S.: Educational data mining: a review of the state of the art. IEEE Transactions on Systems, Man, and Cybernetics, Part C Applications and Reviews, vol. 40 No. 6, pp. 601–618 (2010)
10. Romero, C., Ventura, S.: Data mining in education. Wiley Interdisciplinary Reviews: Data Mining and Knowledge Discovery, 3(1), pp. 12–27 (2013)
11. Sheikh, L.M., Tanveer, B., Hamdani, M.A.: Interesting measures for mining association rules. In: Multitopic Conference, Proceedings of INMIC 2004. 8th International, pp. 641–644. IEEE (2004)
12. Subsecretaria de Educación Media Superior. Encuesta Nacional de Deserción en la Educación, `http://www.sems.gob.mx/sems/encuesta_nacional_desercion_ems`

ISSN 1870-4069

# Free Form Object Recognition Module using A-KAZE and GCS

Karen Lizbeth Flores-Rodríguez, Felipe Trujillo-Romero

Universidad Tecnológica de la Mixteca,
División de Estudios de Posgrado, Oaxaca,
Mexico

karenflores350@hotmail.com, ftrujillo@mixteco.utm.mx

**Abstract.** This paper presents an object recognition module development. This module uses a local feature approach to identify keypoints in free form objects and an unsupervised artificial neural network (ANN) to associate the nearest ones and get clusters of each object learned. The module uses A-KAZE feature descriptor and Growing Cell Structure (GCS) ANN. The module is validated using an own data base, with twenty real objects and twenty different images each one. Here is presented a variety of experiments using from five to fifteen trainning images per object and the rest of them for evaluation. This method gets good results with 100% of discrimination between objects and up to 80% of correct classification.

**Keywords:** A-KAZE, growing cell structure, free form object recognition, local features.

## 1 Introduction

There are plenty of works referents to object recognition showing good results [1–4]. These works prove classification and object recognition is an issue solved for a lot of computer vision methods. These tools can use external features (size, signatures, polygonal approximations) or inner features (color, gray levels, texture). Additionally, the feature classification can be doing with different approach like ANN, support vector machines, statistical methods, etc.The choice of one of these methods depends of the problem, application or data base to work with. One of the current challenges is to get a method who can be used in real time, be faster and not need extra processing resource to be applied. Thinking in a human environment like an office or a house, where a human do his daily activities, it can be find several different objects. There are objects like phones, scissors, staplers, etc. These object are complex to modeling mathematically.

Then, if the goal is recognize them, a good solution is an object recognition method considering free form objects. The most methods like that use local feature to describe the objects in a faster way [5–8]. These methods, detects visually distinctive points in images called: interest points, salient points, keypoints or corner points. The detection includes the keypoints scale, orientation

and description making them a strong feature to learn and recognize an object. The most popular of them are Scale Invariant Feature Transform [9] (SIFT) and Speeded Up Robust Feature [10] (SURF). Recently, in [11], it was develop KAZE, a feature detector and descriptor algorithm comparable to SIFT but with an increase computational cost disadvantage compared to SURF. KAZE evolved to A-KAZE [12] showing an excellent compromise between speed and execution compared to BRISCK [13], ORB [14], SURF, and SIFT. The keypoints alone can be classified with a nearest neighbors algorithm. But talking about free form object where the all 3D form is taking into account and there are a lot of keypoints describing only one object, should be used an optimized method to cluster the data. The best choice is an ANN, whom is an approach with a high popularity and a way for develop adaptive coefficients to make decision function by series of patterns training presentations. Actually, there are a lot of ANN variants and is hard enough to choice one that fully solve a particular problem. In the free form object recognition module, the patterns to be classified are those obtained by the method A-KAZE and it is chosen the self-organizing GCS [15] for classification task which have the advantage to increase and decrease dynamically his form during the training phase.

There are many successful object recognition models who take local features into objects representations. These models can often be broken down into two steps: a coding step, of the most representative features in a scene, and an association step, which summarizes the features over nearest neighborhoods or some similar clusters. Several coding combinations and association schemes have been made. The bag of words or bag of features it will be made more popular, works like [16–18] use it with supervised or unsupervised classification obtaining result about 84% to 91.4%. ANN supervised and unsupervised have been used too, like in [19], the back–propagation algorithm with local signatures and self-organizing maps obtained a 75% correct classification. With unsupervised low level local descriptors [20], a model based on bayes, PCA and combining SIFT-PCA [21] make more distinctive the representation. These obtained a 95% classification. The unsupervised feature learning with convolutional ANN [22], [23] and [24], and local descriptors using SIFT obtained correct classification about 80%, 85.8%, and 92.5%. Another using the same model [25] but with images RGB-d obtained a 93.23%. Cellular ANN and SIFT had been used obtained 90%. The disadvantage is to have large data set and large time. Also many of them use data base like COIL-100, CALTHEC-101 and others. The free form object recognition module contribution is: (i) the automatically data association obtained from A-KAZE with the ANN self-organizing GCS, (ii) the speed because use only a few views, (iii) discriminate well the objects between them, and (iv) easy to be implemented. A performance analysis is carried to prove using an ANN model and keypoints can be applied in a real time module, remains consistent, be fast and be accurate. To evaluate the approach it is considered data cross performances, confusion matrix and receiver operating characteristics (RoC) curve analysis.

## 2 A-KAZE

A-KAZE refers to a method based on KAZE but faster because the dramatic speed-up introduced by Fast Explicit Diffusion (FED) schemes and the low computational demand and storage by Modified-Local Difference Binary (M-LDB). In this section is briefly described the algorithm from [12].

Firstly, define a evolution times set to build the nonlinear scale space in a $O$ octaves and $S$ sub-levels series mapped to pixels scale $\sigma$ with

$$\sigma_i(o,s) = 2^{o+s/S}, o \in [0 \dots O-1], s \in [0 \dots S-1], i \in [0 \dots M], \tag{1}$$

where $M$ is the total filtered images number. Then the discrete scale levels set is converted to time units

$$t_i(o,s) = \frac{1}{2}\sigma_i^2, i = \{0 \dots M\}. \tag{2}$$

The input images are convolved with a standard deviation Gaussian to reduce noise and artefact and to computed the contrast factor as the gradient histogram 70%. With both input images and contrast factor the FED scheme starts, the pyramidal approach algorithm 1 and inner cycle algorithm 2.

**Algorithm 1:** Pyramidal FED, nonlinear diffusion filtering

**Data:** Image $L_0$, contrast $\lambda$, $\tau_{max}$ and evolution times $t_i$
**Result:** Set of filtered images $L_i$, $i = 0...M$

**for** $i = 0 -> M-1$ **do**
- 1. Compute diffusivity $A(L^i)$
- 2. FEDcycle time $T = t_{i+1} - t_i$
- 3. Number of inner steps $n$
- 4. Compute step size $\tau_j$
- 5. Set Prior $L^{i+1,0} = L^i$ $L^{i+1} =$ **FEDCycle**$(L^{i+1,0}, A(L^i), \tau_j)$ **if** $o_{i+1} > o_i$ **then**
  - Downsample $L_{i+1}$ with mask $(\frac{1}{4}, \frac{1}{2}, \frac{1}{4})$
  - $\lambda = \lambda 0.75$

**Algorithm 2:** FED Cycle

**Function FEDCycle** $(L^{i+1,0}, A(L^i), \tau_j)$ **for** $j = 0 -> n-1$ **do**
- $L^{i+1,j+1} = (I + \tau_j A(L^i))L^{i+1,j}$

return $L^{i+1,n}$

The feature detection uses the Hessian determinant for each images filtered $L_i$ in the nonlinear scale space. The differential multi-scale operators set are normalized with a scale factor

$$L^i_{Hessian} = \sigma^2_{i,norm}(L^i_{xx}L^i_{yy} - L^i_{xy}L^i_{yx}). \tag{3}$$

The concatenated Scharr filters is used for computing the second order derivatives with step size $\sigma_{i,norm}$. At each evolution level i, the detector response is check, if is higher than a pre-defined threshold and if is a maxima in a 3x3 pixels window. Then, the 2D keypoint position is estimated with sub-pixel accuracy.

The feature description use M-LDB with the derivatives computed in the feature detection step to compute an average approximation of the same areas in the intensity and gradient images. Finally, the descriptor vector of length 64 is obtained.

## 3 Growing Cell Structure

Next is briefly describe the unsupervised GCS model from [15]. The model is a Kohonen's self-organizing network variant. The main advantage over existing approaches is the model ability to automatically find a suitable network structure and size, achieve through a controlled growth process that also includes occasional units removal. The network dynamics is summarized in the next algorithm 3 and 4.

**Algorithm 3:** GCS

**Data:** $\varepsilon_b$ best matching, $\varepsilon_n$ neighboring and $\lambda$ steps

Start: k-dimensional simplex $V = R^b$

**while** *(≠ desired network size)* **do**

  **AdaptationSteps**

Determine $q$: $h_q \geq h_q \quad (\forall\, c \in A)$

Look $q$ largest distance neighbor $f$: $\| w_f - w_q \| \geq \| w_c - w_q \| \; (\forall\, c \in N_q)$

Insert cell $r$ between $q$ and $f$.

Initialize $r$: $w_r = 0.5(w_q + w_f)$

Redistribute counter: $\Delta\tau_c = \frac{|F_c^{(new)}| - |F_c^{(old)}|}{|F_c^{(old)}|}\tau_c$

Initialize new cell: $\tau_r = -\sum_{c \in N_r} \Delta\tau_c$

After insertion, check $\hat{p_i} < \eta$

Cells remove: $\hat{p} = \tilde{p} \sum_{c \in A} \tilde{f}_c$

**Algorithm 4:** GCS: **AdaptationSteps**

**for** *adaptationsteps* $= 0 - > \lambda$ **do**

  Choose an input signal $\xi$ according to $P(\xi)$

  Locate the best matching unit $s = \phi_w(\xi)$.

  Increase matching:

  $\Delta w_s = \varepsilon_b(\xi - w_s)$

  $\Delta w_c = \varepsilon_n(\xi - w_c) \quad (\forall\, c \in N_s)$

  Increment the signal counter of $s$:

  $\Delta\tau_s = 1$

  Decrease all signal counters by a fraction $\alpha$ in the network $A$:

  $\Delta\tau_c = -\alpha\tau_c \quad (\forall\, c \in A)$

## 4 Object Recognition Module

The free form object recognition module is proposed like the described in the Figure 1. The module is divided in two main phases: *Leraning* and *Recognition*.

In *Learning* phase, it is used different object view images as input. Using A-KAZE extracts keypoints, process the data and pass trough the unsupervised GCS for classification. Each class is reserved into a data base with a label (name of the object). The *Recognition* phase, uses only one object view image as input.

As in the *Learning* phase, it is used A-KAZE to extract keypoints, process the data and pass trough GCS evaluation to obtain the object label.

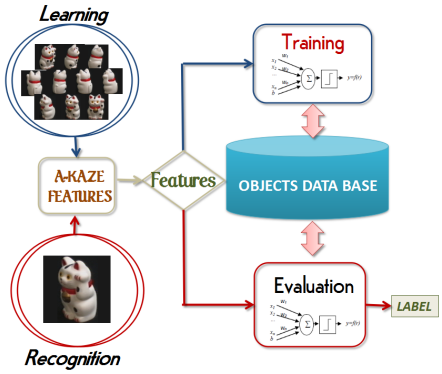


**Fig. 1.** Object recognition module blocks diagram.

### 4.1 Module Description

After extract the keypoints from the images and before pass trough GCS, the data is processed. A-KAZE gets a big data from an image and all the data can be reduced to an histogram. This is proved with the process explanation next:

1. There are four images from an object in different views: front, back, left and right. For each view all the keypoints are extracted.
2. Each view is compared with the right. The Figure 2 presents the 50 best keypoints coincidences connected by a line.

The above shows, that images from one view to other, in an object, share many features. If the object has more images it will have more coincidences between views.

3. All the keypoints are summarized into an histogram per image from the previous object. The keypoints homogenization summarized the view essence.

The histogram keeps the information about an object view because it is learned all the keypoints whom are part of that view. In Figure 3 (a), the four histograms are overlayed to show the similitude between them and the graph errors from each comparison is shown in Figure 3 (b). Also, a comparison between the object 2 in Table 4 and the actual object is carried out and the result are shown in

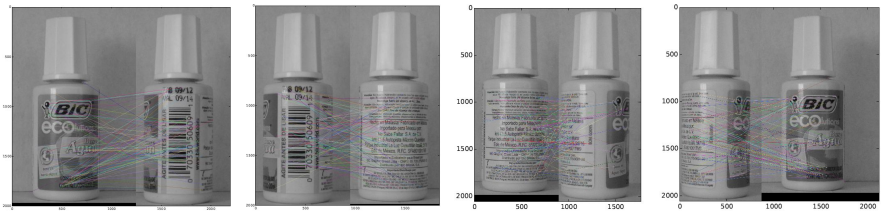

**Fig. 2.** Four images from an object in different views: front, back, left and right view. Graphical representation of keypoints coincidences.

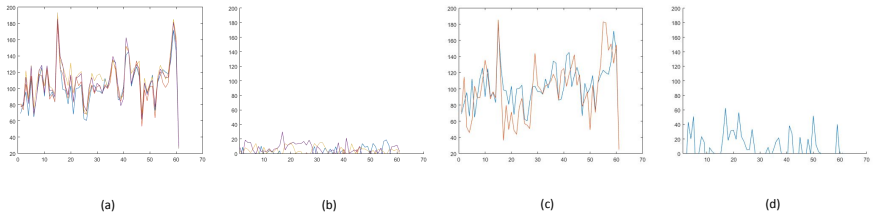


**Fig. 3.** (a) Histograms per image view, (b) Error between views, (c) Two different object histogram, (d) Error graph.

Figure 3 (c) and in Figure 3 (d) it is observed that the error between them is bigger.

4. Once obtained the histograms per object, these are the GCS input. The GCS automatically do a nearest neighbor association of them.
5. The histograms belongs to an object will be classified into a neurons group. Therefore, there will be more than one neuron per object.

**Algorithm 5:** Object recognition module. *Training*

**Data:** $\boldsymbol{I}$ images, $\boldsymbol{N}$ objects, $\boldsymbol{L}$ images per object, $\boldsymbol{E}$ object label
**Result:** ***classes(N)*** Object classes.

**for** $n \leftarrow 1$ ***to*** $N$ **do**
  **for** $l \leftarrow 1$ ***to*** $L$ **do**
    keypoints =A-KAZE($\boldsymbol{I(n,l)}$)
    H(n,l)= $\frac{\Sigma keypoints}{Totalkeypoints}$
classes($\boldsymbol{N,E}$)=GCS($\boldsymbol{H}$)

**Algorithm 6:** Object recognition module. *Evaluation*

**Data:** $\boldsymbol{I}$ image
**Result:** ***class(I)*** object class and $\boldsymbol{E}$ object label

keypoints =A-KAZE($\boldsymbol{I}$)
H($\boldsymbol{I}$)= $\frac{\Sigma keypoints}{Totalkeypoints}$
class($\boldsymbol{I,E}$)=GCS($\boldsymbol{H}$)

### 4.2 Algorithm Training and Classification

The free form object recognition module implementation is as follows. There are *Training* and *Evaluation* tasks. In *Training* task, as is shown in algorithm 5, the input are the images, object number, images number and the object label.

The module accurate depends of the images number per object. Although, in some cases, only five images are enough to learn an object. Using A-KAZE the keypoints are extracted and the histograms per image are builded. All the histograms are sent to ANN GCS to classification. Each class is saved in a data base with a label (object name). The *Evaluation* task, as is shown in algorithm 6, receives only one image per object to recognize as input. As in the *Training* task, uses A-KAZE to extract all the keypoints and builds the image histogram. Then, the histogram is sent to evaluation with the ANN trained. The ANN delivers the nearest class and the recognized object label.

## 5 Experiments and Results

The free form object recognition module validation is as next. It is used an own five real objects data set shown in Table 4. Each of them with twenty views images to different sizes. The experiments are from 5 to 15 images to training and the rest for evaluation. The main parameters of each experiments, described in Table 1 are: training images number, evaluation images, ANN max neurons numbers and training steps. The neurons and epoch values are chosen to be between 100 minimum and 500 maxima depends of the training images number. In GCS $\varepsilon_b = 0.05$, $\varepsilon_n = 0.005$ and $\lambda = NumOfSamples$ adaptation steps for all the experiments. The experiments takes randomly images from the data base for each object in each experiment.

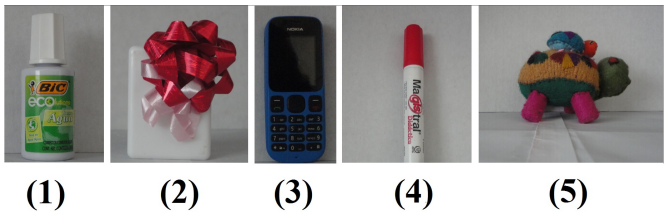


**Fig. 4.** Real objects data set. (1) corrector, (2) gift, (3) cell-phone, (4) marker, (5) turtle.

### 5.1 Results

The experiments results are shown in a confusion matrix for each one and RoC curve analysis for the classification. The confusion matrix is shown in Table 2,

**Table 1.** Main parameters per experiment.

| Experiment | Training | Evaluation | Neurons | Epochs |
|---|---|---|---|---|
| First | 5 | 5 | 100 | 100 |
| Second | 5 | 1 | 100 | 100 |
| Third | 5 | 15 | 200 | 200 |
| Fourth | 10 | 10 | 200 | 500 |
| Fifth | 15 | 5 | 200 | 500 |

these show a consistent classification mistaking the two last objects in each experiment. The training and evaluation performance was done in MATLAB 2015 in a PC with Intel(R) Core(TM) i7-4770 3.40GHz processor, with 12 GB RAM, Windows 8 (64) bits OS.

**Table 2.** Experiments confusion matrix.

| First | | | | | |
|---|---|---|---|---|---|
| | **1** | **2** | **3** | **4** | **5** |
| **1** | 5 | 0 | 0 | 0 | 0 |
| **2** | 0 | 5 | 0 | 0 | 0 |
| **3** | 0 | 0 | 5 | 0 | 0 |
| **4** | 2 | 0 | 0 | 3 | 0 |
| **5** | 0 | 0 | 0 | 0 | 5 |

| Second | | | | | |
|---|---|---|---|---|---|
| | **1** | **2** | **3** | **4** | **5** |
| **1** | 10 | 0 | 0 | 0 | 0 |
| **2** | 0 | 10 | 0 | 0 | 0 |
| **3** | 0 | 0 | 10 | 0 | 0 |
| **4** | 4 | 0 | 0 | 6 | 0 |
| **5** | 1 | 0 | 0 | 0 | 9 |

| Third | | | | | |
|---|---|---|---|---|---|
| | **1** | **2** | **3** | **4** | **5** |
| **1** | 5 | 0 | 0 | 0 | 0 |
| **2** | 0 | 5 | 0 | 0 | 0 |
| **3** | 0 | 0 | 5 | 0 | 0 |
| **4** | 2 | 0 | 0 | 3 | 0 |
| **5** | 0 | 0 | 0 | 0 | 5 |

| Fourth | | | | | |
|---|---|---|---|---|---|
| | **1** | **2** | **3** | **4** | **5** |
| **1** | 1 | 0 | 0 | 0 | 0 |
| **2** | 0 | 1 | 0 | 0 | 0 |
| **3** | 0 | 0 | 1 | 0 | 0 |
| **4** | 1 | 0 | 0 | 0 | 0 |
| **5** | 0 | 0 | 0 | 1 | 0 |

| Fifth | | | | | |
|---|---|---|---|---|---|
| | **1** | **2** | **3** | **4** | **5** |
| **1** | 13 | 0 | 0 | 1 | 1 |
| **2** | 0 | 15 | 0 | 0 | 0 |
| **3** | 0 | 0 | 15 | 0 | 0 |
| **4** | 4 | 0 | 0 | 10 | 1 |
| **5** | 1 | 1 | 2 | 0 | 11 |

**Table 3.** Experiments results.

| Experiment | (%) | Time (sec) |
|---|---|---|
| First | 92 | 0.351 |
| Second | 80 | 0.426 |
| Third | 85.33 | 1.246 |
| Fourth | 90 | 2.344 |
| Fifth | 92 | 3.457 |

However, the experiments percentages and the performance training time presented in Table 3, exhibit two best with 92% correct classification, the rest up to 80% correct classification. The performance training time depends of

the neurons quantity which at the same time depends of the images quantity. Considering the results and only the neurons quantity, the training time increase with a lineal approximation like (4):

$$time = 0.0063(neurons) - 0.2395. \tag{4}$$

The increase in time remaind small from a neuron quantity to other. If the images training increase to 20 the neurons should increase to 700 and the time will be 4.1705 s approximately. Remembering that are 20 images per each of the five objects, then, the module is considering faster.

**Table 4.** Operating characteristics per experiment.

| Object | TP | TN | FP | FN | Sensitivity | Specificity | 1-Specificity |
|---|---|---|---|---|---|---|---|
| (1) | 34 | 129 | 15 | 2 | 0.944 | 0.896 | 0.104 |
| (2) | 36 | 143 | 1 | 0 | 1 | 0.993 | 0.007 |
| (3) | 36 | 142 | 2 | 0 | 1 | 0.986 | 0.014 |
| (4) | 22 | 142 | 2 | 14 | 0.611 | 0.986 | 0.014 |
| (5) | 30 | 142 | 2 | 6 | 0.833 | 0.986 | 0.014 |

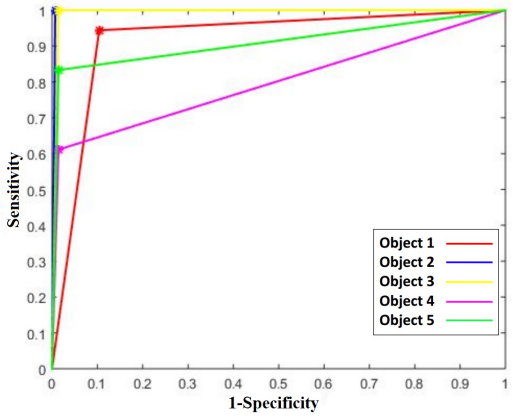


**Fig. 5.** RoC curve of each object for all the experiments.

Additionally, the sensitivity and specificity experiments analysis is obtained using the true positive (TP), true negatives (TN), false positives (FP) and false negatives (FN). The values are in Table 4, corresponding to all the data classify in the five experiments, it means 180 images total. These operating characteristics can be reformulated slightly and then presented graphically as shown below in Figure 5. The plots shows true positive against the false positive rate for the different possible classification result. These curves demonstrates,

the tradeoff between sensitivity and specificity (any increase in sensitivity will be accompanied by a decrease in specificity). The curves follow the left-hand border and the RoC space top border, showing the test accuracy. The object 1, 4 and, 5 curves are closer to the 45-degree RoC space diagonal but still closer to the RoC space top border. These are less accurate but enough to do a good classification.

## 6 Conclusions

This paper presented a free form object recognition module development based on local features and ANN. The features identify free form objects interest points and are used as ANN input to cluster the nearest. It was used A-KAZE and GCS.

The GCS network uses from 100 to 500 neurons maxima in training. The module was validated using an own real object data base with five objects and twenty images per object. The ANN was trained with different images number per object. The obtained results are good ones with 100% classification rate and up to 80% recognition. It means the module can discriminate very well the objects. There are some confusions in the evaluation because it is necessary to give the system images with more features from object views. Future work is: (i) to increase the objects number, (ii) mix more similar objects to see the module performance, and (iii) to implement it in a humanoid robot NAO to do service tasks.

**Acknowledgement.** Acknowledgements to CONACYT for the economic scholarship support to get a master's degree 584190/571271.

## References

1. Pereyra, M., Destefanis, E.: Reconocimiento de objetos para control de calidad mediante la descomposición en figuras geométricas. In: 2 Congreso Nacional de Ingeniería Informática/Sistemas de Información (2014)
2. Gelsi, L., Di Caro, C.A., Fernández, H.A.: Reconocimiento rápido de objetos. Anales AFA, 22, pp. 95–97 (2011)
3. Gómez, J.D.: Proceso de reconocimiento de objetos asistido por computadora, aplicando gases neurales y técnicas de data mining. Revista Científica y Tecnológica de la Facultad de Ingeniería. pp. 12–1 (2007)
4. Roth, P. M., Winter, M.: Survey of appearance-based methods for object recognition. Technical Report: ICG-TR-01/08, Graz University of Technology, Austria (2008)
5. Albanesi, B., Funes, N., Chichizola, F.: Reconocimiento de objetos en video utilizando sift paralelo. In: XVI Congreso Argentino de Ciencias de la Computación. (2010)
6. Salamanca, S., Adán, A., Cerrada C., Adán, M., Merchán, P., Pérez, E.: Reconocimiento de objetos de forma libre a partir de los datos de rango de una vista parcial usando cono curvaturas ponderadas. Revista Iberoamericana de Automática e Informática Industrial, pp. 94–106 (2007)

7. Chen, H., Bhanu, B.: 3d free-form object recognition in range images using local surface patches. Pattern Recognition Letters. 28, pp. 1252–1262 (2007)
8. Guo, Y., Beccamoun, M., Sohel, F., Liu, M., Wan, J.: 3D object recognition in cluttered scenes with local surface features: a survey. IEEE Transactions on Pattern Analysis and Machine Intelligence (2013)
9. Lowe, D.G.: Distinctive image features from scale-invariant keypoints. International Journal of Computer Vision (2004)
10. Bay, H., Ess, A., Tuytelaars, T., Van Gool, L.: SURF: Speeded up robust features. Computer Vision and Image Understanding (CVIU), 110-3, pp. 346–359 (2008)
11. Alcantarilla, P. F., Bartoli, A., Davison, A. J.: Kaze features. ECCV, Springer-Verlag Berlin Heidelberg, pp. 214–227 (2012)
12. Alcantarilla, P. F., Nuevo, J., Bartoli, A.: Fast explicit diffusion for accelerated features in nonlinear scale spaces. In: British Machine Vision Conference (BMVC) (2013)
13. Leutenegger, S., Chli, M., Siegwart, R. Y.: BRISK: Binary robust invariant scalable keypoints. In: IEEE Intl. Conf. on Computer Vision (ICCV), pp. 2548–2555 (2011)
14. Rublee, E., Rabaud, V., Konolige, K., Bradski, G.: Orb: an efficient alternative to siftt or surf. In: IEEE Intl. Conf. on Computer Vision (ICCV), pp. 2564–2571 (2011)
15. Fritzke, B.: Growing cell structures, a self-organizing network for unsupervised and supervised learning. Neural Networks, 7-9, pp. 1441–1460 (1994)
16. Boureau, Y. L., Bach, F., LeCun, Y., Ponce J.: Learning mid-level features for recognition. In: Computer Vision and Pattern Recognition (CVPR), IEEE Conference (2010)
17. Oursland, J.: Real-time scale invariant object recognition using an articial neural network. In: Proceedings of the ISCA 25th International Conference on Computers and Their Applications, CATA (2010)
18. Sudholt S., Rothacker L., Fink G. A.: Learning local image descriptors for word spotting. Document Analysis and Recognition (ICDAR), pp. 651–655 (2015)
19. Ros, J., Laurent, C., Lefebvre, G.: Cascade of unsupervised and supervised neural networks for natural image classification. In: Image and Video Retrieval: 5th International Conference, CIVR, pp. 92–101 (2006)
20. Osendorfer, C., Bayer, J., Urban, S., Van der Smagt, P.: Unsupervised feature learning for low-level local image descriptors. CoRR (2013)
21. Ken, Y., Sukthankar, R.: Pca-sift: a more distinctive representation for local image descriptors. Computer Vision and Pattern Recognition, CVPR, 2 pp. 506–513 (2004)
22. Dosovitskiy, A., Fischer, P., Sprinenberg, J. T., Riedmiller, M., Brox,T.: Discriminative unsupervised feature learning with exemplar convolutional neural networks. CoRR, abs/1406.6909 (2014)
23. Paulin, M., Douze, M., Harchaoui, Z., Mairal, J., Perronnin, F., Schmid, C.: Local Convolutional Features with Unsupervised Training for Image Retrieval. In: IEEE International Conference on Computer Vision, ICCV, (2015)
24. Dong, J., Soatto, S.: Domain-Size Pooling in Local Descriptors: DSP-SIFT. CoRR (2014)
25. Jhuo, I. H., Gao, S., Zhuang, L., Lee, D. T., Ma, Y.: Unsupervised Feature Learning for RGB-D. IEEE Transactions on Image Processing, 24 pp. 4459–4473 (2015)

ISSN 1870-4069

# Quaternion Atomic Phase Magnification for 2D and 3D Motion

E. Ulises Moya-Sánchez[1], Marcela Bonell[1], Gustavo Torres[1], Eduardo Vázquez-Santacruz[2]

[1] Universidad Autónoma de Guadalajara, Guadalajara, Mexico
[2] Universidad Nacional Autónoma de México, Mexico City, Mexico

eduardo.moya@edu.uag.mx, marcelabonell@gmail.com, gustavo.blanco@edu.uag.mx, evazquezsa@conacyt.mx

**Abstract.** The phase computation is used in many applications of signal and image processing such as edge, line, symmetry detection, image analysis and recently to show small motion or color changes. Eulerian video processing allows to show small color changes and motions invisibles to the naked eye. Eulerian motion magnification, was modify using the phase and the Riesz pyramid in order to reduce the noise amplification. In this work we introduced a novel phase magnification approach based on a infinitely differentiable unique compact supported window, an atomic function. Another contribution of our work was apply our quaternion phase and Eulerian magnification to 3D motion, which has not been reported so far, we propose to use simple projections of conformal algebra in order to do the magnification at any plane of the 3D space. We compare the phase (Riesz Pyramids), with the atomic Riesz pyramid, in our comparation our atomic pyramid Riesz preserves more information than the phase Riesz approximation, besides our approach is slower by 2.5 times. Finally, we compare method and the linear magnification (Laplace Pyramid) in terms of the Signal to Noise Ratio (SNR). We found that the phase magnifications has better response to noise than the linear method.

**Keywords:** Quaternion atomic phase, phase magnification, atomic functions, and local phase.

## 1 Introduction

The phase concept is commonly used in many application areas of signal processing such as telecommunications, image processing, geophysics, hypercomplex analysis, and recently to show small motion or color changes, visual microphone and to create an interactive elastic image called visual vibrometry [15,14,16,17,8,9]. There are three different types of phases, the global or Fourier phase, the instantaneous phase and the local phase [7,12]. In this work, we propose a new technique for computing the local phase magnification in order to amplify motion by using a multiscale radial atomic function and 1D atomic function for computing the short-term and long-term temporal

variation on 2D and 3D. There are three main reasons for using the atomic functions. The atomic function have a compact support in space domain, the $n-$order derivative is easy to compute and we can compute the Hilbert and the Riesz transform by using the first derivative [6]. We present some applications in order to measure the breathe rate in 2D and 3D and the heart beat measurement. We use a RGB camera and RGBD (3D) sensors *KinectI* to get 2D and 3D sequences. According to our results, our phase magnification lost less information than the other Riesz approximation, however the computational time of our method response to noise than the linear method.

## 2 Quaternion Algebra

Quaternions $\mathscr{H}$ or $\mathscr{G}_{3,0,0}$ in the Geometric algebra *GA* is correct framework to compute the local phase [11,12,7]. An element of $\mathscr{H}$ consists of a real element adding three imaginary elements $(i, j, k)$:

$$q = a + bi + cj + dk, \tag{1}$$

where $a, b, c, d \in \mathscr{R}$ and $i$, $j$ obey the relations $i^2 = j^2 = -1, ij = k$. The real part of $q$ is noted by $Re(q) = a$ and the pure part is $Pu(q) = bi + cj + dk$ [13]. $\mathscr{H}$ are geometrically inspired, due to the quaternions may be used to represent rotations (as bivector) in $\mathscr{R}^3$ and $\mathscr{R}^4$ and translations (as vector) in $\mathscr{R}^3$ [13]. *GA* allows to distinguish naturally objects and operations [12]. The imaginary components can be described in terms of the basis of $\mathscr{R}^3$ space, $i \to \mathsf{e}_{32}, j \to \mathsf{e}_{13}, k \to \mathsf{e}_{21}$ [12,13].

## 3 Local Phase Information

The Fourier or global phase is the most well known phase and denotes the angular phase of a signal in frequency domain [11]. However, when 2D the structural information is needed, the local phase can be computed [11,7]. The local phase, is used to know what is the phase at a certain position of the real signal [11,12]. The local phase means the computation of the phase restricted to a certain part or bandwidth of the real signal. The local phase is useful to separate the signal structure into impulses (even) and jumps (odd) [15,14]. Additionally, the phase information allows us to use the invariant or equivariant properties of the signal [12]. For instance, it has been shown that the phase has an invariant response to image brightness and it can also be invariant to the rotations [12,14]. For $2D$ signals, the complex approach, Hilbert transform is not enough to compute the magnitude and local phase independently in any direction [12,11]. Then, the quaternionic analytic signal and the monogenic signal have been proposed [11,12,15].

### 3.1 Monogenic Signal

The monogenic signal, was proposed by M. Felsberg and G. Sommer, and generalize the analytic signal to $n-$D. The monogenic signal for $2D$ signals is represented by [7]:

$$f_{\mathbf{M}}(\mathbf{x}) = f(\mathbf{x}) + (i, j) f_{\mathbf{R}}(\mathbf{x}) = f(\mathbf{x}) + (i, j) f(\mathbf{x}) * \frac{\mathbf{x}}{2\pi|\mathbf{x}|^3}. \tag{2}$$

The magnitude of the signal is computed by $|f_{\mathbf{M}}(\mathbf{x})| = \sqrt{(i,j)f_{\mathbf{R}}^2 + f(\mathbf{x})^2}$. Since the monogenic signal is constructed from the original signal and its Riesz transform, we can express the local phase $\phi$ and the local orientation $\theta$ as [12]:

$$\phi = \arctan\left(\frac{|(i,j)f_{\mathbf{R})} * f(\mathbf{x})|}{f(\mathbf{x})}\right), \tag{3}$$

$$\theta = \arctan\left(\frac{jf_{\mathbf{R}} * f(\mathbf{x})}{if_{\mathbf{R}} * f(\mathbf{x})}\right). \tag{4}$$

We use an special window, the radial atomic function, in order to compute the local phase, to a certain part or bandwidth of the real signal.

## 4 Atomic Functions and Monogenic Signal

In this work we use two atomic functions an $up(x)$ for time convolution and a radial atomic function $Plop(x,y)$ in order to compute the Riesz Transform in a multiscale approach.

The atomic functions ($AF$) are compactly supported, infinitely differentiable solutions of differential functional equations with a shifted argument [18]:

$$Lf(x) = \lambda \sum_{k=1}^{M} c(k) f(ax - b(k)), |a| > 1, b, c, \lambda \in N, \tag{5}$$

where $L = \frac{d^n}{dx^n} + a_1 \frac{d^{n-1}}{dx^{n-1}} + ... + a_n$ is a linear differential operator with constant coefficients.

The function $up(x)$ has the following representation in terms of their Fourier transform as [18,5]:

$$up(x) = \frac{1}{2\pi} \int_{\mathscr{R}} \prod_{k=1}^{\infty} \frac{\sin(\nu 2^{-k})}{\nu 2^{-k}} e^{i\nu x} d\nu, \tag{6}$$

$$= \frac{1}{2\pi} \int_{\mathscr{R}} \hat{up}(\nu) e^{i\nu x} d\nu. \tag{7}$$

A radial atomic function was mentioned in [6] as $up(\sqrt{x^2+y^2})$ (see Fig 1). However in [6], the function $Plop(x,y)$ was defined as a radial infinite differentiable function with compact support (see Fig 1):

$$\hat{Plop}(\nu,\upsilon) = \prod_{h=0}^{\infty} \sum_{k=0}^{\infty} \frac{[-(u^2+\nu^2)]^k}{3^{2k(h+1)}[(k+1)!]^2}, \tag{8}$$

and is solution of the following functional-differentail equation:

$$\nabla^2 Plop(x,y) = \lambda \int_{\partial S} Plop[3(x-\xi_1), 3(y-\xi_2)] ds + \mu Plop(3x, 3y), \tag{9}$$

where $\nabla^2 = \Delta = e_1 \frac{\partial^2}{\partial x^2} + e_2 \frac{\partial^2}{\partial y^2}$, $\xi_1^2 + \xi_2^2 = 4/9$, $\mu = -4\pi\lambda/3$ and $\lambda = 3^5/4\pi$.

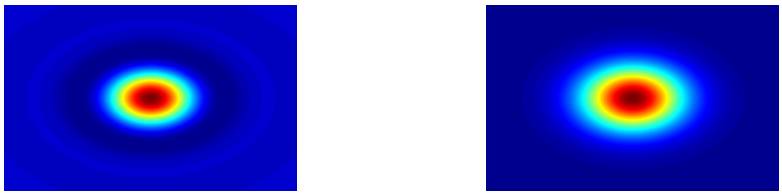

**Fig. 1.** Left: $\hat{up}(\sqrt{\nu^2+\upsilon^2})$; right: $\hat{Plop}(\nu,\upsilon)$.

### 4.1 Riesz Transform using Atomic Functions

The Hilbert transform acts as an involution on the space of solutions of linear differential-functional equations solutions such as atomic functions [19]. The Riesz transform can be seen as a generalized Hilbert transform to $n-$dimensions [12]. A Riesz transform based on an atomic function was presented at [6] using this equation:

$$f_{\mathbf{R}}(\mathbf{x}) = f(\mathbf{x}) * \left( \nabla^2 Plop(\mathbf{x}) * -\frac{1}{2\pi} sign(|\mathbf{x}|) log(|\mathbf{x}|) \right). \tag{10}$$

Atomic-Riesz pyramid coefficients consist of a real part and two imaginary parts with two Riesz transforms based on equation 10:

$$f_{\mathbf{M}}(\mathbf{x}) = f(\mathbf{x}) + i f_{\mathbf{R}_1}(\mathbf{x}) + j f_{\mathbf{R}_2}(\mathbf{x}), \tag{11}$$

and this information is used to determine the local amplitude $A = ||f_{\mathbf{M}}||$, local phase $\phi$ and local orientation $\theta$:

$$f_{\mathbf{M}} = A\cos(\phi) + iA\sin(\phi)\cos(\theta) + jA\sin(\phi)\sin(\theta), \tag{12}$$

$$\log \frac{f_{\mathbf{M}}}{||f_{\mathbf{M}}||} = iA\phi\cos(\theta) + jA\phi\sin(\theta). \tag{13}$$

Equation 13 uses a normalized quaternion,and is invariant to whether the local phase and orientation are $\phi$ and $\theta$ or the antipode $-\phi$ and $\theta+\pi$.

## 5 Linear and Phase Magnification

Eulerian video magnification (linear magnification), was introduced by F. Durand, W. Freeman et al [1,8,9] is able to amplify small motions or color changes in videos. In their work, the temporal brightness changes in each frame sub-bands are amplified in order to amplify motions or color changes.

Figure 2 shows the Euler magnification approach on an image, by increasing temporal variation it is possible to increase spatial motion or color.

In order to do the implementation of the linear magnification Wadhwa et al. [8] use a Laplace pyramid in addition to temporal filter. The main problem of linear magnification is that noise power is amplified.

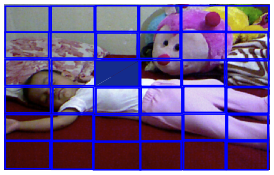

**Fig. 2.** Euler magnification approach on a frame, where the fluid par- ticles is tracked over time.

Several papers has demonstrated that the local phase using bandpass filtered can be used for local structure description and motion estimation. Also it has been shown the link between phase and motion and could be exploited in an Eulerian manner for motion magnification [14,20]. Additionally, the main problem of linear magnification were solved by amplifying temporal phase variations using a Riesz pyramid approximation [1,10]. In this work we propose use an unique atomic function to compute our Riesz transform aproximation and to compute some temporal filters in 1 dimension.

### 5.1 Local Phase Magnification based on Atomic Functions

As a summary, the first step to phase magnification is to express the image sequence in terms of the quaternion Riesz pyramid. The next step is to filter the local phase in a temporal way we have used an $up(x)$. Then an amplify factor ($\alpha$) was applied to the local phase(magnitude and local orientation are not affected) , finally the Quaternion Riesz pyramid of the $n$ frames is reconstructed. This method is very time consuming due to we need 3 images ( or 3 pyramids) for each sequence pyramids instead of one pyramid a Laplacian approach. The local phase computation has an ambiguous sign, therefore a filter a sequence of unit quaternions can be used. According to [8,9] the local orientation $\theta$ is supposed as constant over time at every pixel [9]. The equation 13 can be expressed in terms of $n-frames$:

$$iA\phi_n \cos(\theta) + jA\phi_n \sin(\theta). \tag{14}$$

At every pixel, a temporal filtering $1D$ on this quantity to isolate motions or changes of interest. In this case we propose using an 1D atomic function $up(x)$. Spatial filtering can be achieved by weighted blur with Plop function on the $i$ and $j$ components:

$$iPlop(x,y)A\phi_n \cos(\theta) + jPlop(x,y)A\phi_n \sin(\theta). \tag{15}$$

Motion amplify coefficients in the phase approach are in the same way as phase-shift a complex number. A quaternion expression is amplified by $\alpha$ factor such as

$$A\cos(\alpha\phi) + iA\sin(\alpha\phi)\cos(\theta) + jA\sin(\alpha\phi)\sin(\theta). \tag{16}$$

When multiply $I_M$ this unit quaternion by the original coefficient $(\mathbf{x}) + if_{\mathbf{R}_1}(\mathbf{x}) + jf_{\mathbf{R}_2}(\mathbf{x})$ the real part can be expressed by [9]:

$$I_M = A\cos(\alpha\phi) - Af_{\mathbf{R}_1}\sin(\alpha\phi)\cos(\theta) - Af_{\mathbf{R}_2}\sin(\alpha\phi)\sin(\theta). \tag{17}$$

In the results section we compare our approach with the method reported in [9] in terms of the Riesz pyramid reconstruction information and the time of computation.

## 6 3D Magnification

The phase magnification was only defined by 2D projections. We use a RGBD sensor (Kinect I) in order to compute a 3D magnification. In this case we use a RGBD sensor in order to obtain the 3D information, therefore we have $(x,y)$ plane and the depth value is a query of the value coordinates, actually it is straightforward (see the distance such as brightness of the image) to apply the magnification in this image sequence.

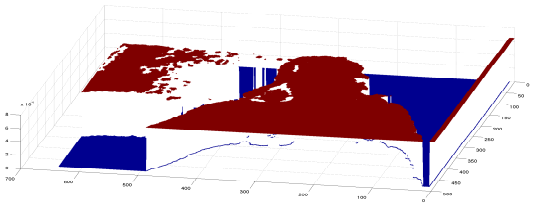

**Fig. 3.** Example of one 3D frame measure by kinect one.

However, using geometric algebra it is posible select any plane of magnification using the project or reject of the 3D points to another plane. The products of the Geometric Algebra has a geometric meaning and the dot product is related with the projection and the wedge product with the rejection.

Let $p_l = (x,y,z)$ the 3D points in our case measured by the RGBD sensor. It is posible to project the 3D point into anothers planes ( not only use $\pi_{x,y} = e_1 \wedge e_2$) of interest using this equation in the conformal space:

$$P_{project} = (\pi \cdot p_l)\pi, \tag{18}$$

$$P_{reject} = (\pi \wedge p_l)\pi, \tag{19}$$

where $\pi = e_l \wedge e_m$ is plane where the 3D points will be projected, $P_{project}$ are the 3D points projected in a new plane, in the case of the rejection points $P_{reject}$ will be on orthogonal plane. For instance if we want to project in the $\pi_{y,z} = e_2 \wedge e_3$. A similar equation (using a dot product) can be used to project lines, planes, spheres among others objects. We belive that this is a good example about how use geometric algebra in low and mid level image processing.

## 7 Results and Analysis

### 7.1 2D Magnification

The original gray image and its Region of Interest (ROI) in the chest of a baby sleeping is shown in the Fig. 4. In order to show the difference between the original sequence and the magnified sequence. We select this ROI due to is a very significant information

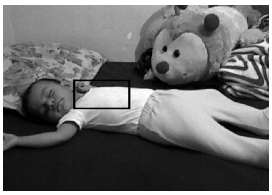

**Fig. 4.** ROI of the image sequence for 2D magnification.

about the baby. This application can be used to make visible or measure the breathe rate using an simple camera.

Phase magnifications using the Riesz pyramid are presented in the Fig. 5. From left to right: original ROI, phase amplification of ROI and difference of each frame. In order to see the evolution of the signal we show from top to down we show 5 frames at $t = 0 : 0.5 : 2sec$. Its posible to see in the difference image how the edge

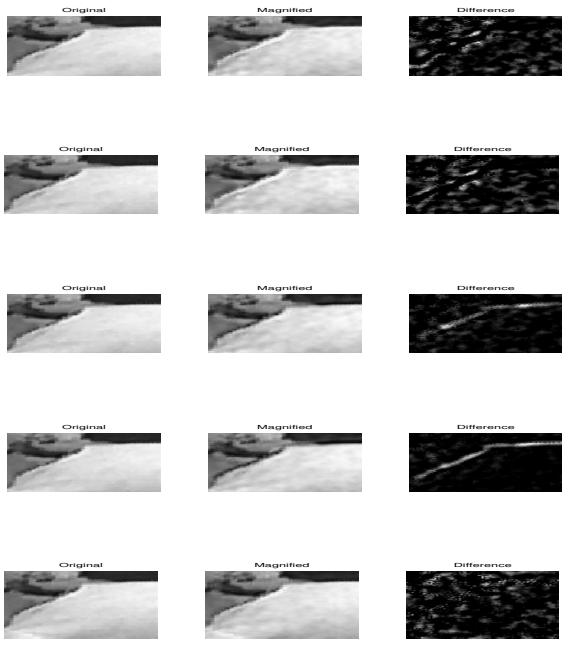


**Fig. 5.** From left to right: Original frame, linear magnification of a ROI of the image sequence and the difference between the original frame and its magnification.

An application of this technique is to measure the heart beat. In this case we present

the original image and its magnification Fig. 6 we can see in the subtraction of the images the white region related with the pulse rate. One of the important uses of sensing physiological signals of the human being, is the determination of stress levels or emotions in an automatic way and this two parameter can be used. We measure the heart beat using the maximum value and we get a 110 $bpm$.

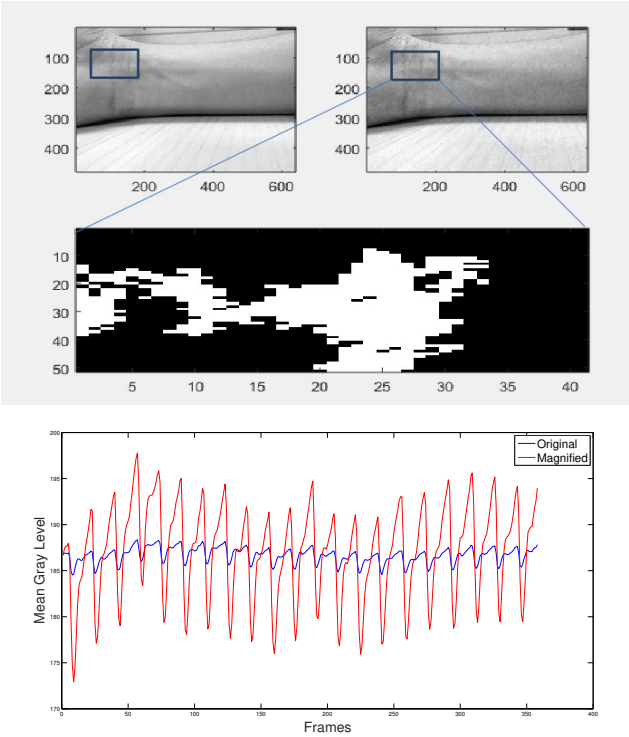


**Fig. 6.** Magnification of a ROI of the image sequence to get the heart beat.

### 7.2 Riesz Pyramids Comparison

In order to compare both approaches we compute de reconstruction (4 level in both cases) of a couple of images. The first image is a $256 \times 256$ with a white central point such as point spread function. In this case we show the original image, the reconstruction and finally an image subtraction. We measure de mean value of the difference image and the standard deviation. Our method obtain $mean = -2.6221 \times 10^{-24}$ $stdv = 1.0588 \times 10^{-22}$ in the difference image Fig. 7. In Riesz aproximation proposed by Wadwha was used fast Riesz computation using a 0D filter approximation based on five coefficients Chebyshev polynomials and the McClellan transform, the mean value

of the difference was $mean = 2.6622 \times 10^{-7}$ and a $stdv = 7.1790 \times 10^{-5}$. Its posible to see that our Riesz pyramid reconstruction presents less difference between the original.

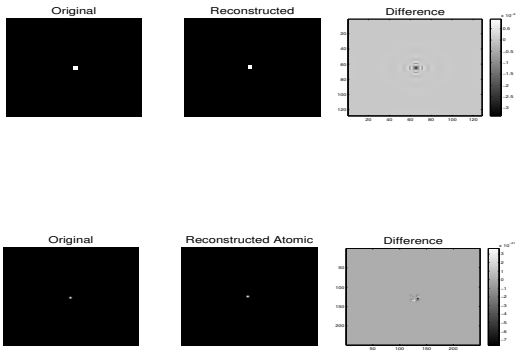


**Fig. 7.** From left to right: original image, the reconstruction of the image using the Riesz pyramid and finally the difference between the original and the reconstructed image. In the upper row a the result using Riesz pyramid proposed by Wadwha et all and in the down row our Riesz pyramid approximation using atomic functions.

### 7.3 3D Magnification

One contribution of this work is amplify a 3D sensor image sequence. We use a Kinect, which provides a RGB-Depth images with $640 \times 480$ images at 30 $fps$. Due to IR Fig. 8 images has more noise than RGB images, therefore, we use a phase technique in order to improve a linear Eulerian magnification method in two aspects: it supports larger magnification and it has better noise performance.

**Fig. 8.** IR image. It is possible to see the IR pattern has a lot of noise.

In this case we work with the original plane acquisition, which is by definition an $x, y$ plane where all 3D points are projected. We select the same chest baby in order to show the breath frequency. In Fig. 9 we present one frame and the selected region of interest used in the Fig. 10. We use the depth map from the Kinect, we present the 3D motion magnification Fig 10.

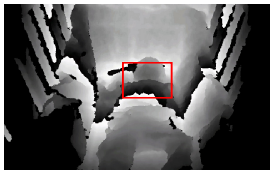

**Fig. 9.** Depth image. We select a ROI of 3D image using the Kinect.

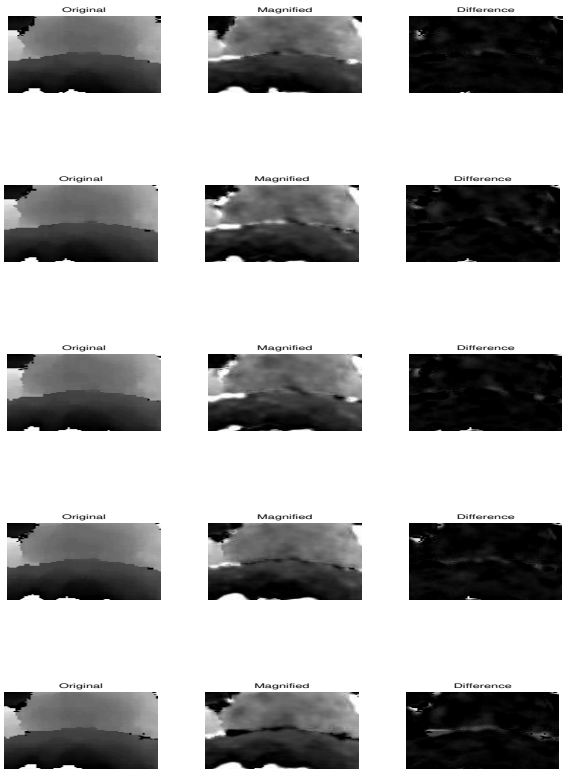


**Fig. 10.** Depth image phase magnification of the selected ROI. From left to right, original ROI, phase amplification of ROI and difference of each frame between the original ROI and the magnified frame. From top to down we show 5 frames at $t = 0 : 0.5 : 2s$.

In the selected ROI, we compute the Signal to Noise Ratio in terms of the mean value of the ROI (signal) and the standard deviation of the ROI (Noise) of the magnification areas. We can see that the linear magnification Fig. 11 has more variations, in contrast phase magnification Fig. 12 has less noise at the breath peaks. This results shows that it is posible to make a 3D phase magnification. In a future work we can

show the 3D magnification in different planes using conformal geometry. This result has the same behavior that the reported by Wadwha et all. Where the linear magnification amplify the noise of the signal. We believe that our results could be used with another 3D sensors based on the projection and rejection equation it easy to project all the point to a plane of magnification. In a future work we hope to apply this 3D with another 3D objets such as lines, spheres among others.

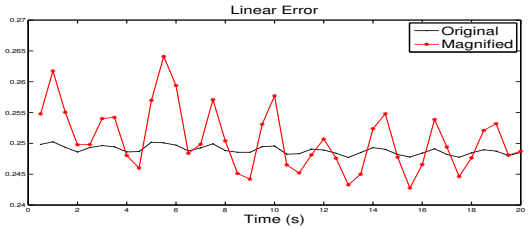


**Fig. 11.** Standard deviation of the selected ROI using a linear magnification.

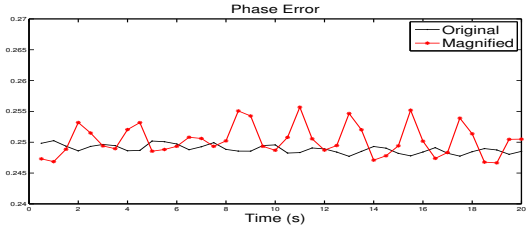


**Fig. 12.** Standard deviation of the selected ROI using a Phase magnification.

## 8 Conclusions

As a conclusion, we have presented a new local phase quaternionic method based on a unique compact supported window infinitely differentiable, the atomic function $up(x)$. We compute a Riesz pyramid based on atomic functions and compare with the Wadhwa Riesz approximation, our method present less difference between the gray scale value of each image. However, the fast phase computation made by Wadwha takes 2.5 less time than our method. Additionally we do not see a significance difference in the final magnification. In our method we see in some levels an alliasyng effect at the high pass filtered images. Additionally we have presented a 3D magnification based on IR depth sensor *KinectI* in the front plane of the sensor. We present a projection equation in conformal geometry in order to compute another magnification in others projections. Due to IR images of both sensor have more noise than RGB images we

use a phase technique to improve the linear Eulerian magnification method in two aspects: it supports larger magnification and it has better noise performance. Finally we compare, the Riesz Pyramids method and the linear magnification in terms of the Signal to noise ratio (SNR), we found that the phase magnifications has better response than the linear method. The phase motion magnification method has higher quality, however it is also more expensive for computing which is similar result previously reported. Also, considering another future application in forensic science, we can apply our tools in order to detect small changes in images about facial gestures or small changes by blood pressure, pulse and respiration in faces images given some questions put to person. In this sense, we will have a detector of small changes in people's faces images (2D or 3D models) to a set of questions, only using cameras and image processing.

**Acknowledgment.** Thanks to our research team and volunteers of our videos and we want to thank to CONACYT-SNI.

## References

1. Rubinstein, M.: Analysis and Visualization of Temporal Variations in Video. PhD thesis, Massachusetts Institute of Technology (2014)
2. Davis, A., Bouman, K. L., Chen, J. G., Rubinstein, M., Durand, F., Freeman, W.T.: Visual vibrometry: Estimating material properties from small motions in video. In: IEEE Conference on Computer Vision and Pattern Recognition (CVPR) (2015)
3. Moya-Sánchez, E.U., Bonell, M.: Quaternion Atomic Phase Magnification for 3D Motion. In: Early Proceedings of the AGACSE Conference (2015)
4. Moya-Sánchez, E.U., Bayro-Corrochano, E.: Quaternion and Clifford Fourier Transforms and Wavelets. Ch 4: Quaternionic Local Phase for Low-level Image Processing Using Atomic Functions Trends in Mathematics, pp. 57–83, Springer (2013)
5. Bayro-Corrochano, E., Ulises Moya-Sánchez, E.: Ch 8: Quaternion Atomic Function for Image Processing, Leo Dorts Joan Lasenby. Guide to Clifford Algebras in Practice, Spinger (2011)
6. Moya-Sánchez, E.U., Bayro-Corrochano, E.: Hilbert and Riesz transforms using atomic function for quaternionic phase computation. Adv. Appl. Clifford Algebr. 23, No. 4, pp. 929-949 (2013)
7. Felsberg, M., Sommer, G.: The monogenic signal. IEEE Trans. Signal Process., 49(12), pp. 3136–3144 (2001)
8. Wadhwa, N., Rubinstein, M., Durand, F., Freeman, W.T.: Riesz Pyramids for Fast Phase-Based Video Magnification. In: IEEE International Conference on Computational Photography (ICCP) (2014)
9. Wadhwa, N., Rubinstein, M., Durand, F., Freeman, W.T.: Quaternionic Representation of the Riesz Pyramid for Video Magnification, http://people.csail.mit.edu/nwadhwa/riesz-pyramid
10. Wadhwa, N., Rubinstein, M., Durand, F., Freeman, W.T.: Pseudocode for Riesz Pyramids for Fast Phase-Based Video Magnification Tecnical Report (2014)
11. Bülow, T.: Hypercomplex spectral signal representations for the processing and analysis of images. PhD thesis, Christian- Albert, Kiel University, Kiel, Germany (1999)
12. Felsberg, M.: Low-level image processing with the structure multivector. PhD thesis, Christian- Albert, Kiel University, Kiel, Germany (2002)

13. Lounesto, P.: Clifford Algebras and Spinors. Cambridge University Press (2001)
14. Kovesi, P.: Invariant measures of image features from phase information. PhD thesis, University of Western Australia (1996)
15. Lennart, W.: Local feature detection by higher order Riesz transforms on images. Master's thesis, Christian- Albert, Kiel University, Kiel, Germany (2008)
16. Ell, T.A., Sangwine, S.J.: Hypercomplex Fourier Transforms of Color Images. IEEE Trans Image Proc, 16(1), pp. 22–35 (2007)
17. Hitzer, E.M.S.: Quaternion Fourier Transform on Quaternion fields and Generalizations. J Adv Appl Clifford Alg, 17(3), pp. 497–517 (2007)
18. Kolodyazhnya, V.M., Rvachev, V.A.: Cybernetics and Systems Analysis, 43 (2007)
19. Weiss, J.: The Hilbert transform of wavelets are wavelets. Technical Report, Applied Mathematics Group (1995)
20. Bayro Corrochano, E.: The theory and use of the quaternion wavelet transform. Journal of Mathematical Imaging and Vision, 24, pp. 19–35 (2006)

ISSN 1870-4069

# Deep Analysis of a Basic Traffic Model

Diego Uribe, Luis Lugo, Enrique Cuan

Instituto Tecnológico de la Laguna,
División de Estudios de Posgrado e Investigación, Torreón, Coahuila,
Mexico

{diego, lclr, kcuan}@itlalaguna.edu.mx

**Abstract.** In this article we analyze the basic elements to be considered in vehicular traffic by using modeling based on agents. One of the most important activities of a traffic engineer is to measure the capacity of a road in order to optimize the road infrastructure of a city. The incorporation of the microscopic and macroscopic characteristics of vehicular traffic flows are the key elements for developing a realistic model for measuring the capacity of a particular road. By using a basic traffic model, we present, on the one hand, the empirical relationships of a vehicular traffic system in terms of density, flow and speed; on the other hand, we show how the use of agent-based modeling to simulate vehicular traffic system proves to be a plausible alternative. Also, this work makes clear the shortcomings of a basic traffic model that must be considered for developing a more realistic traffic simulation system.

**Keywords:** Agent-based modeling, traffic model, micro and macro levels.

## 1 Introduction

Nowadays, heavy traffic in big cities is the cause of many urban problems: wasted time, poor fuel efficiency, high pollution, stress and unfortunately, an increase in the accident rate [2]. So the need for a network of intelligent transportation system to be able to cope with these multiple problems is evident.

Among the multiple tasks of traffic engineers, traffic flow analysis is perhaps the most important activity. Indeed, the optimization of the transport infrastructure largely depends on a through analysis of the traffic flow detecting areas and time periods of increased traffic density is critical for making decisions such as expanding the number of lanes, installing traffic lights, or altering the scheduled times of existing traffic lights.

Likewise, among the multiple tools available to the traffic engineer, a vehicular traffic simulator is an essential tool because it allows analyzing hypothetical scenarios corresponding to several possible vehicular flows. Also, this tool is essential as facilitates the estimation of real-time road traffic information. In fact, by using a vehicular traffic simulator, a traffic engineer embarks on preanalysis of the urban area to be investigated. The purpose of this activity is

to establish various hypotheses to be verified, or disproved, based on the road traffic information obtained in real time.

According to the definition of a complex system as a system characterized by an environment in which multiple individual and independent elements interact with each other giving rise to an emerging phenomenon [3, 5], to analyze vehicular traffic from this perspective is rather a plausible approach. In fact, taking into account the multiple factors to be considered when driving a vehicle (e,g. the presence of other vehicles, road conditions, traffic lights, traffic accidents, pedestrian crossing), a traffic system may also be characterized as a complex system.

In this way, since agent based modeling is a computational methodology that allows us to model complex systems [15], we analyze in this work the basic elements to be considered in vehicular traffic by using modeling based on agents. To be more specific, the vehicles are represented as agents, whereas the road is represented as the environment in which the vehicles travel and interact. The micro and macro level that characterize a complex system are also analyzed by using a basic traffic model based on agents in order to present the empirical relationships of a traffic system in terms of density, flow and speed.

Also, as a fundamental part of our analysis work we point out the shortcomings of the traffic model that must be considered for developing a more realistic traffic simulation system. Since velocity is an intrinsic parameter to any traffic model, an appropriated representation of distance and time is essential for a traffic simulation system [8]. In other words, taking care of the distance is essential for a safe control of the speed. Thus, its fundamental to study the representation of distance and time in this model.

The theoretical framework of the methodology adopted in the traffic model is described in section 3. As it is briefly mentioned lines above, the model represents the simulation of a vehicular traffic system based on agents so the properties, behaviour and interactions between autos is detailed. Then, the empirical relationships of a traffic system in terms of density, flow and speed are presented in section 4 as well as the basic parameters for an elemental runtime analysis. Related work as other models for describing traffic flows is also mentioned in the next section.

## 2 Related Works

In this section, we briefly narrate other models for describing traffic flows. Traffic flow theory is a scientific field relatively young. The first traffic problems in the past century were solved by the implementation of rule of thumb methods. However, at the beginning of the 1950s, the turning point in the field of traffic engineering came when Glen Wardrop described traffic flows by using mathematical representations [12].

The first popular traffic flow model, commonly known as the LWR model, was based on fluid dynamics, a discipline for studying fluids (liquids and gases) in motion [6, 11]. In fact, traffic flow model makes use of numerical analysis

and algorithms to solve and analyze problems that involved fluid flows. The interactions of liquids and gases are used as an analogy to model the interactions among vehicles.

Another interesting work was the traffic model implemented by Prigogine and Herman who drew an analogy between gas-kinetic and the velocity distributions [10]. It is basically a stochastic model of traffic flow in which the microgoals of each driver are modified by the interaction with other drivers. Then, the central idea is to predict how much the microgoals of the driver have been modified by making use of a kinetic equation defined in terms of the desire of the driver and the interactions with other vehicles.

Statistical physics represents a more recent framework in traffic flow modelling. Particularly, the cellular automata model developed by Nagel and Schreckenberg is based on particles systems where the cells have varying states over time [9].

## 3 Theoretical Framework

The theoretical framework that supports the basic traffic model to be analyzed in this article is described in this section. First, we briefly define the microscopic and macroscopic properties of traffic flow to study vehicular transport systems. Then, we present the essential concepts of agent-based modeling, the methodology for designing and building the basic traffic model.

### 3.1 Microscopic and Macroscopic Properties of a Traffic Flow

Broadly speaking, the drivers and vehicles, that is, the actors of a vehicular transport system denote the microscopic characteristics, whereas the interactions between drivers denote the macroscopic characteristics of traffic flows [7].

The microscopic properties of a traffic flow are described, first, in terms of a single vehicle, and then, by considering two consecutive vehicles. The main characteristic to describe a vehicle in a traffic lane are: *length*, *position*, *velocity*, and *acceleration*.

Driving safely requires to be aware of how close another car is. Thus, by considering two consecutive vehicles in a traffic lane, we have two very important properties:

- *space headway*: it is defined as the space gap between two consecutive vehicles: a follower and its leader (i.e. predecessor), that is measured from the followers rear bump to its leaders rear bump. Such space gap is usually expressed in metres.
- *time headway*: it is defined as the time to travel the space headway at the current velocity. Such time gap is usually expressed in secs.

The macroscopic properties of a traffic flow are considered in terms of an aggregate level of multiple vehicles in a traffic stream. We begin with density:

a measure to determine how crowded a section of a road is. In other words, the concentration or *density* of traffic, denoted by $k$, is estimated by the following expression:

$$k = \frac{n_x}{x}, \tag{1}$$

where $n_x$ denotes the number of vehicles in the section of a road to be measured, $x$ denotes the length of the section of a road, and $k$ is expressed in terms of veh/m.

The second macroscopic property is concerned with time: a temporal measure to determine the number of vehicles passing at a particular point of the road during a particular period of time. In other words, the *flow* of traffic, denoted by $q$, is estimated by the following expression:

$$q = \frac{n_t}{t}, \tag{2}$$

where $n_t$ denotes the number of vehicles in a particular period of time, $t$ denotes a particular period of time, and $q$ is expressed in terms of veh/s.

Average speed is the third macroscopic property and it is concerned with multiple rather than individual speeds. There are two different ways to estimate the average speed: the spatial measurement and the temporal measurement [1]. Assuming n vehicles in a traffic stream where the particular speed of each vehicle is registered in a specific point and a particular time, the temporal measurement of the *average speed*, denoted by $u_t$, is estimated by the following expression:

$$u_t = \frac{\sum_{i=1}^{n}(u_i)}{n}, \tag{3}$$

where $n$ denotes the number of vehicles, and $u_i$ denotes the speed of an individual vehicle.

### 3.2 Agent-based Modeling

The approach for developing the basic traffic model is based on one of the primary methodologies to study complex problems: agent-based modeling. A complex system is defined as a system characterized by an environment in which multiple individual and independent elements interact with each other giving rise to an emerging phenomenon [3, 5]. The complexity of a system is observed in natural and social phenomena that are non-deterministic and have distributed mechanisms and control. Thus, to simulate the interactions among agents to recreate the macroscopic properties that emerge is fundamental to make sense of the phenomena to investigate.

Agent based modeling is a computational methodology that allows us to model complex systems [15]. More precisely, ABM is a computational modelling paradigm that enable us to describe a complex system in terms of agents, environment, and interactions. While agents denote the basic ontological unit of the model, the environment represents the world in which the agent lives. In this work, we make use of Agent based modeling to represent vehicular traffic

flows. To be more specific, the vehicles are represented as agents, whereas the road is represented as the environment in which the vehicles travel and interact. The micro and macro leves that characterise a complex system are also analysed to present the empirical relationships of a traffic system in terms of density, flow and speed.

## 4 Basic Traffic Model and Discussion

The empirical relationships of a traffic system in terms of density, flow and speed are presented in this section. First, we describe the basic traffic model used to illustrate the relationships between the macroscopic traffic flow characteristics, and then, the section concludes with a discussion about the shortcomings of the traffic model that are essential to be considered for developing a more realistic traffic simulation system.

### 4.1 Empirical Relationships of a Traffic System

The traffic model used to exemplify the empirical relationships of a traffic system in terms of density, flow and speed is the model developed by Wilensky [13]. This model represents a traffic lane in which the velocity of the cars is a function in terms of the available space between them. In other words, an individual driver might accelerate o decelerate according to the distance between his vehicle and the next: the space headway. The model also proves how traffic jams emerges spontaneously from slow-moving vehicles creating a ripple effect backward.

Moreover, the traffic model used to illustrate the relationships of a traffic system has been developed with NetLogo [14]. NetLogo is a programming language used to create models based on agents and has also proved to be a well suited tool for modeling complex systems evolving over time. One of the most appealing features of NetLogo is the capacity to investigate the connections between the micro-level behavior of individuals and macro-level patterns that emerge from their interactions [4].

The relation between speed and density is shown in Figure 1. It can be noticed how the speed falls as the number of cars increases. In other words, we observe a negative correlation between speed and density: as density increases, speed decreases and vice versa. We can also describe this relation in terms of the drivers comfort: as long as the density in a particular road is lower, the driver travels at his desired speed. On the contrary, the speed range available to a driver is limited to the extent that the density on the road increases.

Figure 2 shows the relation between flow and density. In this case, two stages can be noticed: increasing and decreasing of the flow as traffic density rises. In other words, we observe at the beginning a positive correlation reaching the maximum of flow and then, a negative correlation: as density increases, flow decreases.

In this way, Figure 2 shows two essential points to determine how much traffic might be allocated in a road space. First, when flow is at its highest, we

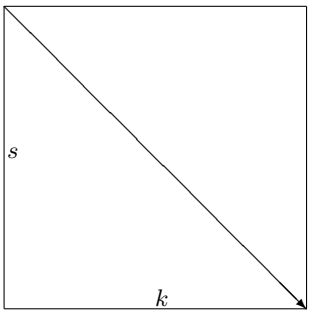


**Fig. 1.** The relation between speed ($s$ ) and density ($k$).

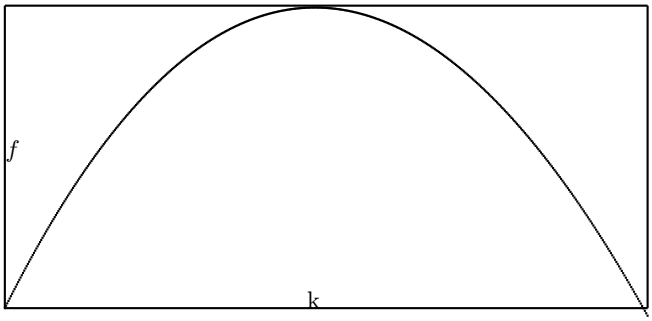


**Fig. 2.** The relation between flow ($f$ ) and density ($k$).

can consider this value to characterise the capacity of a particular road. Second, when density is at its highest value, we can consider this value to denote the emergence of a traffic jam.

Figure 3 shows the relationships between density, flow and speed by using the traffic model developed with NetLogo. Figures 3a, 3b, and 3c have been obtained with a density value of 10, 20, and 30 respectively. In other words, the traffic model has been run through different values of density. In this way, the relation between speed and density can be noticed: we see how speed is dropping whereas density increases.

From the perspective of the relationships between flow and density, the traffic engineer can define the capacity of the road in terms of a not very constrained speed. In other words, as long as the driver is able to accelerate to keep a target speed, previously defined by the traffic engineer, the flow is on the way to its highest point. Otherwise, the driver enters a state of deceleration that can eventually lead to a traffic jam. In this particular case, Figure 3 shows how a medium speed can be achieved with a density value of 20.

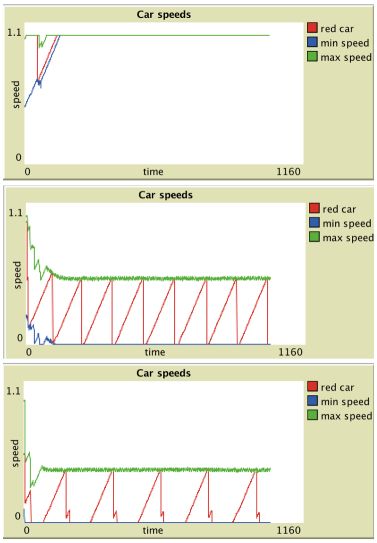


**Fig. 3.** The relationships between density, flow, and speed.

### 4.2 Discussion

Another fundamental part of our analysis work is the consideration of the shortcomings of the traffic model used to exemplify the relationships of a vehicular system. The purpose of further analysis of the model is to identify essential elements to be considered for developing a more realistic traffic simulation system.

Since velocity is an intrinsic parameter to any traffic model, an appropriated representation of distance and time is essential for a traffic simulation system [8]. As it was previously mentioned, the model depicts a traffic lane in which the velocity of the cars is determined according to the available space between them: a driver might accelerate o decelerate to the extent of the distance between his vehicle and the next. In other words, taking care of the distance is essential for the safety control of the speed. Thus, its fundamental to study the representation of distance and time in this model.

To achieve a better representation of the distance between cars we focus our attention in one of the fundamental microscopic traffic characteristics: the *space headway*. As we mentioned in section 3, the space headway between two consecutive vehicles: a follower and its leader (i.e. predecessor), is defined as the space gap measured from the followers rear bump to its leaders rear bump. Such space gap is usually expressed in meters [7].

In the case study discussed in this article, the traffic model developed with NetLogo measures the distance in terms of patches. A patch is the basic unit used by NetLogo to represent the environment in which the agents interact. In fact, NetLogo represents the environment (called "*world*") as a bi-dimensional space that is divided up into a grid of patches.

Thus, being NeLogo a generic tool for agent-based modeling, the configuration of the environment, and therefore the definition and interpretation of a patche depends on the domain to be modelled. For example, in the classic Wolf-Sheep Predation model, the environment is represented by a landscape where a patche" denotes a minute portion of the landscape, that is, a minute portion of grass. On the other hand, in our case study model, the environment is represented by a road space where a "*patche*" denotes an undefined portion of the space headway, that is, an undefined measure of distance.

Even though the distance has not been properly defined, Figure 4 shows how the model allows us to observe the correlation between speed and space headway. When we run the model under the same density of traffic and different values of headway, speed gradually decreases as the headway increases, which denotes a more preventive driving habit.

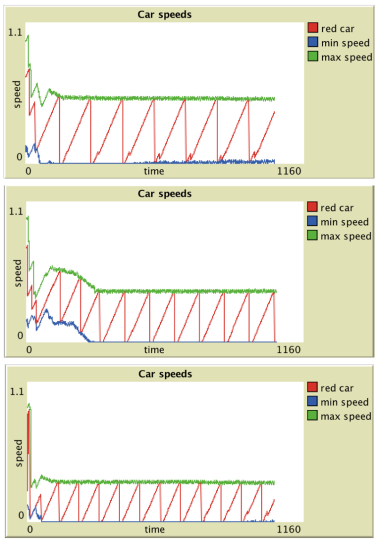


**Fig. 4.** The correlation between speed and space headway.

We conclude our discussion to emphasize how important a proper environment settings is. In fact, to determine the scale of the environment in which agents play is a fundamental stage in the development of any model. In the particular case of NetLogo, it is essential to define the maximum size of the environment in terms of a scale to perform all calculations involving distance. For instance, to model a road space of 1000 meters, an option would be to configure the space with 1000 patches which denotes a simple 1:1 scale. However, since a large number of patches affects the performance of the model, a configuration of a 1:5 scale would be more advisable. In this way, the road space would be represented with 200 patches.

## 5 Conclusions and Future Work

We focus our attention in the basic elements to be considered in vehicular traffic by using modeling based on agents. By making use of a basic traffic model, we present the empirical relationships of a vehicular traffic system in terms of density, flow and speed. We also show how relevant the microscopic and macroscopic characteristics of vehicular traffic flows are for developing a realistic traffic model. Furthermore, the shortcomings of a basic traffic model were discussed to emphasize how important an appropriated representation of distance and time is for a traffic simulation system.

Many dynamic aspects of traffic flows have a huge influence over the developing a realistic traffic model. Dynamic and complex aspects to be modeled such as the conditions of the road (e.g. wet roads) and human factors (e.g. reaction time) are undoubtedly interesting aspects to investigate and to include in the developing of a traffic simulation system.

## References

1. Bell, M., Bonsall, P., Leake, G., May, A., Nash, C.: Transport Planning and Traffic Engineering. Butterwörth-Heinemann, Elsevier (2006)
2. Greengard, S.: Smart Transportation Networks Drive Gains. Communications of the ACM 58(1), 25–27 (2015)
3. Holland, J.: Hidden Order: How Adaptation Builds Complexity. Helix Books/Addison-Wesley (1995)
4. Janota, A., Rastocny, K.: Multi-agent Approach to Traffic Simulation in NetLogo Environment Level Crossing Model. In: 5th International Conference Transport Systems Telematics TST05- 2005 (2005)
5. Kauffman, S.: At Home in the Universe: The Search for the Laws of Self-Organization and Complexity. Oxford University Press (1995)
6. Lighthill, M., Whitham, G.: On kinematic waves: II. A theory of traffic flow on long crowded roads. In: Proceedings of the Royal Society. vol. A229, pp. 317–345 (1955)
7. Maerivoet, S., De Moor, B.: Traffic Flow Theory. eprint arXiv:physics/0507126 (2005)
8. Mayrhofer, C.: Performance, Scale and Time in Agent-based Traffic Modelling with NetLogo. Journal for Geographic Information Scien 1, 567–570 (2015)
9. Nagel, K., Schreckenberg, M.: A cellular automaton model for freeway traffic. Journal de Physique I France 2, 2221–2229 (1992)
10. Prigogine, I., Herman, R.: Kinetic Theory of Vehicular Traffic. Elsevier, New York (1971)
11. Richards, P.I.: Shockwaves on the highway. Operations Research 4, 42–51 (1956)
12. Wardrop, J.: Some theoretical aspects of road traffic research. In: Proceedings of the Institution of Civil Engineers. vol. 1 (1952)
13. Wilensky, U.: NetLogo Traffic Basic Model. Center for Connected Learning and Computer-Based Modeling, Northwestern University, Evanston, IL (1997), http://ccl.northwestern.edu/netlogo/models/TrafficBasic
14. Wilensky, U.: NetLogo. Center for Connected Learning and Computer-Based Modeling, Northwestern University, Evanston, IL (1999), http://ccl.northwestern.edu/netlogo/

15. Wilensky, U., Rand, W.: An Introduction to Agent-Based Modeling. The MIT Press. Cambridge Massachusetts (2015)

ISSN 1870-4069

# Robust Stability Analysis for Linear Systems with Uncertain Fast-Varying Time Delay arising from Networked Control Systems

Juan-Eduardo Velázquez-Velázquez, Rosalba Galván-Guerra

Instituto Politécnico Nacional, UPIIH, Hidalgo,
Mexico

{jvelazquezv, rgalvang}@ipn.mx

**Abstract.** This contribution is concerned with the robust stability analysis for linear systems with time-varying delay arising from networked control systems. The time-varying delay is supposed to be bounded and fast-varying. By constructing a new complete Lyapunov-Krasovskii functional, delay-dependent robust stability conditions are derived in terms of Linear Matrix Inequalities. The derivative of the new complete nominal Lyapunov-Krasovskii functional along the trajectories depends on the complete state and the state derivative.

**Keywords:** Robust stability, time delay systems, Lyapunov-Krasovskii functional, networked control systems.

## 1 Introduction

Conventional control systems are composed of interconnected controllers, sensors and actuators following a point-to-point architecture. As an alternative, the use of a multipurpose shared network to connect spatially distributed elements results in flexible architectures and generally reduces installation and maintenance costs [7]. These kind of systems are known as Networked Control Systems (NCSs). The relevance of NCSs is due to their broad range of application as mobile sensor networks [14], remote surgery [12], automated highway systems and unmanned aerial vehicles [15, 16]. In contrast to using several dedicated independent connections, the use of a shared network introduces new challenges as the presence of time-varying network-induced delays, aperiodic sampling or packet dropouts. Since an implementable model usually needs to possess some stability properties, in this work we are interested in the robust stability analysis for a class of networked control systems (NCSs) where the control loops are closed through a real-time network forming a delay control system.

The dynamical systems with time delays commonly known as Time-Delay Systems (TDSs) is a continuous field of interest and development. Principally, because time-delay is one of the main causes of instability of systems. Nowadays, with the increasing expectations of dynamics performance the robust stability analysis of TDSs is of practical significance. Time-delay robustness is often studied for situations in which the delay is uncertain but remains constant throughout time. While much research has

been done and stability criteria have been derived for systems with uncertain constant time-delays, the recent research has been focused in the case where the time delay is time varying. The significance of such research effort is tied to the interest in designing control algorithms for large-scale networked systems.

Most of the results devoted to the stability of TDSs with uncertain delays consider as assumption the stability of the system free of delays, and next, in the time domain, use appropriate Lyapunov-Razumikhin functions or Lyapunov-Krasovkii Functionals (LKFs) combined with Linear Matrix Inequalities (LMIs) to derive some upper bounds on the delay values $\mu$. This type of delays is considered as uncertain *small* delays with *zero nominal* values and perturbations from $[0, \mu]$ [17, 3, 13]. There are cases where the previous assumption, the stability of system free of delays fails, but it may be stable for some *non-zero* delay. This type of delays is called *non-small* delays [1] and their stability analysis cannot be performed by using simple LKFs [5]. In order to treat effectively the fast-varying delay commonly the proposed LKFs involve terms such as $\int_{-h}^{0}\int_{t+\theta}^{t}\dot{x}(s)W\dot{x}(s)dsd\theta$ and then the derivative along trajectories of the involved functionals present quadratic derivative terms. This is the reason why in [2] negative quadratic terms, depending on $\dot{x}(t)$ were inserted into $\dot{v}_n$. There, the compressive techniques for stability analysis of uncertain time-delay systems: free weighting matrices and application of Jensens inequality [5] were extended to the case of complete LKF. The derivative of the complete LKF in [2] depends on the present state only.

The complete type LKF introduced in [11] are constructed on the base of the solution of a linear matrix differential-difference equation on a finite time interval which satisfies additional symmetry and boundary conditions. This solution is called a delay Lyapunov matrix and it inherits properties of the classical quadratic Lyapunov functions for ordinary delay free differential equations. These LKFs prove to be useful in the robustness analysis of time delay systems [11]. In [10], the complete LKF was constructed for the uncertain system, which did not explicitly depend on the bounds of the uncertainties. As a result, the stability conditions were rather complicated, and induced some conservatism. In [4] a 'complete' LKF, depending on two delay Lyapunov like matrices, is constructed whose derivative along the trajectories depend on the state and its derivative which allows a less conservative treatment of the delay perturbation.

In this contribution, inspired in [11], [4], and [2], we enlarge the class of functionals by adding the functionals whose time derivative includes a given derivative term and functionals which correspond to the perturbed system. It is worth to mention, that the construction of the new proposed functional depends only on the delay Lyapunov matrix. The new complete LKF is used to obtain delay-dependent robust stability conditions for TDSs arising from NCSs. The paper is organized as follows: the problem statement is presented in Section II. Because of their key role in obtaining the sufficient robust stability conditions, some basic results concerning the quadratic LKF of complete type are recalled in Section III and also a new LKF is constructed. In Section IV we show how the new functional of complete type is used for the robust stability analysis of the system with uncertain time-varying delay. The main result of the contribution is illustrated with an example. In Section V some concluding remarks end the contribution.

## 2 Problem Statement

In this work we consider a simple NCS setup shown in Fig. 1 with "initial" and "causal" delays $\tau_a, \tau_b$. By considering lumped delays a simple delayed model of the linear NCS is (see [18] for more details)

$$\dot{x}(t) = Ax(t) + Bu(t - \tau_a - \tau_b), \quad u(t) = Kx(t), \tag{1}$$

where $x(t) \in \mathbb{R}^n$ is the state variable, $u(t) \in \mathbb{R}^m$ is a control input vector; $A \in \mathbb{R}^{n\times n}$, and $B \in \mathbb{R}^{n\times m}$ are known real constant matrices. The corresponding closed-loop system has the following TDS with time-varying state form:

$$\dot{x}(t) = A_0x(t) + A_1x(t - \tau(t)), \quad x(t) = \varphi(t), \quad t \in [-\bar{h}, 0], \tag{2}$$

where $x(t) \in \mathbb{R}^n$ is the system state at time $t$, $t \geq 0$; $A_0 = A$, $A_1 = BK$ are known constant real matrices with appropriate dimensions, $\varphi$ is a continuously differentiable vector-valued initial function and $\bar{h}$ is an upper-bound on the time delay $\tau(\cdot)$. The state $x_t$ is defined by $x_t(\theta) = x(t + \theta)$ for $\theta \in [-\bar{h}, 0]$. The uncertain delay $\tau(t)$ is supposed to

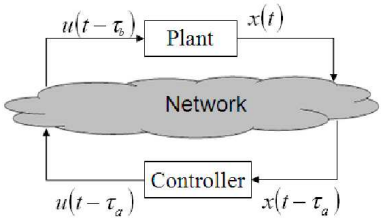


**Fig. 1.** A simple NCS with delays.

have the form $\tau(t) = h + \eta(t)$, where $h > 0$ is a nominal constant value and $\eta(\cdot)$ is a time-varying perturbation. We assume that $\eta(t)$ is a *sign-varying* piecewise continuous function satisfying

$$|\eta(t)| \leq \mu \leq h, \tag{3}$$

with known upper-bound $\mu$, i.e. $\tau \in [h - \mu, h + \mu]$. We consider the following assumption:

**A1** Given the constant nominal value of the delay $h > 0$, the nominal TDS

$$\dot{x}(t) = A_0x(t) + A_1x(t - h), \tag{4}$$

is exponentially stable.

*Problem 1.* Determine the value of $\mu$ for which the uncertain TDS with time-varying state (2) remains stable provided that the nominal system (4) is exponentially stable.

## 3 Preliminaries

As suggested in [4] we consider the following form of LKF:

$$v = v_n + v_a, \tag{5}$$

where $v_n$ is a nominal complete LKF which corresponds to the necessary and sufficient conditions for stability of the nominal system (4) and $v_a$ consists of additional terms and depends on $\mu$ and $v_a \to 0$ for $\mu \to 0$. Therefore, for $\mu \to 0$ $v \to v_n$. The latter will guarantee that if the conditions for the stability of the nominal system are feasible, then the stability conditions for the perturbed system will be feasible for small enough $\mu$.

The LKFs of complete type are such that their derivative along the solutions of the system is more substantial than a quadratic form of the state, allowing to prove that they admit a quadratic lower bound [11]. Under assumption **A1**, given a continuous initial function $\varphi(\theta)$ in $\theta \in [-h, 0]$, there exists a nominal complete LKF [11] of the form

$$v_0(x_t, W) = x^T(t)U(0)x(t) + 2x^T(t)\int_{-h}^{0} U(-h-\theta)A_1 x(t+\theta)d\theta + \int_{-h}^{0}\int_{-h}^{0} x^T(t+\theta_2)A_1^T$$
$$\times U(\theta_2-\theta_1)A_1 x(t+\theta_1)d\theta_1 d\theta_2 + \int_{-h}^{0} x^T(t+\theta)\left[W_1 + (h_1+\theta)W_2\right]x(t+\theta)d\theta, \tag{6}$$

whose time derivative along nominal system (4) is $\frac{d}{dt}v_0(x_t)\Big|_{(4)} = -w_0(x_t)$, where

$$w_0(x_t) = x^T(t)W_0x(t) + x^T(t-h)W_1x(t-h) + \int_{-h}^{0} x^T(t+\theta)W_2x(t+\theta)d\theta, \tag{7}$$

and $W = W_0 + W_1 + hW_2$.

Observe that functional (6) is defined by the matrix valued function $U(\cdot)$ known as delay Lyapunov matrix. This matrix is as important for the functionals, as the classical Lyapunov matrix is for the quadratic Lyapunov functions in the case of delay free systems. Also note that the derivative of the LKF (7) depends on the complete state of the system.

**Definition 1.** *[9] The $n \times n$ matrix $U(s)$ is a delay Lyapunov matrix of system* (4) *associated with a symmetric matrix $W$ if it satisfies the properties:*

$$U'(s) = U(s)A_0 + U(s-h)A_1, \quad s \geq 0, \tag{8}$$

$$U(-s) = U^T(s), \quad s \geq 0, \tag{9}$$

$$-W = U(0)A_0 + A_0^T U(0) + U(-h)A_1 + A_1^T U(h). \tag{10}$$

The existence and uniqueness issues of the delay Lyapunov matrix are investigated in [9, 8]. With the choice of $W = W_0 + W_1 + hW_2$ we can obtain a delay Lyapunov matrix $U(\cdot)$ as the solution of Eq. (8) satisfying conditions (9) and (10), which can be used for

the construction of the LKF (6). The functional (6) is said to be of complete type if matrices $W_i$, $i = 0,1,2$, are positive definite.

In order to treat effectively the fast-varying delay it is necessary that the derivative along trajectories of the involved functionals present quadratic derivative terms. Then in the following subsection we construct a new LKF whose derivative along trajectories of the nominal system (4) presents quadratic derivative terms. The construction of the new LKF unlike the one presented in [4] depends only in the delay Lyapunov matrix, see Definition 1.

### 3.1 A New LKF for The Nominal TDS

A broader class of functionals can be useful for achieving less conservative delay-dependent stability conditions for uncertain non-small delays. We look now for functionals of complete type that along with the nominal system (4) satisfy

$$\dot{v}_n(x_t) = -w_n(x_t), \tag{11}$$

with $w_n(x_t) = w_0(x_t) + \bar{w}_n(x_t)$, where $w_0(\cdot)$ is defined in (7) and

$$\bar{w}_n(x_t) = \dot{x}^T(t)Z\dot{x}(t) + x^T(t)ZA_0\dot{x}(t) + \dot{x}^T(t)A_0^TZx(t).$$

We assume that the matrix $Z$ is symmetric and such that

$$\begin{bmatrix} W_0 + A_0^TZA_0 + ZA_0A_0 + A_0^TA_0^TZ & A_0^TZA_1 + ZA_0A_1 \\ A_1^TZA_0 + A_1^TA_0^TZ & W_1 + A_1^TZA_1 \end{bmatrix} > 0. \tag{12}$$

Substituting into $\bar{w}_n(x_t)$, $A_1x(t-h)$ by $\dot{x}(t) - A_0x(t)$ and considering the nominal system (4), we find that

$$\bar{w}_n(x_t) = -x^T(t)A_0^TZA_0x(t) + x^T(t-h)A_1^TZA_1x(t-h) + \frac{d}{dt}x^T(t)(A_0^TZ + ZA_0)x(t).$$

Next, by assumption **A1** the integration from 0 to $\infty$ of expression (11) gives

$$v_n(x_t) = -x^T(t)[A_0^TZ + ZA_0]x(t) + \int_0^\infty x^T(t)[W_0 - A_0^TZA_0]x(t)dt$$
$$+ \int_0^\infty x^T(t-h)[W_1 + A_1^TZA_1]x(t-h)dt + \int_0^\infty \int_{-h}^0 x^T(t+\theta)W_2x(t+\theta)d\theta dt.$$

If we define

$$W = W_0 + W_1 + hW_2 - A_0^TZA_0 + A_1^TZA_1, \tag{13}$$

we can obtain a LKF constructed with delay Lyapunov matrix $U(\cdot)$ associated with matrix (13). The functional $v_n(x_t, W)$ is of the form

$$\begin{aligned} v_n(x_t,W) =& x^T(t)[U(0) - A_0^T Z - ZA_0]x(t) + 2x^T(t)\int_{-h}^{0} U(-h-\theta)A_1 x(t+\theta)d\theta \\ &+ \int_{-h}^{0}\int_{-h}^{0} x^T(t+\theta_2)A_1^T U(\theta_2-\theta_1)A_1 x(t+\theta_1)d\theta_1 d\theta_2 \\ &+ \int_{-h}^{0} x^T(t+\theta)\left[W_1 + A_1^T Z A_1 + (h+\theta)W_2\right]x(t+\theta)d\theta. \end{aligned} \tag{14}$$

Observe that the new LKF (14) depends only in the delay Lyapunov matrix, see Definition 1. Also note that it preserves the structure of the nominal functional (6).

## 4 Robust Stability Analysis

In this section, for the robust stability analysis of the perturbed system (2) the nominal system (4) is assumed to be stable. We derive the values $\mu$ for which system (2) remains asymptotically stable for all perturbation values $\eta(t)$ satisfying (3). To obtain such bounds following [10], for $t \geq 0$, we represent the perturbed system in the form

$$\dot{x}(t) = A_0 x(t) + A_1 x(t-h) - A_1 \int_{t-h-\eta(t)}^{t-h} \dot{x}(s)ds. \tag{15}$$

We consider the LKF (5), $v = v_n + v_a$, where $v_n$ is the new complete LKF (14) and $v_a$ is the LKF which corresponds to the uncertainty

$$\begin{aligned} v_a(x_t) =& \mu \int_{t-h}^{t} x^T(s)Sx(s)ds + \int_{-\mu}^{\mu}\int_{t+\theta-h}^{t} \dot{x}^T(s)R\dot{x}(s)dsd\theta \\ &+ \mu r \int_{-h}^{0}\int_{t+\theta}^{t} x^T(s)A_1^T U(\theta+h)U^T(\theta+h)A_1 x(s)dsd\theta, \end{aligned} \tag{16}$$

with $S$, $R$, are $n \times n$ positive matrices and $r$ a positive scalar. Observe that $v \to v_n$ when $\mu \to 0$.

Then, by using only the delay Lyapunov matrix properties (8)-(10), the time derivative of (5) along the trajectories of the perturbed system (15) is obtained. First, for the new LKF (14) by straightforward computation we obtain that $\dot{v}_n(x_t, W) = -w_n(x_t) + \Delta$, where

$$\Delta = -2\left[A_1 \int_{t-h-\eta(t)}^{t-h} \dot{x}(s)ds\right]^T \left[\left[U(0) - A_0^T Z - ZA_0\right]x(t) + \int_{-h}^{0} U^T(h+\theta)A_1 x(t+\theta)d\theta\right].$$

Considering the perturbed system (15), $\dot{v}_n(\cdot)$ is rewritten as

$$\dot{v}_n(x_t) = -w_0(x_t) - \dot{x}^T(t)Z\dot{x}(t) - 2x^T(t)ZA_0\dot{x}(t) - 2\left[A_1 \int_{t-h-\eta(t)}^{t-h} \dot{x}(s)ds\right]^T$$
$$\times\left[\Big[U(0) - ZA_0\Big]x(t) + Z\dot{x}(t) + \int_{-h}^{0} U^T(h+\theta)A_1x(t+\theta)d\theta + \frac{1}{2}ZA_1 \int_{t-h-\eta(t)}^{t-h} \dot{x}(s)ds\right].$$

Next, we calculate the derivative of the functional $v_a(x_t)$ along the trajectories of the perturbed system (15):

$$\dot{v}_a(x_t) = \mu x^T(t)Sx(t) - \mu x^T(t-h)Sx(t-h) + 2\mu\dot{x}^T(t)R\dot{x}(t) - \int_{t-h-\mu}^{t-h+\mu} x^T(s)R\dot{x}(s)ds$$
$$+ \mu r x^T(t)A_1^T\mathscr{U}A_1x(t) - \mu r\int_{-h}^{0} x^T(t+\theta)A_1^TU(\theta+h)U^T(\theta+h)A_1x(t+\theta)d\theta,$$

where

$$\mathscr{U} = \int_{-h}^{0} U(\theta+h)U^T(\theta+h)d\theta. \tag{17}$$

Applying the Jensen integral inequality [5], we obtain the following estimations:

$$\int_{t-h-\mu}^{t-h+\mu} \dot{x}^T(s)R\dot{x}(s)ds \geq \int_{t-h-\eta(t)}^{t-h} \dot{x}^T(s)R\dot{x}(s)ds \geq \frac{1}{\mu}\int_{t-h-\eta(t)}^{t-h} \dot{x}^T(s)ds R \int_{t-h-\eta(t)}^{t-h} \dot{x}(s)ds,$$

$$\int_{-h}^{0} x^T(t+\theta)A_1^TU(\theta+h)U^T(\theta+h)A_1x(t+\theta)d\theta$$
$$\geq \frac{1}{h}\int_{-h}^{0} x^T(t+\theta)A_1^TU(\theta+h)d\theta \int_{-h}^{0} U^T(\theta+h)A_1x(t+\theta)d\theta.$$

It is a fact that the use of free-weighting matrices reduce more the conservatism of the delay-dependent stability conditions [6]. Then we insert into $\dot{v}(x_t)$ negative quadratic terms, depending on $\dot{x}(t)$ by adding the following zero term:

$$\delta = 2\left[-\dot{x}(t) + A_0x(t) + A_1x(t-h) - A_1 \int_{t-h-\eta(t)}^{t-h} \dot{x}(s)ds\right]^T \Big[N_1x(t) + N_2\dot{x}(t)\Big] = 0,$$

where $N_1$ and $N_2$ are free $n \times n$ matrices.

Considering the previous estimations and inserting the zero term $\delta$, the time derivative of the LKF (5) admits the following estimation:

$$\dot{v}(x_t) \leq \zeta^T \Phi \zeta,$$

where

$$\zeta^T = \left[ x^T(t)\ \dot{x}^T(t)\ \frac{1}{\mu} \int_{t-h-\eta(t)}^{t-h} \dot{x}^T(s)ds\ \int_{-h}^{0} x^T(t+\theta)A_1^T U(\theta+h)d\theta\ x^T(t-h) \right]$$

and

$$\Phi = \begin{bmatrix} \phi_{11} & \phi_{12} & \phi_{13} & \phi_{14} & \phi_{15} \\ * & \phi_{22} & \phi_{23} & \phi_{24} & \phi_{25} \\ * & * & \phi_{33} & \phi_{34} & \phi_{35} \\ * & * & * & \phi_{44} & \phi_{45} \\ * & * & * & * & \phi_{55} \end{bmatrix}, \tag{18}$$

here $\phi_{11} = -W_0 + A_0^T N_1 + N_1^T A_0 + \mu r A_1^T \mathscr{U} A_1 + \mu S$, $\phi_{12} = A_0^T N_2 - N_1^T - Z A_0$, $\phi_{13} = -\mu \left[ U(0) - Z A_0 + N_1 \right]^T A_1$, $\phi_{14} = 0$, $\phi_{15} = N_1^T A_1$, $\phi_{22} = -Z - N_2 - N_2^T + 2\mu R$, $\phi_{23} = -\mu \left[ Z + N_2 \right]^T A_1$, $\phi_{24} = 0$, $\phi_{25} = N_2^T A_1$, $\phi_{33} = -\mu R - \mu^2 A_1^T Z A_1$, $\phi_{34} = -\mu A_1^T$, $\phi_{35} = 0$, $\phi_{44} = -\frac{\mu r}{h} I_{n\times n}$, $\phi_{45} = 0$, $\phi_{55} = -W_1 - \mu S$, hereafter $*$ stands for symmetric elements of the symmetric matrix. We have proved the following result which solves Problem 1.

**Theorem 1.** *Assume that the nominal TDS* (4) *satisfies* ***A1****. Given $n \times n$-positive definite matrices $W_i$, $i = 0, 1, 2$. Let $Z$ be defined by* (12)*, $U(\cdot)$ be defined by* (8)-(10) *with $W$ satisfying* (13)*, and $\mathscr{U}$ be defined by* (17)*. Then, the uncertain system* (15) *is asymptotically stable for a continuous time-varying function $|\eta(t)| < \mu$ if there exist $n \times n$-matrices $N_1$, $N_2$, and $n \times n$-positive definite matrices $R$ and $S$, and a positive scalar $r$ such that the LMI: $\Phi < 0$ holds, where $\Phi$ is that of* (18)*.*

### 4.1 A Benchmark Comparison

In this subsection, the combination of functionals with prescribed time derivative including quadratic derivative terms, the functionals corresponding to the uncertainty and the free weighting matrices is discussed. In the contribution [2], it should be noted that functional $v_a$ does not vanish when $\mu \to 0$. The LMI condition is similar to the one here obtained. In the contribution [2], the free matrix $N2$ is necessary in order to guarantee the negativity of the corresponding LMI for any upper-bound $\mu$. This fact is evidenced in element $\phi_{22}$. This gives sense to the introduction of the derivative quadratic term $-\dot{x}(t)Z\dot{x}(t)$ in the derivative of the proposed LKF (14). Additional benefits are obtained with the use of the past state $x(t-h)$ in the derivative of the LKF (14) as can be appreciated in element $\phi_{55}$.

For [4], firstly it should be noted that a little error is committed when the derivative of the nominal LKF along the perturbed system is calculated. Considering the nominal complete LKF $V_n$ (equation (19)) proposed in [4] and the system with uncertain delay (15), the correct derivative of the LKF along the perturbed system is

$$\dot{V}_n(x_t) = -x^T(t)\tilde{W}_0 x(t) - \dot{x}^T(t)\tilde{W}_1 \dot{x}(t) + \tilde{\Delta}, \tag{19}$$

where $\tilde{\Delta} = -2\left[A_1 \int_{t-h-\eta(t)}^{t-h} \dot{x}(s)ds\right]^T \left[\tilde{U}(0)x(t) + \tilde{W}_1\dot{x}(t) + \int_{-h}^{0} Q^T(h+\theta)A_1x(t+\theta)d\theta + \frac{1}{2}\tilde{W}_1A_1 \int_{t-h-\eta(t)}^{t-h} \dot{x}(s)ds\right]$. Here matrices $\tilde{U}(\cdot)$ and $Q(\cdot)$ are defined by (20a) and (29b) in [4], respectively. It is worth to mention that matrix $\tilde{U}(\theta) = \tilde{U}_0(\theta) + \tilde{U}_1(\theta)$ is defined in terms of a nominal delay Lyapunov matrix $\tilde{U}_0(\theta)$ and on a matrix satisfying an algebraic expression $\tilde{U}_1(\theta) = A_0^T X(\theta)A_0 + A_1^T X(\theta+h)A_0 + A_0^T X(\theta-h)A_1 + A_1^T X(\theta)A_1$ and $X(\theta) = \int_0^{\infty} K^T(t)W_1K(t+\theta)d\theta$. $K(\cdot)$ is the fundamental matrix for system (4). It should be pointed out that the key of the construction of the LKF proposed in [4] resides in the matrix $\tilde{U}_0(\theta)$. This is the principal difference with our contribution, the construction of the new LKF (14) just depends on a delay Lyapunov matrix $U(x_t, W)$ defined by (8)-(10) with $W$ satisfying (13). The cost for construct the new complete LKF (14) in a simple fashion is the introduction of cross terms in the derivative of the form $x^T(t)ZA_0\dot{x}(t)$. This will result in conservative estimation of upper-bound $\mu$ but marginal compared with the stability criteria if the same technique is applied to the LKF proposed in [4].

*Example 1.* Consider the system:

$$\dot{x}(t) = \begin{pmatrix} 0 & 1 \\ -1 & -2 \end{pmatrix} x(t) + \begin{pmatrix} 0 & 0 \\ -1 & 1 \end{pmatrix} x(t-\tau(t)). \tag{20}$$

For $\tau(t) = h + \eta(t)$, where $h = 1$ and $\eta(t)$ is a *sign-varying* piecewise continuous function satisfying $|\eta(t)| \leq \mu$.

With $W_0 = 1I$, $W_1 = W_2 = 0.0001I$, by applying Theorem 1 we find that for $\mu = 0.11$ the LMI involved is feasible. Hence, the system with uncertain non-small delay $\tau(t) = 1 + \eta(t)$ with $|\eta(t)| \leq 0.11$ is asymptotically stable. This upper-bound is the same as the one obtained with the LKF proposed in [4] with the correct derivative (19) and following the majorization procedure presented there. Following [2] with $W_0 = 1I$, $W_1 = W_2 = 0$ we find $\mu = 0.049$.

With $W_0 = 1.5I$, $W_1 = 0.0001I$, $W_2 = W_1$ we get from (12) that

$$Z = \begin{bmatrix} 1.6662 & 0.7424 \\ 0.7424 & 0.8237 \end{bmatrix}.$$

With $W = W_0 + W_1 + h_1W_2 - A_0^T ZA_0 + A_1^T ZA_1$, following a semi-analytic procedure we obtain

$$U(0) = \begin{bmatrix} 5.8238 & 1.1312 \\ 1.1312 & 0.9164 \end{bmatrix} \text{ and } \mathscr{U} = \begin{bmatrix} 28.2404 & 3.6132 \\ 3.6132 & 0.9188 \end{bmatrix}.$$

Then, by applying Theorem 1 we find that for $\mu = 0.15$ the LMI involved is feasible. Hence, the system with uncertain non-small delay $\tau(t) = 1 + \eta(t)$ with $|\eta(t)| \leq 0.15$ is asymptotically stable. By considering the approach of free weighting matrices applied to the LKF presented in [4] with $\tilde{W}_1 = \tilde{W}_2 = I_{2\times 2}$ and the additional functional (16) one may find a less conservative bound $\mu = 0.17$.

## 5 Concluding Remarks

In the present contribution a modification of complete LKFs is developed. The new complete LKF is used for the robust stability analysis of TDSs with uncertain fast-varying time delay arising from NCSs. It is evident that the computation of the delay Lyapunov matrices is crucial for a successful application of the quadratic functionals to the analysis of the uncertain time-delay systems. Given matrices $W_0$, $W_1$, and $W_2$, matrices $U(0)$ and $\mathscr{U}$ are used to obtain sufficient stability condition. A numerical example illustrates the design procedure.

## References


1. Fridman, E.: A new Lyapunov technique for robust control of systems with uncertain non-small delay. Jornal of Mathematical Control and Information 23, 165–179 (2006)
2. Fridman, E., Niculescu, S.: On complete Lyapunov-Krasovskii functional techniques for uncertain systems with fast varying delays. Int. Journal of Robust and Nonliear Control 18, 364–374 (2008)
3. Fridman, E., Shaked, U.: A descriptor system approach to $H_\infty$ control of linear time-delay systems. IEEE Trans. Automat. Contr. 47(2), 253–270 (2002)
4. Fridman, E.: Stability of systems with uncertain delays: a new 'complete' Lyapunov-Krasovskii functional. IEEE Trans. Automat. Contr. 51, 885–890 (2006)
5. Gu, K., Kharitonov, V., Chen, J.: Stability of Time-Delay Systems. Boston (2003)
6. He, Y., Wang, Q., L.Xie, C.Lin: Further improvement of free weighting matrices technique for systems with time-varying delay. IEEE Trans. Automat. Contr. 52, 293–299 (2007)
7. Hespanha, J.P., Naghshtabrizi, P., Xu, Y.: A survey of recent results in networked control systems. PROCEEDINGS-IEEE 95(1), 138 (2007)
8. Kharitonov, V.L.: Lyapunov matrices: Existence and uniqueness issues. Automatica 46, 1725–1729 (2010)
9. Kharitonov, V., E.Plischke: Lyapunov matrices for time-delay system. Systems & Control Letters 55, 697–706 (2006)
10. Kharitonov, V., Niculescu, S.: On the stability of linear system with uncertain delay. IEEE Trans. Automat. Contr. 48(1), 127–132 (2003)
11. Kharitonov, V., Zhabko, A.: Lyapunov-Krasovskii approach to the robust stability analysis of time-delay system. Automatica 39, 15–20 (2003)
12. Meng, C., Wang, T., Chou, W., Luan, S., Zhang, Y., Tian, Z.: Remote surgery case: Robot-assisted teleneurosurgery. In: IEEE Int. Conf. Robot. and Auto. (ICRA'04). vol. 1, pp. 819–823 (2004)
13. Moon, Y., Park, P., Kwon, W., Lee, Y.: Delay-dependent robust stabilization of uncertain state-delayed systems. Int. Journal of Control 74(14), 1447–1455 (2001)
14. Ogren, P., Fiorelli, E., Leonard, N.: Coperative control of mobile sensor networks: Adaptive gradient climbing in a distributed environment. IEEE Trans. Automat. Contr. 49(8), 1292–1302 (2004)
15. Seiler, P., Sengupta, R.: Analysis of communication losses in vehicle control problems. In: Proc. 2001 Amer. Contr. Conf. vol. 2, pp. 1491–1496 (2001)
16. Seiler, P., Sengupta, R.: An $H_\infty$ approach to networked control. IEEE Trans. Automat. Contr. 50(3), 356–364 (2005)
17. de Souza, C., Li, X.: Delay-dependent robust $H_\infty$ control of uncertain linear state-delayed system. Automatica 35, 1313–1321 (1999)
18. Sun, J., Jiang, J.P.: Stability of uncertain networked control systems. Procedia Engineering 24, 551–557 (2011)

ISSN 1870-4069

# Botnet Detection using Clustering Algorithms

Francisco Villegas Alejandre, Nareli Cruz Cortés, Eleazar Aguirre Anaya

Instituto Politécnico Nacional,
Centro de Investigación en Computación, Mexico City,
Mexico

b140572@sagitario.cic.ipn.mx,{nareli,eaguirre}@cic.ipn.mx

**Abstract.** In this paper, some clustering techniques are analyzed to compare their ability to detect botnet traffic by selecting features that distinguish connections belonging to or not belonging to a botnet. By considering the history of network's connections, some clustering algorithms are used to derive a set of rules to decide which should be considered as a botnet. Our main contribution is to evaluate different clustering techniques to detect botnets based on their detection rate (true and false positives). The algorithms used are *K-medoids* and *K-means* clustering. Datasets used in this paper were extracted from the repositories ISOT and ISCX. Results on *K-medoids* were better for almost all the experiments than *K-means*.

**Keywords:** Malware detection, botnet, clustering algorithms.

## 1 Introduction

Botnets are a group of infected computers (bots) remotely controlled by a botmaster through a channel Command and Control (C&C). Botnets can be classified as centralized and decentralized. In centralized botnets, bots contact the server C&C to receive instructions. Meanwhile, in decentralized botnets, only one of bot receives the message from C&C server, then this bot is responsible for transmitting the message to other bots, and those bots to more bots, and so on.

Leonard et al. divided the life cycle of the botnet in four phases: training, C&C, attack, and post-attack [6]. During the training phase, the botmaster infects other machines through the Internet, these infected machines now become bots controlled by the botmaster and receive instructions from the botmaster during phase C&C. During the attack, bots perform malicious activities based on the instructions received. During the phase post-attack, some bots could be detected and removed, for this reason, the botmaster analyzes the botnet (occasionally) to detect bots still active.

In this research, an approach based on clustering algorithms to detect botnets at the phase C&C using connections between devices, is presented. Network connections are used to identify the behavior of botnets. A connection network is the traffic between two specific endpoints. The connections are used to organize packages as 5-tuple in the following manner: <source IP address, destination IP address, source port, destination port, protocol>.

This document is organized as follows: in Section 2 some related algorithms to detect botnets are mentioned, in Section 3 the detection process used in this work to detect botnets is mentioned, in Section 4 the different types of experiments carried out are explained, in Section 5 the results of experimentation are mentioned, in Section 6 the conclusions of the paper are mentioned.

## 2 Related Works on Algorithms for Detecting Botnets

Some works related to the algorithms based on connections into time intervals to detect botnets at the phase of C&C, are following:

K. Huseynov et al. [1] performed a comparison between the algorithms *K-means* and *Ant Colony System* to detect decentralized botnets. They used features based on the host, to propose a method able to detect the botnets quickly and accurately. Their results show that the algorithm *K-means* has a better performance than *Ant Colony System*. The algorithm *K-means* obtained 82.1% of detection rate with 2.4% false positives, and the Ant Colony System scored a very low detection rate with 67.8% and high rate of false positives, about 23.5%. The dataset used was ISOT.

S. Garg et al. [2] performed a comparison of three machine learning techniques commonly used for the detection of decentralized botnets: *C4.5*, *Nearest Neighbours*, and *Bayesian Network*. They used features based on connection intervals of time. Additionally, feature selection was executed. They showed the effectiveness of some of the features on the dataset ISOT, the algorithms with the best results were *C4.5* and *Nearest Neighbors*.

Saad et al. [3] performed a comparison among five machine learning techniques for decentralized botnets detection. The results of the experiments based on the dataset ISOT showed that it is possible to detect botnets with high precision during the phase C&C. The classification techniques were: *Support Vector Machine (SVM)*, *Naive Bayes*, *Gaussian Classifier*, *Artificial Neural Network*, and *Nearest Neighbours*, where *SVM* obtained the best detection rate, about 98%.

D. Zhao et al. [4] used the *RepTree* algorithm to detect botnets using the dataset ISOT. The results showed a detection rate of 98.1% for a reduced dataset and 98.3 % for the full set with time windows of 300 seconds (8.58 seconds for training and 29.4 seconds of testing). They analyzed the detection rate and false positives of botnets with various time windows, where the best time window was 300 seconds. Furthermore, they built a server to detect botnets in real time and tested with two centralized botnets: black energy and weasel, obtaining 100% of detection rate.

P. Narang et al. [5], instead of the traditional 5-tuple flow-based detection approach, used a 2-tuple conversation-based approach which is port-oblivious, protocol-oblivious, and it does not require Deep Packet Inspection. They named their detector PeerShark; it also classified different P2P applications like Emule and Utorrent, furthermore, they also detect Storm and Waledac p2p traffic with a detection rate of more than 95%. They executed tests with 3 different algorithms

*Bayesian Network*, *C4.5*, and *Adaboost with Rep trees* to detect the decentralized botnets and the best algorithm was the C4.5. The dataset used was ISOT.

## 3 Proposal

Our proposal consists of the definition of some clusters that defines the limits for a botnet detection strategy. The detection process receives as input a feature vector and a training set. The clustering algorithm receives that training set and the feature vector to generate clusters that define the behavior of the training set, after that, the clusters are transformed into a set of if-then-else rules, that can distinguish between botnets and non-botnets in new datasets (testing sets). Figure 1 refers to the detection process carried out in this research.

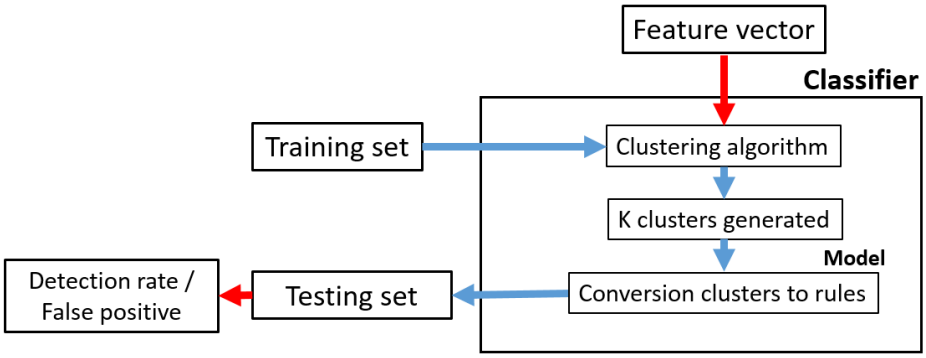


**Fig. 1.** The general idea of the proposed detection process.

### 3.1 Feature Vector

The initial 8-feature vector used in this work is shown in Table 1. The first column refers to the names given to the features and the second column is the description of the features.

### 3.2 Conversion from Clusters to Rules

The clustering algorithm receives the training set and the feature vector to generate clusters that define the behavior of the training set. The training set contains data points representing botnet connections. Each data point contains 8 values representing the feature vector. The clustering algorithm forms groups of data points called clusters. These clusters are converted into rules represented as a vector, where each rule has 8 limits with the lowest value from every feature in all the data points and 8 limits with the highest value from every feature in all the data points.

**Table 1.** Feature vector using connections.

| Name | Description |
|---|---|
| APL | Average payload length per connection |
| MDPS | Number of a different size of packets transferred to a total number of frames per connection |
| Payload | Total number of bytes per connection excluding the header. |
| TPT | Total bytes transmitted per connection |
| Duration | Duration of the connection |
| Flen | Large of the first packet of the connection |
| ToByte | Bytes from origin to destination |
| NPacketsAB | Number of packages from origin to destination |

An example of the conversion from clusters to rules:

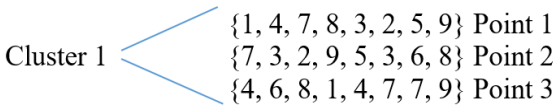


Rule 1 {1-7, 3-6, 2-8, 1-9, 3-5, 2-7, 5-7, 8-9} generated from cluster 1, where the cluster1 contains 3 data points with 8 features. To generate the rule1 from the cluster1, the lowest-highest value is taken from every feature in the data point.

### 3.3 Clasification

Once the rules have been generated, the classification is achieved by applying the rules forming a if-then-else model in a testing set containing botnet and non-botnet connections. The point classified as botnet or non-botnet depends on if it meets the conditions of at least a rule or not.

Being so, if the new point meets the conditions of a rule (where the new point should be between all the limits of the rule) is considered botnet, otherwise is considered a non-botnet.

The if-then-else model is composed as follows:
If any rule is accomplished
    A botnet is detected
Else
    A no botnet is detected
An example of this, where rule1 classify 3 points of a testing set:
Rule 1 {1-7, 3-6, 2-8, 1-9, 3-5, 2-7, 5-7, 8-9}
Testing set containing 3 points:
{2, 4, 7, 8, 3, 2, 5, 9} Point1. Considered as Botnet by rule 1

{0, 4, 7, 8, 3, 2, 5, 9} Point2. Considered as No Botnet by rule 1
{8, 7, 9, 9, 6, 1, 4, 9} Point3. Considered as No Botnet by rule 1

## 4 Experiments

We performed specific experiments, varying the number of clusters to obtain the number of clusters with highest detection rate and lowest false positives for every centralized and decentralized botnet. In our experiments, two datasets were used. hese datasets are:
· ISOT. Which contains decentralized botnets.
· ISCX. Which contains centralized botnets.

In the next subsections, first a description about the datasets used for the experiments are mentioned, then a description of the experiments carried out are mentioned.

### 4.1 Datasets

A description of the two datasets used for the experimentation are mentioned. These datasets contain representative data for centralized and decentralized botnets as well as normal traffic, focusing only on the connections of this traffic. From these datasets the training set, as well as the testing set are extracted. These two datasets are the following:

**ISOT:** This dataset was created by Information Security and Object Technology (ISOT) research laboratory at the University of Victoria [9]. Basically, it is a mixture of many existing datasets (malicious and non-malicious). Malicious traffic in the dataset ISOT were extracted from the French chapter of the Honeynet Project [10] and it includes three different decentralized botnets: Waledac, Storm, and Zeus. In total, the dataset of ISOT contains 14.1 GB of data in pcap format. The description of this dataset is shown in Table 2, in which the first column represents the type of botnet, the second represents the number of connections, and the third column represents the type of botnet.

**Table 2.** Description of dataset ISOT.

| Botnet | Number of connections | Type |
|---|---|---|
| ISOT Storm | 22,888 | Decentralized |
| ISOT Waledac | 34,442 | Decentralized |
| ISOT NO Botnet | 77,586 | NO Botnet |

**ISCX:** This dataset was created by Information Security Centre of Excellence ISCX (ISCX) research laboratory at the University of New Brunswick [7]. It

has been generated in a physical test environment using actual devices that generate traffic (SSH, HTTP, and SMTP). It contains the centralized botnets Neris and RBot. In total, the dataset ISCX contains 5.6GB of data in pcap format. The description of this dataset is shown in Table 3, in which the first column represents the type of botnet, the second represents the number of connections, and the third column represents the type of botnet.

**Table 3.** Description of dataset ISCX.

| Botnet | Number of connections | Type |
|---|---|---|
| ISCX Neris | 33,084 | Centralized |
| ISCX RBot | 34,217 | Centralized |
| ISCX NO Botnet | 76,175 | NO Botnet |

### 4.2 Design of Experiments

To validate our proposal we did four types of experiments, each experiment is repeated four times, varying the parameter number of clusters (rules) in each one (cluster values of 100, 200, 500, 1000). To get the number of the clusters with highest detection rate and lowest false positives in the phase of C&C for a specific botnet, the botnets evaluated were: the decentralized botnets Storm and Waledac are shown in Table 4a and 4b, and the centralized botnet Neris and RBot in Table 4c and 4d.

Furthermore, to perform a comparison of results with the related work, a general experiment called ISOT was performed. The main goal in this experiment is to obtain the detection rate for the decentralized botnets.

The ISOT experiment contains the decentralized botnet Storm and Waledac shown in Table 4e.

The first column of the tables corresponds to the type of botnet in the dataset; the second column to the class or label of data; and the third column the number of connections used for that botnet. The *K-medoids* algorithm was programmed in the Java language and the *K-means* is the one implemented in weka [8].

**Table 4a.** Experiment 1 to detect Storm.

| Botnet | Class | Connections |
|---|---|---|
| Storm | Storm | 22,888 |
| NO Botnet | No Storm | 22,888 |

**Table 4b.** Experiment 2 to detect Waledac.

| Botnet | Class | Connections |
|---|---|---|
| Waledac | Waledac | 34,442 |
| NO Botnet | No Waledac | 34,442 |

**Table 4c.** Experiment 3 to detect Neris.

| Botnet | Class | Connections |
|---|---|---|
| Neris | Neris | 33,084 |
| NO Botnet | No Neris | 33,084 |

**Table 4d.** Experiment 4 to detect RBot.

| Botnet | Class | Connections |
|---|---|---|
| RBot | RBot | 34,217 |
| NO Botnet | No RBot | 34,217 |

**Table 4e.** General experiment for ISOT.

| Botnet | Class | Connections |
|---|---|---|
| Storm | Botnet | 22,888 |
| Waledac | Botnet | 34,442 |
| NO Botnet | No Botnet | 77,586 |

## 5 Results

*K-means* and *K-medoids* algorithms were used for clustering. These two algorithms were chosen, influenced by state of art in clustering algorithms, due to their popularity. Some other clustering algorithms can be used. The state of art obtained better results.

Two values were used to evaluate the clustering algorithms: false positives, and detection rate.

The results of the specific experiments are illustrated in the Figures 2a, 3a, 4a, 5a for the detection rate obtained with that number of clusters (rules) for each botnet, and the figures 2b, 3b, 4b, 5b for the false positives according to the detection rate obtained with that number of rules for each botnets. The results of the general experiment ISOT are illustrated in the Figures 6a and 6b, for the detection rate and false positives respectively. These figures show detection rate and false positives for both clustering algorithms *K-means* and *K-medoids*, varying the number of rules parameter. Results are better when the detection rate is higher and the false positives are lower, an opposite correlation between detecion rate and false positives. To obtain the best correlation between detection rate and false positives, maintaining the detection rate as high as possible and the false positives as low as possible.

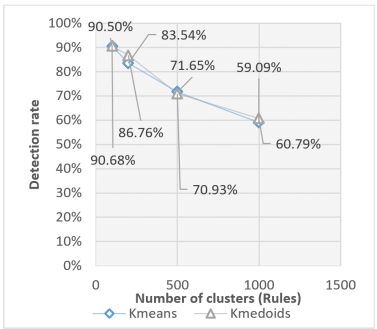


**Fig. 2a.** Detection rate for Storm.

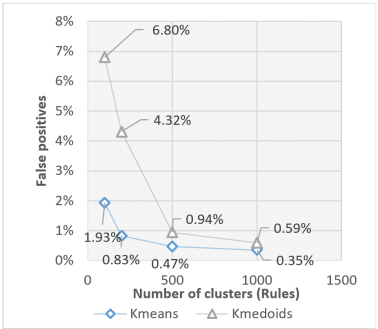


**Fig. 2b.** False positives for Storm.

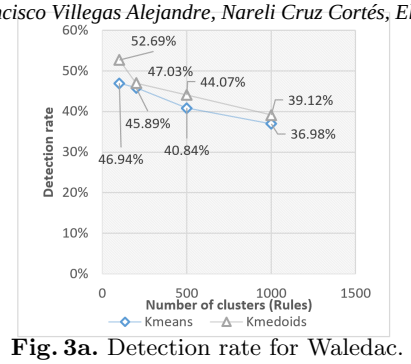


**Fig. 3a.** Detection rate for Waledac.

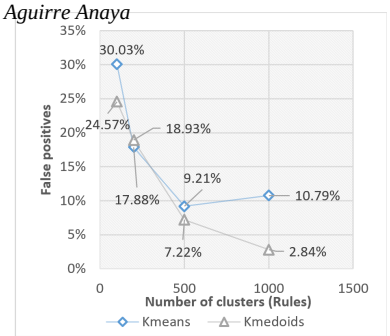


**Fig. 3b.** False positives for Waledac.

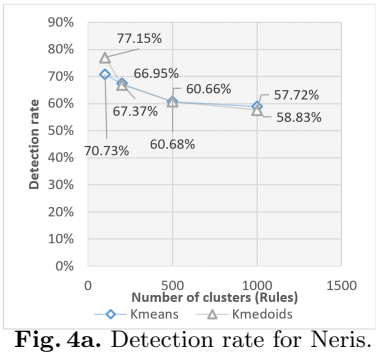


**Fig. 4a.** Detection rate for Neris.

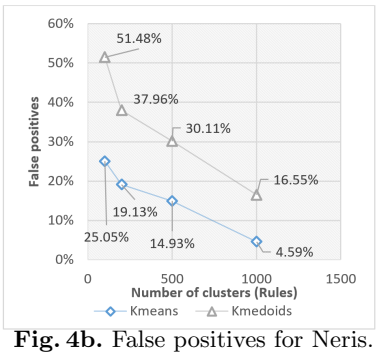


**Fig. 4b.** False positives for Neris.

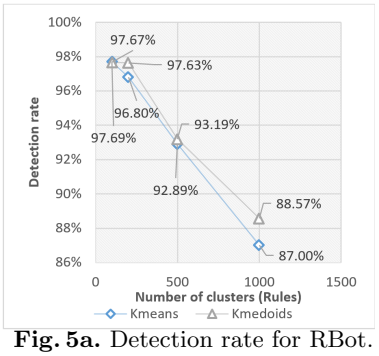


**Fig. 5a.** Detection rate for RBot.

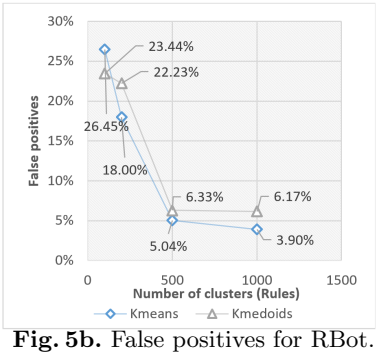


**Fig. 5b.** False positives for RBot.

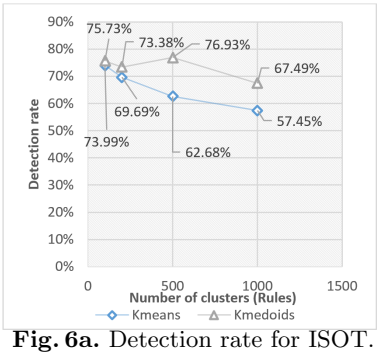


**Fig. 6a.** Detection rate for ISOT.

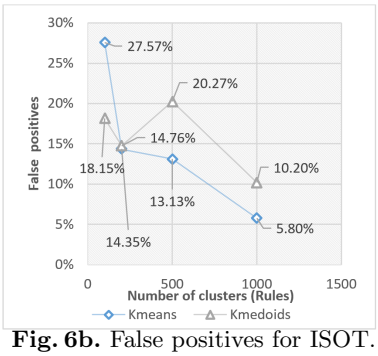


**Fig. 6b.** False positives for ISOT.

**Comparison of Results:** In Table 5, a comparison of results with the related work is shown. The table shows the reference to the related work in its first column; the second column the algorithms used; the third column is the dataset used; in the fourth and fifth column the detection rate and false positives.

**Table 5.** Comparison of results.

| Reference | Algorithm | Dataset | Detection rate | False positives |
|---|---|---|---|---|
| K. Huseynov [1] | *K-Means* | ISOT | 82.1% | 2.4% |
| K. Huseynov [1] | *Ant Colony System* | ISOT | 67.8% | 23.5% |
| S. Saad [3] | *SVM* | ISOT | 97.8% | 5.1% |
| D. Zhao [4] | *RepTree* | ISOT | 98.3% | 0.01% |
| P. Narang [5] | *C4.5* | ISOT | 98.7% | 0.04% |
| This research | *K-means* | ISOT | 69.99% | 14.35% |
| | *K-medoids* | ISOT | 73.37% | 14.76% |

The *K-means* algorithm and *K-medoids* show almost similar results. The number of clusters (rules) with high detection rate, but low false positives are 500 in average. The *K-means* algorithm got better results for the bot neris with a detection rate of 57.72% and false positives 4.59% with 1000 clusters, and for the bot storm with 90.68% detection rate and false positives of 1.93% with 100 clusters than the algorithm *K-medoids*. On the other hand, the algorithm *K-medoids* got better results for the bot rbot with a detection rate of 93.19% and false positives of 6.33% with 500 clusters. Furthermore, for the bot waledac with 44.07% and false positives 7.22% with 500 clusters than *K-means*, this is because they have a better correlation between detection rate and false positives.

The algorithm *K-medoids* obtained better results in the general experiment ISOT with 73.33% detection rate and 14.76% false positives. The algorithm *K-means* obtained 69.99% detection rate and 14.35% false positives. The clusters (rules) with better correlation in the general experiment were 200.

The comparative of results in Table 5 show that our proposal obtained worst results than K. Huseynov [1], S. Saad [3], D. Zhao [4], and P. Narang [5] with the algorithms *K-means*, *SVM*, *RepTree*, and *C4.5*. On the other hand, our proposal obtained better results than K. Huseynov [1] with the *Ant Colony System* algorithm.

Perhaps the comparisons are not so fortunate for the results of the proposed method and may be because they have used different basis of features, the next phase of experimentation would force to consider tests on the exact base of features that each method in the state of the art uses generating and confronting a pair of results to confirm or discard clustering as a strategy for the detection of botnets.

## 6 Conclusions

In this work, two clustering algorithms were evaluated for the formation of rules to detect botnets via network connections. In this study the detection rate and false positives of different types of botnets were evaluated, our proposed method is allowed to detect the botnets in the phase of C&C accurately for some botnets by generating rules.

Based on the results we can conclude that the *K-means* algorithm is better to detect Neris and Storm than *K-medoids*. The *K-medoids* algorithm is better for detecting Rbot, Waledac, and the general experiment with decentralized botnets (Storm and Waledac) than *K-means*. These algorithms detect the botnets accurately for Storm and RBot with detection rate over 90% and false positives under 7% with a very low number of clusters (rules) 500 in average. Our main objective was accomplished partially because the algorithm *K-medoids* has better results only for 2 botnets and for the general experiment. This means that the *K-medoids* can be used as an alternative to *K-means* algorithm only for these types of experiments. Therefore, evaluation of other clustering algorithms is needed to achieve this objective.

Our results can be improved with another technique of detection. Furthermore, the results can be improved with a method of feature selection, this is the purpose of our future work.

**Acknowledgment.** The authors would like to thank to the *Instituto Politécnico Nacional* (IPN), the *Centro de Investigación en Computación* (CIC), and the *Consejo Nacional de Ciencía y Tecnología* (CONACYT) for the support in this research.

## References

1. Huseynov, K., Kim, K., Yoo, P.: Semi-supervised Botnet Detection Using Ant Colony System. In: 31th Symposium on Cryptography and Information Security, Kagoshima, Japan, Jan. 21-24 (2014)
2. Garg, S., Singh, A., Sarje, A., Peddoju, S.: Behaviour Analysis of Machine Learning Algorithms for detecting P2P Botnets. Department of Computer Science and Engineering, Indian Institute of Technology, Roorkee, India (2013)
3. Saad, S., Sayed, B., Felix, J., Traore, I., Zhao, D., Ghorbani, A., Ku, W., Hakimian, P.: Detecting P2P botnets through network behavior analysis and machine learning. In: Privacy, Security and Trust (PST), on Ninth Annual International Conference, July 19-21 (2011)
4. Zhao, D., Traore, I., Sayed, B., Lu, W., Saad, S., Ghorbani, A., Garan, D.: Botnet detection based on traffic behavior analysis and flow intervals. In: 27th IFIP International Information Security Conference (2013)
5. Narang, P., Ray, S., Hota, C., Venkatakrishnan, V.: PeerShark: Detecting Peer-to-Peer Botnets by Tracking Conversations. In: IEEE Security and Privacy Workshops (SPW), San Jose, CA, May 17-18 (2014)

6. Leonard, J., Xu, S., Sandhu, R.: A Framework for Understanding Botnets. In: Proceedings of the International Workshop on Advances in Information Security (WAIS at ARES), Fukuoka, Japan, Fukuoka Institute of Technology, March 16-19 (2009)
7. Shiravi, A., Shiravi, H., Tavallaee, M., Ghorbani, A.A.: Toward developing a systematic approach to generate benchmark datasets for intrusion detection. IComputers & Security, vol. 31, no. 3, pp. 357–374 (May 2012)
8. Ian, E., Witten, H., Trigg, L., Hall, M., Holmes, G., Cunningham, S.: Weka: Practical Machine Learning Tools and Techniques with Java Implementations (1999)
9. Information security and object technology (ISOT) research lab, ISOT Botnet dataset, University of Victoria, obtained from: http://www.uvic.ca/engineering/ece/isot/datasets/index.php
10. The Honeynet Project, French Chapter of Honeynet, obtained from: http://www.honeynet.org/chapters/france
11. Szab'o, G., Orincsay, D., Malomsoky, S., Szab'o, I.: On the validation of traffic classification algorithms. In: Proceedings of the 9th international conference on Passive and active network measurement (PAM'08), Berlin, Heidelberg, pp. 72–81, Springer-Verlag, (2008)
12. LBNL and ICSI, LBNL Enterprise Trace Repository, obtained from: http://www.icir.org/enterprise-tracing.

ISSN 1870-4069

# System Identification of a Quad-rotor in X Configuration from Experimental Data

Victor Manuel Aboytes Reséndiz, Edgar Rivas Araiza

Universidad Autónoma de Querétaro, Querétaro, Mexico

victoraboytes@outlook.com

**Abstract.** Quad-rotors have been a very popular topic for research in the current literature because of its capability to perform different tasks autonomously. This paper focuses on the modeling of a quad-rotor aircraft dynamics based on experimental data. It will be demonstrated that a linear model could represent its dynamics despite of quadrotor's strong nonlinearities. Also, it will be shown how a quad-rotor aircraft system works, its typical mathematical model according with literature and a brief history of Unmanned Aerial Vehicles.

**Keywords:** Quadrotor, system identification, modeling, linear model.

## 1 Introduction

Technology has been evolving through the years and has given us the possibility to build and create complex machines. We are witnessing the new era of robots, where the use of quad-rotor machines, known as drones, in our daily lives has been on the increase. Thanks to technology, these aircrafts can handle many tasks autonomously in natural and man-made environments. Therefore, strong knowledge in the areas of electronics, control, and mechanics is important to understand the behavior of these aerial robotic systems.

### 1.1 A Brief History of UAVs

Contrary to many people's belief, drones or Unmanned Aerial Vehicles [1] (UAVs) are not a recent invention, going back a few decades. The UAVs have a rich history that goes back many years back and as a result of this, the human kind can use and explore the many possibilities that these rotorcrafts offer us.

The idea of building flying machines was first conceived around 2,500 years ago in ancient Greece and China. According to [2], the first known autonomous flying machine has been credited to Archytas from the city of Tarantas in southern Italy, also known as Archytas the Tarantine. In the same era, in China, in about 400 BC, the first document that showed the idea of a vertical flight aircraft was found.

Many centuries later, an aircraft, called aerial screw or air gyroscope [3], capable of hovering was designed by Leonardo Da Vinci in 1483. The first manned

flight took place in 1783 using a hot air balloon designed by the Montgolfier brothers. As a result of these events, several flying machines were designed until the first helicopter was created in 1860s and later the fixed wing aircraft was introduced.

Today UAVs are more complex and reliable than before, thanks to the advancement of technology. Nowadays, aircrafts can manage different tasks [4], such as: inspection of structures, transportation of medical supplies, communication through network for rescue missions, and more.

### 1.2 Related Work

There are several kinds of methods to identify the unknown UAV's parameters considering their dynamics. Measurement of vehicle parameters, such as inertias, lift, and drag coefficients are commonly used to obtain nonlinear models. However, such values are difficult to obtain with a certain level of accuracy. Therefore, scientists have applied different methodologies to acquire UAV's parameters.

Genetic Algorithm (GA) is a globally optimal method for solving optimization problems such as quad-rotors system. Real-coded GA and Distributed Genetic Algorithm (DGA) [5–7] are used to determine the unknown parameters.

Least square method, maximum likelihood estimation, neural network identification, the fuzzy system identification, and wavelet network identification methods are used in identification of model [8,9]. Some examples of these identification methods are: ARX Model is an identification method to determine linear systems [10–12], RBF-ARX Model combine the linear ARX model structure with Radial Basis Function Neural Network (RBF) [13,14] and Fuzzy Modeling which describes the dynamic characteristics of complex and nonlinear dynamics.

### 1.3 Motivation for System Identification

The model of a quad-rotor commonly involves dynamic forces, momentums, and torques produced by the physical aircrafts elements such as propellers, sensing units, motors, airframes, and so on. Here lies the main problem when the rotorcraft's mathematical model is required. Different quad-rotor's elements, as mentioned before, change the dynamics and the parameters of a model and many of those parameters are difficult to obtain in an experiment.

Having an alternative method to obtain the quad-rotors model would improve the process of the design of the control algorithm without affecting the type of propellers, BLDC motors or airframe the aircraft has. This identification method has several advantages:

1. It reduces the amount of time wasted on obtaining the quad-rotor's parameters of the model in an experiment. This costs a lot of work and does not guarantee accuracy and can not detect important dynamics.
2. The algorithm can be used for modeling similar quad-rotor systems with larger or shorter propellers, bigger or smaller motors, different weight of the structure, and so on.

## 2 Quad-rotor

There are different configurations for an aircraft depending on the number of motors. These configurations are: Tricopter, quadcopter, hexacopter, and octocopter. Another difference, beside the number of motors, is the shape of the frame. Therefore, there exists different variations of aircrafts even though the number of motors remains the same. The type of rotorcraft used in this paper is a quad-copter in X configuration.

### 2.1 Quad-rotor Characteristics

The quad-rotor rotorcraft is an aircraft with four rotors in a square. Due to this configuration, it is possible to hover, mover forward, sideward, up, down, and turn about the roll, pitch, and yaw axes separately. The four rotors spin clockwise and counter-clockwise like it is shown in Fig. 1. Clockwise (CW) motors, shown in blue, use normal propellers and counter-clockwise (CCW) motors, shown in red, use pusher propellers.

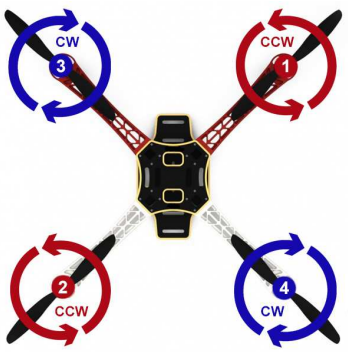


**Fig. 1.** Quad-rotor in X configuration.

This four-rotor aircraft has some advantages over typical helicopter. Due to rotation of the motors (clock and counter-clockwise), gyroscopic effects, and aerodynamic torques tend to cancel in flight.

Throttle input is the sum of the thrust of each motor (motors 1, 2, 3, and 4). This force makes the quad-copter fly. Roll movement is obtained by increasing or reducing the speed of rear motors (motors 2 and 4) and reducing or increasing front motors (motors 3 and 1) respectively. Pitch movement is obtained similarly using lateral motors. Lastly, yaw movement is obtained by increasing or decreasing the speed of the counter-clockwise motors while decreasing or increasing the speed of the clockwise motors. Figure 2 shows the UAV's angles of rotation.

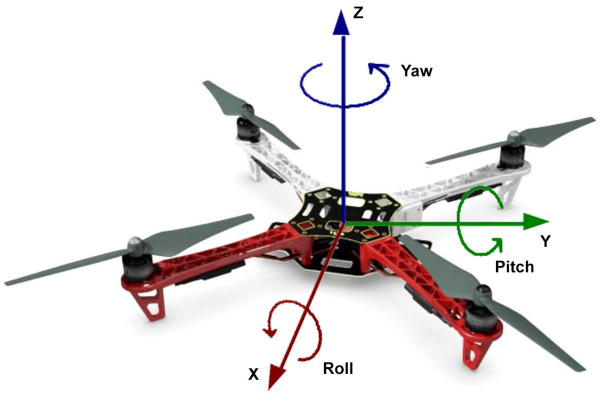


**Fig. 2.** Quad-rotor angles of rotation.

### 2.2 Quad-rotor System

A description of the quad-rotor used for the experiments:

1. Quad-rotor frame: The quad-rotor consist of a rigid body with 4 arms mounted in X configuration. A motor is mounted at the end of each arm.
2. Motors: Each rotor consists of a brushless motor (BLDC) and a propeller. Each of the motors are controlled by Electronic Speed Controllers (ESC). The input of an ESC is a Pulse Width Modulated signal. This signal is measured for the purpose of system identification on later stages.
3. Microcontroller Unit (MCU): A MCU is mounted on the central body of the quad-rotor. The MCU used is the Pixhawk which basically a 32bit STM32F427 Cortex M4 core with FPU. The Pixhawk hardware is integrated with different sensors like: 3-axis accelerometer/gyroscope, magnetometer, and barometer. It has different communication protocols such as: UART, CAN, $I^2C$, SPI. This MCU was selected because it is an open source project and we can design and program our own code using the Pixhawk.

## 3 Quad-rotor Dynamic Model

The dynamic model of the quad-rotor is firstly formulated in this section. Then a model based on experimental data will be obtained.

### 3.1 Rigid Body Dynamics

Quad-rotor's dynamics are represented by two reference frames: earth fixed $O_E$ and body fixed $O_B$ frame. See Fig. 3. $O_E$ is the fixed frame to the earth where $X$ points to the south, $Y$ points to the west, and $Z$ point up. On the other

hand, $O_B$ is the fixed frame of the quad-rotor's body whose $x$, $y$, and $z$ are defined along the axes of the quadcopter. As a consequence 12 variables define the dynamical system of the quad-rotor [15].

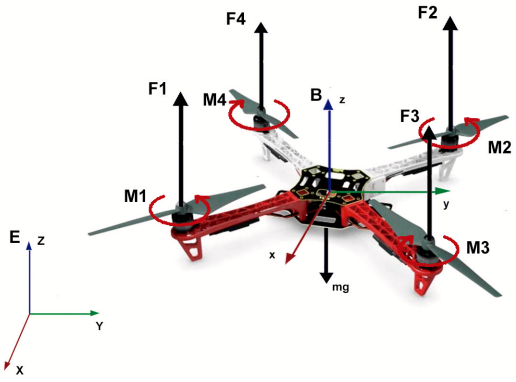


**Fig. 3.** Quad-rotor frame of reference.

1. Six states define the position of the system in the three dimensional space: Cartesian coordinate $(x, y, z)$ points to the center of gravity of the quadcopter and their time derivative $(u, v, w)$ defines the speed of the center of gravity relative to the earth.
2. Six states define the attitude of the system: Euler angles $(\phi, \theta, \psi)$ represent the roll, pitch, and yaw respectively and their time derivatives $(p, q, r)$ describe the rotation of the quad-rotor.

According to Fig. 3, $F_1$,$F_2$, $F_3$, and $F_4$ are the forces applied to the rigid body by the motors. The effect of these forces produces roll angle $(\phi)$, pitch angle $(\theta)$, and yaw angle $(\psi)$. Four control inputs can be defined according to these four forces acting on the quad-rotors rigid body:

$$\begin{aligned} U_1 &= F_1 + F_2 + F_3 + F_4, \\ U_2 &= (F_2 - F_4)l, \\ U_3 &= (F_3 - F_1)l, \\ U_4 &= M_1 + M_2 - M_3 - M_4. \end{aligned} \tag{1}$$

$F_i$ and $M_i$ are the thrust and torque generated by rotor $i$ $(i \in \{1, 2, 3, 4\})$ and $l$ represents the length of the arm from the rotor to the center of mass. In [16]

and [17], the Eq. (1) can be expressed in terms of equations, governing dynamics of the quadrotor as:

$$\begin{aligned}
\ddot{x} &= \frac{U_1}{m}\left(\cos\phi\sin\theta\cos\psi + \sin\phi\sin\psi\right), \\
\ddot{y} &= \frac{U_1}{m}\left(\cos\phi\sin\theta\sin\psi - \sin\phi\cos\psi\right), \\
\ddot{z} &= \frac{U_1}{m}\cos\phi\cos\theta - g, \\
\ddot{\phi} &= \frac{U_2}{I_{xx}} + \dot{\theta}\dot{\psi}\left(\frac{I_{yy} - I_{zz}}{I_{xx}}\right) - \frac{J_R}{I_{xx}}\dot{\theta}\Omega_R, \\
\ddot{\theta} &= \frac{U_3}{I_{yy}} + \dot{\phi}\dot{\psi}\left(\frac{I_{zz} - I_{xx}}{I_{yy}}\right) - \frac{J_R}{I_{yy}}\dot{\phi}\Omega_R, \\
\ddot{\psi} &= \frac{U_4}{I_z z} + \dot{\phi}\dot{\theta}\left(\frac{I_{xx} - I_{yy}}{I_{zz}}\right).
\end{aligned} \tag{2}$$

The position of the center of mass in the inertial coordinate system is $(x, y, z)$; $\phi$, $\theta$, and $\psi$ are the quad-rotor's attitude; $m$, $I_{xx}$, $I_{yy}$, and $I_{zz}$ are the mass and the moments of inertia respectively; $J_R$ and $\Omega_R$ are the moments of inertia and angular velocity of the propeller blades; and $g$ is the gravity.

## 4 Quad-rotor Identification Model from Experimental Data

The quad-rotor system can be treated as MIMO (Multiple Inputs and Multiple Outputs) system. See Fig. 4. The variables of interest are

1. 4 inputs (4 PWM signals),
2. 3 outputs (Euler angles).

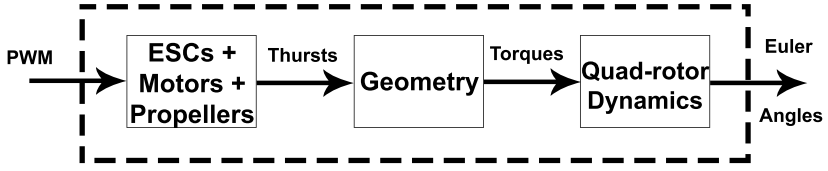


**Fig. 4.** Quad-rotor block diagram.

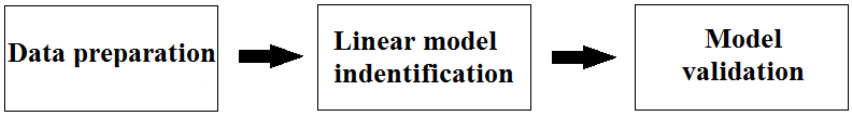


**Fig. 5.** Flow diagram of the system identification.

### 4.1 System Identification Algorithm

The Fig. 5 shows the flow diagram of the identification algorithm. The first step to obtain the model is to prepare the data for system identification. Once the data is obtained from experiments, it has to be imported into Matlab environment. The data has to be represented in time and frequency domains using the iddata function. This function creates an iddata object containing a time-domain output signal $y$ and an input signal $u$. Also, the sample time of the experimental data has to be specified. Then a data selection is done to create independent data sets for estimation and validation.

The second step is to determine which model will be used to represent the linear system. The transfer function model is a numeric model that represents a linear system with fixed numerical coefficients. Those fixed coefficients are the numerator and denominator of the transfer function. For the Matlab System Identification Toolbox, the transfer function model describes the relationship between the inputs and outputs of a dynamic system using a ratio of polynomials.

The transfer function model, in continous time, has the following form:

$$Y(s) = \frac{num(s)}{den(s)}U(s), \tag{3}$$

where $Y(s)$ and $U(s)$ represent the Laplace transforms of the output and input, respectively. The equation (3) represents a single-input single-output (SISO) contionus transfer function. A multi-input multi-output (MIMO) transfer function has $n$ SISO transfer function depending on the input-output system. It has the following form:

$$\begin{aligned} G(s) &= \frac{num(s)}{den(s)}, \\ Y_1(s) &= G_{11}U_1(s) + G_{12}U_2(s) + \ldots + G_{1n}U_n(s), \end{aligned} \tag{4}$$

where $G_{ij}(s)$ is the SISO transfer function between the $i^{th}$ output and $j^{th}$ input. The validation model is the last step to verify the accuracy of the model obtained. The validation data is used to check how the model system behaves and after that, do some refinements if the model requires it.

### 4.2 Obtaining the Models from System Identification

Matlab has a System Identification Toolbox which is used to identify a linear model of the quad-rotor system. Experimental data was obtained and tested to get transfer functions from the roll and pitch axis. The best transfer functions that fit the data are the following:

$$\begin{aligned}
&\text{From input } u_1 \text{ to output } y_1 : \\
&\frac{-2.102 \times 10^{-10}}{\begin{array}{l} s^{11} + 0.4659s^{10} + 0.8069s^9 + 0.2817s^8 + 0.1927s^7 \\ +0.05124s^6 + 0.01715s^5 + 0.003271s^4 + 0.0005535s^3 \\ + 7 \times 10^{-5}s^2 + 4.797 \times 10^{-6}s + 3.605 \times 10^{-7} \end{array}}, \\
&\text{From input } u_2 \text{ to output } y_1 : \\
&\frac{-9.898 \times 10^{-10}}{\begin{array}{l} s^{11} + 0.5932s^{10} + 1.051s^9 + 0.4688s^8 + 0.2964s^7 \\ +0.09754s^6 + 0.03072s^5 + 0.00695s^4 + 0.001157s^3 \\ + 0.0001635s^2 + 1.199 \times 10^{-5}s + 8.575 \times 10^{-7} \end{array}},
\end{aligned} \tag{5}$$

$$\begin{aligned}
&\text{From input } u_3 \text{ to output } y_2 : \\
&\frac{-2.521 \times 10^{-8}}{\begin{array}{l} s^{10} + 0.3857s^9 + 1.114s^8 + 0.3282s^7 + 0.4312s^6 + 0.09092s^5 \\ + 0.069s^4 + 0.009134s^3 + 0.004089s^2 + 0.0002373s + 4.474\times^{-5} \end{array}}, \\
&\text{From input } u_4 \text{ to output } y_2 : \\
&\frac{-2.531 \times 10^{-8}}{\begin{array}{l} s^{10} + 0.3851s^9 + 1.113s^8 + 0.3276s^7 + 0.4306s^6 + 0.09073s^5 \\ + 0.06887s^4 + 0.009111s^3 + 0.004079s^2 + 0.0002366s + 4.476 \times 10^{-5} \end{array}}.
\end{aligned} \tag{6}$$

From Matlab System Identification Toolbox, it is possible to obtain a pair of transfer functions that represent the dynamics of the roll and yaw axis. This model can be used on later stages to design a controller with better performance.

## 5 Results

The dataset obtained was divided in two sized data for both roll and pitch axis. First part was used to find the transfer functions of Eq. (5) and Eq.(6). The second part was used as validation data, in order to validate the model estimated.

### 5.1 Model Validation

The Fig. 6 shows the simulation of the roll and pitch axis from the estimated models respectively. The performance of the estimated models is quite good, although there are some parts in the figure where those models cannot represent the dynamics of the quad-rotor. This behavior is expected because the dynamics models are linear and the quad-rotor dynamics are normally represented by nonlinear models.

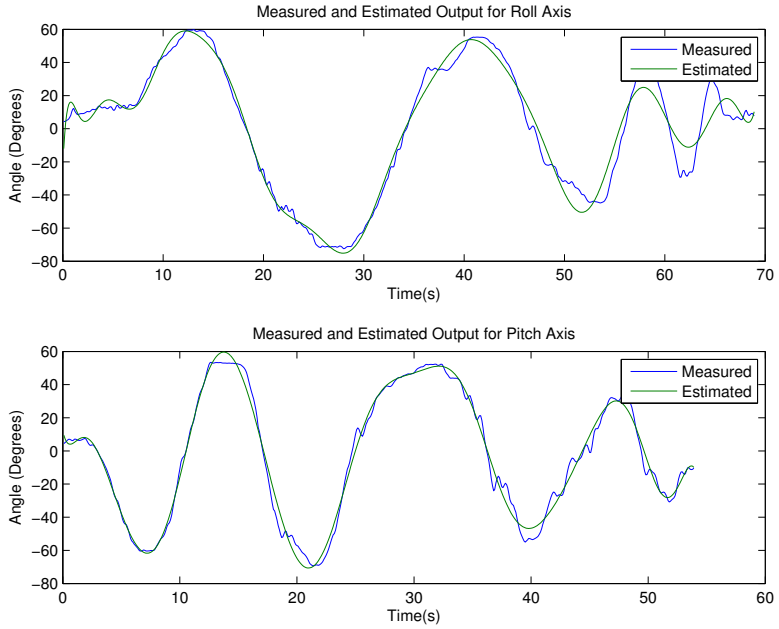


**Fig. 6.** Measured and estimated output for roll and pitch axis.

## 6 Conclusion

This paper presents a system identification method of a quad-rotor in X configuration based on a linear model. The estimated models represent the quad-rotor dynamics quite well, despite some irregularities in the estimated outputs system. It can be seen that the rapid changes in the quad-rotor dynamics, could be difficult to estimate for the linear models proposed in this paper.

The Matlab System Identification Toolbox is demonstrated to be a good tool for a quick modeling of a quad-rotor system. The transfer functions for the roll and pitch axis shows that a linear model can estimate the quad-rotor dynamics, even though the system have strong non-linearities.

Future research include the design of a controller based on the models proposed in this paper, the implementation of a neural network to obtain a nonlinear model which will improve the estimated output system, and the design of a stabilization control for the quad-rotor.

## References

1. Valavanis, K.P., Vachtsevanos, G.J.: Definitions and Terminology. Handb. Unmanned Aer. Veh., pp. 1–3022 (2015)

2. Hughes, V., Macnichol, E.F., Williams, F.C.: Technology and autonomous mechanisms in the Mediterranena: from ancient Greece to Byzantium. MCS.2014.2359589, pp. 110–119 (2014)
3. Valavanis, K.P., Vachtsevanos, G.J.: Aviaton history and unmanned flight. Handb. Unmanned Aer. Veh., pp. 1–3022 (2015)
4. Floreano, D., Wood, R.J.: Science, technology and the future of small autonomous drones. Nature 521, pp. 460-466, doi: 10.1038/nature14542 (2015)
5. Yang, J., Cai, Z., Lin, Q.: System identification of quadrotor UAV based on genetic algorithm. In: Proc. 2014 IEEE Chinese Guided Navigation Control Conf., pp. 2336-2340, doi: 10.1109/CGNCC.2014.7007533 (2014)
6. Chang, W.D.: Nonlinear system identification and control using a real-coded genetic algorithm. Appl Math Model 31, pp. 541–550, doi: 10.1016/j.apm.2005.11.024 (2007)
7. Wang, G., Xia, H., Yuan, X.: Modeling the yaw dynamics of an unmanned helicopter through modes partition method. Sci China Technol Sci 55, pp. 182–192, doi: 10.1007/s11431-011-4576-9 (2012)
8. Jin, H., Li, X., Zhang, X., Li, Y.: Study on the Modeling Methods of the Quadrotor Unmanned Helicopter. pp. 4855–4859 (2015)
9. Xiii, T., May, F.: Genetic fuzzy identification method for quadrotor UAVs. DEVELOPMENT OF MICROCONTROLLER-BASED SINGLE PHASE, Int J Eng pp. 237–240 (2015)
10. Sarioglu, A., Kural, A.: Modeling and ARX identification of a quadrotor Mini-UAV. In: 2015 9th International Conference on Electrical and Electronics Engineering (ELECO), pp. 1196–1200, IEEE (2015)
11. Salameh, I.M., Ammar, E.M., Tutunji, T.A.: Identification of quadcopter hovering using experimental data. In: 2015 IEEE Jordan Conference on Applied Electrical Engineering and Computing Technologies (AEECT), pp. 1–6, IEEE (2015)
12. Wu, H., Sun, D., Zhou, Z.: Model Identification of a Micro Air Vehicle in Loitering Flight Based on Attitude Performance Evaluation. IEEE Trans., Robot 20, pp. 702–712 (2004)
13. Wu, J., Peng, H., Chen, Q.: RBF-ARX model-based modeling and control of quadrotor. In: 2010 IEEE International Conference on Control Applications, pp. 1731–1736, IEEE (2010)
14. Dongli, Y., Jianguo, Y., Xinmin, W., Qingbiao, X.: A Study of Information Fusion for UAV Based on RBF Neural Network. In: 2007 IEEE International Conference on Control and Automation, pp. 2839–2842, IEEE (2007)
15. Schreurs, R.J.A., Weiland, S., Tao, H.: Open loop system identification for a quadrotor helicopter system. In: IEEE Int Conf. Control Autom. ICCA, pp. 1702–1707, doi: 10.1109/ICCA.2013.6565145 (2013)
16. Bouabdallah, S., Murrieri, P., Siegwart, R.: Design and control of an indoor micro quadrotor. In: IEEE Int Conf Robot Autom 2004 Proceedings ICRA '04 2004 5, pp. 4393-4398, doi: 10.1109/ROBOT.2004.1302409 (2004)
17. Dydek, Z.T., Annaswamy, A.M., Lavretsky, E.: Adaptive control of quadrotor UAVs: A design trade study with flight evaluations. IEEE Trans Control Syst Technol 21, pp. 1400–1406, doi: 10.1109/TCST.2012.2200104 (2013)
18. Dong, W., Gu, G.Y., Zhu, X., Ding, H.: A high-performance flight control approach for quadrotors using a modified active disturbance rejection technique. Rob Auton Syst 83, pp. 177–187, doi: 10.1016/j.robot.2016.05.005 (2016)

ISSN 1870-4069

# Mammogram Image Segmentation Using Bioinspired Novel Bat Swarm Clustering

David González-Patiño[1], Yenny Villuendas-Rey[2], Amadeo J. Argüelles-Cruz[1]

[1] Instituto Politécnico Nacional, Centro de Investigación en Computacion, Mexico City, Mexico

[2] Instituto Politécnico Nacional, Centro de Innovación y Desarrollo Tecnológico en Cómputo, Mexico City, Mexico

yenny.villuendas@gmail.com, davidglezp-92@hotmail.com, aarguelles@ipn.mx

**Abstract.** Segmentation is one of the main tasks related to breast cancer classification. Automatic and semiautomatic algorithms have been proposed lately, and in this paper, a new method to segment mammography images is proposed using novel bat algorithm (NBA) and unsupervised metric measures as objective function. Results showed a useful method to segment mammographies using bioinspired algorithms based on bat optimization.

**Keywords:** Mammogram, bioinspired, novel bat algorithm, swarm, breast cancer.

## 1 Introduction

Recent studies have showed that breast cancer is one of the main causes of death in women around the world [1]. In Mexico, breast cancer is the main reason of deaths in adult women in ages among 30 and 54 years [2][3]. It is also one of the currently most common cancers in Mexico, with high risk. Risks are estimated based on new cancer cases between people free of this disease [4].

Detecting breast cancer using x-ray mammograms in early phases is the best way to prevent breast cancer deaths. This is the reason why mammographies are recommended in order to obtain an early detection of breast cancer among women older than 26 years and it is highly recommended to obtain a mammography study for women from 40 to 49 years old [1].

In Mexico it is very important to improve screening analysis to promote early detection for breast cancer because only 5-10% cases of breast cancer in Mexico are detected in early phases [1].

Mammograms are images obtained by mammography. Typically, these images are gray scaled, and the cancer lesion are differentiated due to their texture and color [5]. Automatic detection of lesions in mammogram includes the segmentation of the region of interest, in order to separate the lesion from the rest of the mammary tissue. To

accomplish this task, several segmentation techniques have been used [6–9]. However, development of simple and accurate segmentation algorithms is still a challenge in digital image processing [7].

Segmentation algorithms can be divided in two main categories: region and edge based [7]. The first category assigns each pixel to a region while the other category constructs an image based on the boundaries of a specific object.

Region based segmentation can be modeled as an optimization problem, considering the search space as all possible categories for each pixel, and the objective function as a quality measure for the segmentation.

Metaheuristics algorithms are inspired in nature processes and are used in a lot of optimization problems due to their power and easy implementations. They also try to find the optimal and practical solution to nonlinear or very complex problems [10].

In this paper we focus on this topic, implementing a new method to segment mammograms to later assist diagnosis using segmentation based on regions. Our method is based on the recently proposed Novel Bat Algorithm (NBA) [11]. Novel Bat Algorithm is a swarm intelligence algorithm based on the echolocation behavior of bats and this characteristic can be associated with an objective function.

The paper is organized as follows. Section 2 addresses some previous works in the field of automatic or semi-automatic breast cancer segmentation for mammograms. Section 3 explains the algorithm used for mammogram segmentation, while section 4 presents the experimental results. The paper finalizes with conclusions and future work.

## 2 Previous Works

Around the world, mammograms has been used to detect breast cancer, however there are another techniques used for diagnosis of breast cancer, being the most commonly used: ultrasounds [12], Magnetic Resonance Imagery (MRI) [13] and other more invasive methods like biopsies [14].

Semi-automatic and automatic segmentation is useful for the specialist because it provides a simpler image and the lesion can be detected easily. The algorithms proposed for mammogram segmentation are varied and some of them have been proposed since 1998 [15] using a clustering algorithm extracting texture features and matrices based on lengths.

In 2012 Rahmati et al. proposed a method to segment lesions in mammographies, based on a maximum likelihood active contour [9]. This algorithm separates the image in 2 parts: lesion and background.

Recently was proposed a method for mammographies segmentation using Deep Neural Networks, this method was proposed in 2016 by Dubrovina et al. [16] and uses a new model for classification in mammograms.

Similarly Sargent and Park [8] designed in the same year a method for segmentation of medical images such as mammograms, tomograms and scanned images using side-by-side images comparisons.

Until now, there is no method proposed based on Novel Bat Algorithm for breast cancer mammograms segmentation. In this paper, we proposed a method to use this algorithm using metrics based on lengths as optimization function.

## 3 Proposed Segmentation Algorithm

Segmentation algorithms are used to split the background and the region of interest in images, in the following, we will explain the proposed method based on Novel Bat Algorithm proposed by Xian-Bing Meng et al. in 2015 [11] based on the Bat Algorithm proposed by Xin-She Yang in 2012 [17].

Using the variables called loudness and pulse rate, which represent the proximity to other bats; the Novel Bat Algorithm generates random solutions using the currently optimal solutions. This algorithm was used in this paper because it explores a lot of solutions because of the randomly generated solutions in order to find the best solution.

This algorithm is inspired in the echolocation of bats, a characteristic that helps bats to sense distances and provides them knowledge about the objects of interest and backgrounds.

The pseudoalgorithm of Novel bat algorithm uses an objective function for the optimization process. The pseudoalgorithm adapted to the segmentation problem is showed below.

The frequency of each bat is defined in equation 1, and is calculated using minimum and maximum frequencies and a random value between 0 and 1 given by a uniform distribution:

$$f_i = f_{min} + (f_{max} - f_{min})\beta. \tag{1}$$

Velocity and position for each bat is defined in equation 2 and 3 respectively, position is given by previous position and velocity, and on the other hand velocity is given by the previous velocity and the difference between actual position and currently best position defined as $x_*$:

$$v_i^t = v_i^{t-1} + (v_i^t - x_*)f_i\,, \tag{2}$$

$$x_i^t = x_i^{t-1} + v_i^t\,. \tag{3}$$

The flow chart in Figure 1 was done according to the pseudoalgorithm proposed by Xian-Bing Meng [17].

We need to initialize the bat population with random values in the range from 0 to 255 because these are the values of possible gray levels.

The algorithm iterates a defined number of times and for each iteration the algorithm will generate solutions adjusting frequencies and velocities for each bat.

New solutions are generated randomly and they are accepted if they are better than previous solutions evaluating them in the objective function.

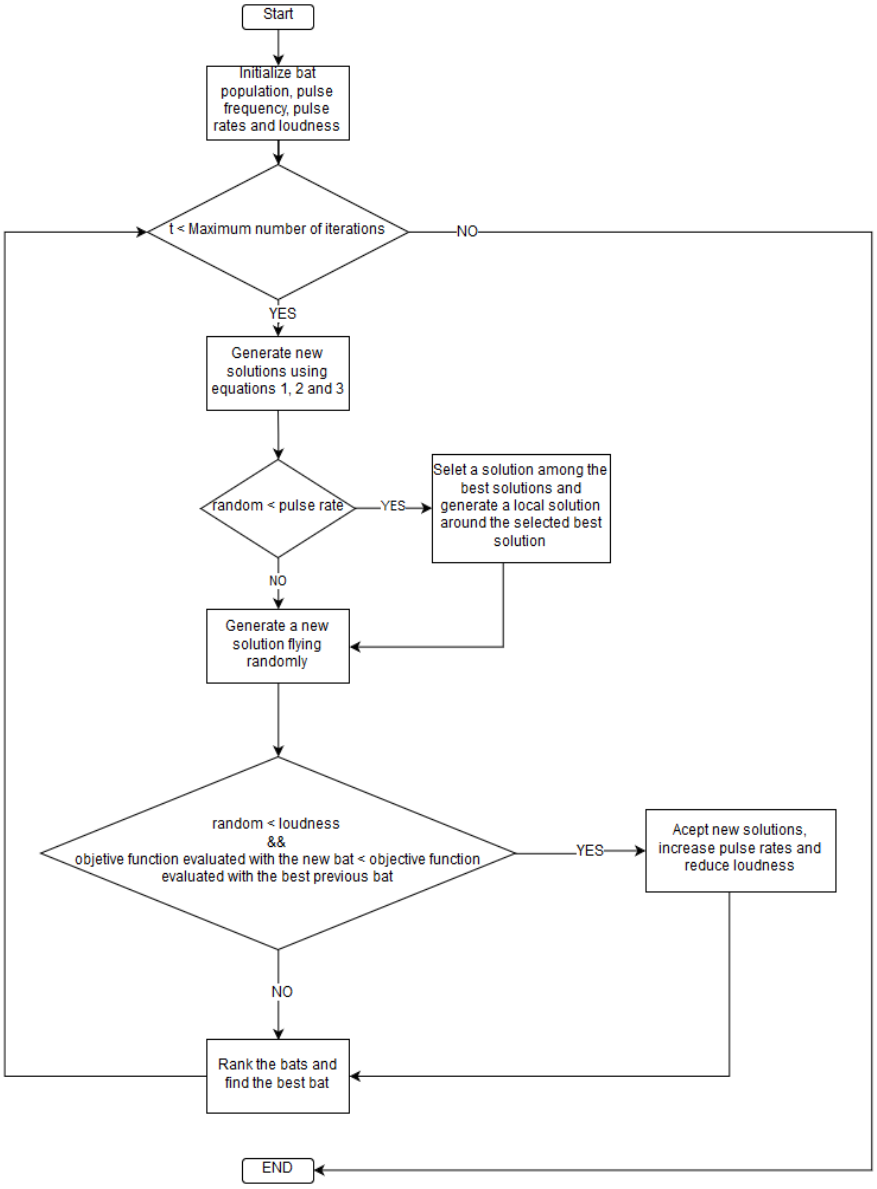


**Fig. 1.** Flow chart for Novel Bat Algorithm.

The Novel bat algorithm was originally programmed in Matlab by Xian-Bing Meng in 2015 [11], this algorithm was tested in Matlab and for this paper the modified algorithm was programmed in C# using Microsoft Visual C# 2010 based on the same algorithm.

For the implementation presented in this paper each bat represents a gray level and a partition of the image as represented in figure 2.

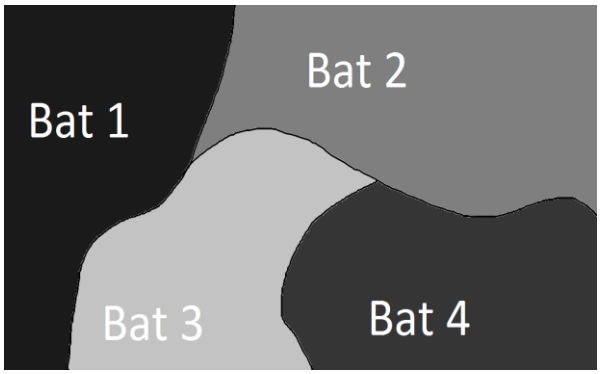


**Fig. 2.** Representation of gray levels for segmentation, each bat represents a region of the image.

The algorithm was modified for processing mammographies images using formula 4 as objective function:

$$\frac{\text{Minimum distance between pixels in different group}}{\text{Maximum distance between pixels in same group}}. \tag{4}$$

The metric used to calculate the distance between each bat was the Minkowski distance for order 1. The bounds used for this implementation were based on gray levels; this means only numbers from 0 to 254 were used.

The segmentations were evaluated according to the work presented by Hui Zhang et al. in 2007 [18]. That work is a survey of evaluations in image segmentations using unsupervised methods. To evaluate the segmentations we used average squared color error (F, equation 5) which penalizes over-segmentations; the survey proposed an improved measure to evaluate average squared color error (F', equation 6).

F' is an extension of F and it penalizes segmentations that have a lot of small regions of the same size:

$$\mathrm{F} = \sqrt{N} \sum_{j=1}^{N} \frac{ej^2}{\sqrt{Sj}}, \tag{5}$$

$$\mathrm{F'} = \frac{1}{1000 * SI} \sqrt{\sum_{b=1}^{MaxArea} N(b)^{1+\frac{1}{b}}} \sum_{j=1}^{N} \frac{ej^2}{\sqrt{Sj}}, \tag{6}$$

where N represents number of regions in the image and Sj are the quantity of pixels in the region j.

SI represents the area of the image and N(b) is number of regions of the segmented image that have exactly b units of area.

In equation 2 and 3 the squared color error of region j $ej^2$ is defined in equation 7:

$$ej^2(Rj) = \sum_{p \in Rj} (Cx(p) - \hat{C}x(Rj))^2. \quad (7)$$

Cx(p) represents the value of component x for pixel p. And finally the average value of component x in the region j is defined in equation 8:

$$\hat{C}x(Rj) = \frac{\sum_{p \in Rj} Cx(p)}{Sj}. \quad (8)$$

These errors measures were used in the performance tests.

## 4 Experiments

The algorithm proposed in this paper was tested using the dataset Breast Cancer Digital Repository [19] provided by the Faculty of Medicine in the University of Porto, in Portugal.

This dataset contains 200 lesions proven by biopsies of 190 women, also including 362 segmentations in the mammograms. The images used were gray scaled. The boundaries for each lesion were identified by expert radiologists.

We used the NBA based segmentation algorithm proposed in this paper (SNBA) for segmentations in two and three regions. Each region was assigned with a color and colors are not representative to their original pixel color.

Several experiments were tested for this paper and all images were processed using two and three bats. The measures were calculated for all the segmented images and compared to the same measures calculated using the segmentations made by the radiologist.

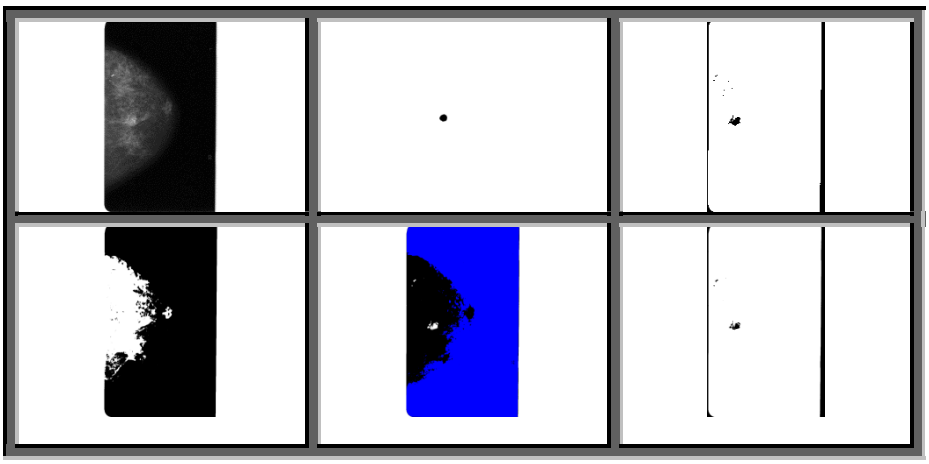

**Fig. 3.** (Top left) Original mammogram, (Top middle) Segmented image by expert radiologist, (Top right) Segmented image using OTSU method, (Bottom left) Image after processing using the algorithm proposed in this paper using two bats for the segmentation, (Bottom middle) Image after processing using the algorithm proposed in this paper using three bats for the segmentation, (Bottom right) Image after obtaining the segmentation cluster of interest in the segmentation for three bats algorithm.

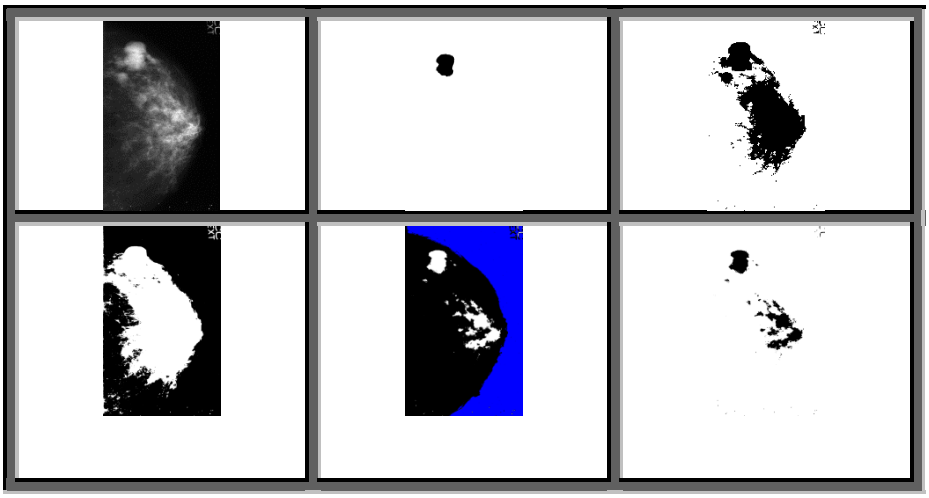

**Fig. 4.** (Top left) Original mammogram, (Top middle) Segmented image by expert radiologist, (Top right) Segmented image using OTSU method, (Bottom left) Image after processing using the algorithm proposed in this paper using two bats for the segmentation, (Bottom middle) Image after processing using the algorithm proposed in this paper using three bats for the segmentation, (Bottom right) Image after obtaining the segmentation cluster of interest in the segmentation for three bats algorithm.

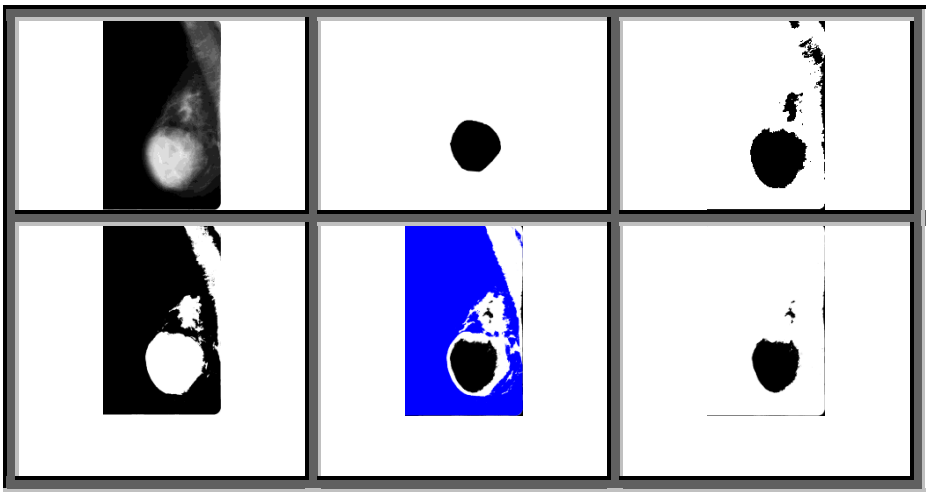

**Fig. 5.** (Top left) Original mammogram, (Top middle) Segmented image by expert radiologist, (Top right) Segmented image using OTSU method, (Bottom left) Image after processing using the algorithm proposed in this paper using two bats for the segmentation, (Bottom middle) Image after processing using the algorithm proposed in this paper using three bats for the segmentation, (Bottom right) Image after obtaining the segmentation cluster of interest in the segmentation for three bats algorithm.

**Table 1.** Measures of error for segmented images.

| Figure | Measure of error | Segmented image using two bats (SNBA) | Segmented image using three bats (SNBA) | Cluster of interest (SNBA) | Segmented image using OTSU method |
|---|---|---|---|---|---|
| **3** | **F** | 3.20039 **x10$^{5}$** | 1.58467 **x10$^{5}$** | 1.58467 **x10$^{5}$** | 1.58611 **x10$^{5}$** |
| | **F'** | 2.693 **x10$^{-4}$** | 1.333 **x10$^{-4}$** | 1.333 **x10$^{-4}$** | 1.334 **x10$^{-4}$** |
| **4** | **F** | 1.940457 **x10$^{6}$** | 2.414146 **x10$^{6}$** | 2.414146 **x10$^{6}$** | 2.155042 **x10$^{6}$** |
| | **F'** | 16.29 **x10$^{-4}$** | 20.27 **x10$^{-4}$** | 20.27 **x10$^{-4}$** | 18.09 **x10$^{-4}$** |
| **5** | **F** | 9.985477 **x10$^{6}$** | 9.296394 **x10$^{6}$** | 8.606007 **x10$^{6}$** | 9.751196 **x10$^{6}$** |
| | **F'** | 84.03 **x10$^{-4}$** | 78.23 **x10$^{-4}$** | 72.42 **x10$^{-4}$** | 82.06 **x10$^{-4}$** |
| **6** | **F** | 9.985477 **x10$^{6}$** | 9.296394 **x10$^{6}$** | 8.606007 **x10$^{6}$** | 8.268497 **x10$^{6}$** |
| | **F'** | 84.03 **x10$^{-4}$** | 78.23 **x10$^{-4}$** | 72.42 **x10$^{-4}$** | 69.58 **x10$^{-4}$** |

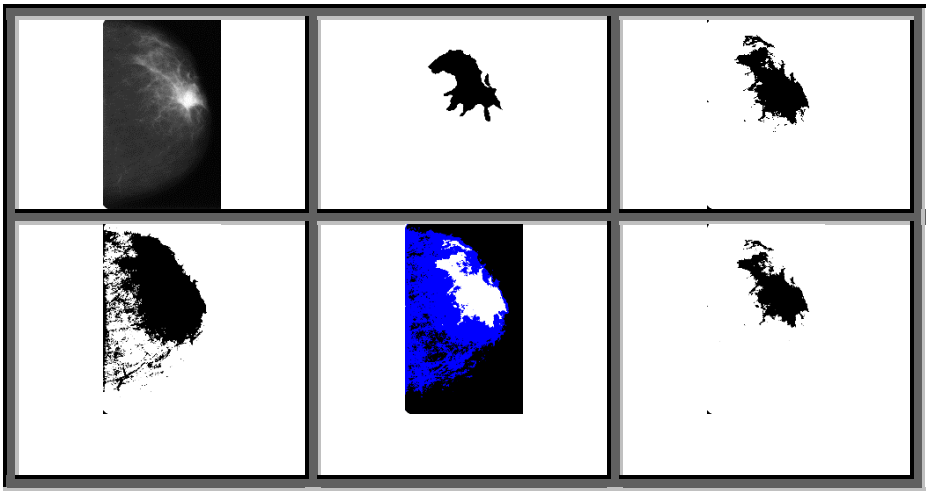

**Fig. 6.** (Top left) Original mammogram, (Top middle) Segmented image by expert radiologist, (Top right) Segmented image using OTSU method, (Bottom left) Image after processing using the algorithm proposed in this paper using two bats for the segmentation, (Bottom middle) Image after processing using the algorithm proposed in this paper using three bats for the segmentation, (Bottom right) Image after obtaining the segmentation cluster of interest in the segmentation for three bats algorithm.

Measures are presented in Table 1. As we can observe segmented images using the algorithm proposed in this paper (SNBA) showed a smaller error in comparison to other segmentations used.

As shown in Table 1, the proposed SNBA algorithm is able to obtain a good segmentation by using only three bats (representing the regions corresponding to cancer lesion, mammary tissue and background, respectively). However, some noisy pixels are marked as cancer lesion, and further processing will be needed to remove them. Some columns showed very similar errors representing no significant changes in the segmented images.

## 5 Conclusions

This paper presents a new method to segment images using bioinspired Novel Bat Algorithm (NBA). As many bioinspired algorithms, the NBA used here has some parameters that can be adjusted to improve the performance of the segmentation process. In a similar way, the quantity of bats can be adjusted to obtain better segmentations. The adjustment of parameters can improve the convergence rate of this algorithm and it is a good line of investigation. In addition, the investigation detects some noisy pixels marked as cancer lesion, and further processing will be needed to address this issue.

**Acknowledgments.** The authors would like to thank the Instituto Politécnico Nacional (Secretaría Académica, Comisión de Operación y Fomento de Actividades Académicas, Secretaría de Investigación y Posgrado, Centro de Investigación en Computación, and Centro de Innovación y Desarrollo Tecnológico en Cómputo), the Consejo Nacional de Ciencia y Tecnología (Conacyt), and Sistema Nacional de Investigadores for their economical support to develop this work.

## References

1. Knaul, F.M., Nigenda, G., Lozano, R., Arreola-Ornelas, H., Langer, A., Frenk, J.: Breast cancer in Mexico: a pressing priority. Reprod. Health Matters, 16, pp. 113–123 (2008)
2. Borja-Aburto, V.H., Dávila-Torres, J., Rascón-Pacheco, R.A., González-León, M., Fernández-Gárate, J.E., Mejía-Rodríguez, I., de Jesús González-Izquierdo, J., los Ríos, P.M.: Cancer mortality in the Mexican Social Security Institute, 1989-2013. Salud Publica Mex. 58, pp. 153–161 (2016)
3. Lozano, R., Knaul, F.M., Gómez-Dantés, H., Arreola-Ornelas, H., Méndez, O.: Tendencias en la mortalidad por cáncer de mama en México, 1979-2006. Observatorio de la Salud. Doc. Trab. Compet. y Salud, Fund. Mex. para la Salud (2008)
4. Wun, L.-M., Merrill, R.M., Feuer, E.J.: Estimating lifetime and age-conditional probabilities of developing cancer. Lifetime Data Anal. 4, pp. 169–186 (1998)
5. Yaffe, M.J.: Digital mammography. In: PACS, pp. 363–371 (2006)
6. Byrd, K., Zeng, J., Chouikha, M.: Performance assessment of mammography image segmentation algorithms. In: 34th Applied Imagery and Pattern Recognition Workshop

(AIPR'05), p. 6 (2005)
7. Timp, S., Karssemeijer, N.: A new 2D segmentation method based on dynamic programming applied to computer aided detection in mammography. Med. Phys. 31, pp. 958–971 (2004)
8. Sargent, D., Park, S.Y.: Automatic segmentation of mammogram and tomosynthesis images. In: SPIE Medical Imaging (2016)
9. Rahmati, P., Adler, A., Hamarneh, G.: Mammography segmentation with maximum likelihood active contours. Med. Image Anal. 16, pp. 1167–1186 (2012).
10. Doerner, K.F., Gendreau, M., Greistorfer, P., Gutjahr, W., Hartl, R.F., Reimann, M.: Metaheuristics: progress in complex systems optimization. Springer Science & Business Media (2007)
11. Meng, X.-B., Gao, X.Z., Liu, Y., Zhang, H.: A novel bat algorithm with habitat selection and Doppler effect in echoes for optimization. Expert Syst. Appl. 42, pp. 6350–6364 (2015)
12. Kelly, K.M., Dean, J., Comulada, W.S., Lee, S.-J.: Breast cancer detection using automated whole breast ultrasound and mammography in radiographically dense breasts. Eur. Radiol. 20, pp. 734–742 (2010)
13. Warner, E., Plewes, D.B., Hill, K.A., Causer, P.A., Zubovits, J.T., Jong, R.A., Cutrara, M.R., DeBoer, G., Yaffe, M.J., Messner, S.J., others: Surveillance of BRCA1 and BRCA2 mutation carriers with magnetic resonance imaging, ultrasound, mammography, and clinical breast examination. Jama, 292, pp. 1317–1325 (2004)
14. Albertini, J.J., Lyman, G.H., Cox, C., Yeatman, T., Balducci, L., Ku, N., Shivers, S., Berman, C., Wells, K., Rapaport, D., others: Lymphatic mapping and sentinel node biopsy in the patient with breast cancer. Jama, 276, pp. 1818–1822 (1996)
15. Sahiner, B., Chan, H.-P., Petrick, N., Helvie, M.A., Goodsitt, M.M.: Computerized characterization of masses on mammograms: the rubber band straightening transform and texture analysis. Med. Phys. 25, pp. 516–526 (1998)
16. Dubrovina, A., Kisilev, P., Ginsburg, B., Hashoul, S., Kimmel, R.: Computational mammography using deep neural networks. Comput. Methods Biomech. Biomed. Eng. Imaging Vis, pp. 1–5 (2016)
17. Yang, X.-S., Hossein Gandomi, A.: Bat algorithm: a novel approach for global engineering optimization. Eng. Comput. 29, pp. 464–483 (2012)
18. Zhang, H., Fritts, J.E., Goldman, S.A.: Image segmentation evaluation: A survey of unsupervised methods. Comput. Vis. image Underst, 110, pp. 260–280 (2008)
19. Moura, D.C., López, M.A.G.: An evaluation of image descriptors combined with clinical data for breast cancer diagnosis. Int. J. Comput. Assist. Radiol. Surg. 8, pp. 561–574 (2013)

ISSN 1870-4069

# Recurrent Trainable Neural Networks for Complex Systems Identification: A Hybrid System Approach

Juan-Eduardo Velázquez-Velázquez[1], Rosalba Galván-Guerra[1], Ieroham Baruch[2], Silvestre Garcia-Sanchez[1]

[1] UPIIH-IPN, Pachuca de Soto, Hgo., Mexico

[2] CINVESTAV-IPN, Department of Automatic Control, Mexico

{jvelazquezv,rgalvang,sgarcias}@ipn.mx, baruch@ctrl.cinvestav.mx

**Abstract.** This paper is devoted to the development of an Identification Framework for unknown Complex Systems. The proposal is based on Recurrent Trainable Neural Networks following a Hybrid System approach. The complex system is identified by using hybrid input-output data defined by a given set of switching hypersurfaces. The effectiveness of the proposed approach is shown using a commutable pendulum with chaotic behavior.

**Keywords:** Complex systems identification, hybrid systems, recurrent trainable neural networks.

## 1 Introduction

It is well known that interpreting and predicting the behavior of complex dynamical systems is challenging, mainly because the causes and effects are not obviously related. One way to establish the direct and indirect relationships of causes and effects in a complex system is via an identification framework. The identification problem consists of obtaining a model that allow us to infer how the system will respond to other inputs that we have not yet measured by approximating the output trajectory of the system. In the complex systems context, there are several approaches with quite different viewpoints on system modeling: dynamical systems, discrete event systems, cellular automata models, neural network models, finite state machines, cognitive maps, multi-agent models and Hybrid Systems (HS) (see [3] and the references there in). These paradigms differ, rather, by concepts and views on the problems and approaches to solve them, than the applications areas [1, 7, 10, 13, 16, 17]. In this contribution, we follow the HS approach.

The identification theory for continuous state systems is well developed in the literature [18]. However, HS add extra complexity due to the interaction of continuous and discrete dynamics. The identification of complex systems following a HS approach has been devoted to the identification of switched affine and piecewise affine models. The main issues and difficulties connected with HS identification are discussed in [22].

Normally the identification is based on statistical techniques that need a reasonable amount of data and assume stationarity: they require that the underlying system does not change its parameters over time. If the parameters of the system are drifting or externally switched from time to time, the statistical algorithms can be applied to short segments of the data, thereby monitoring changes in the characteristic quantities. However, such methods may suffer from the curse of dimensionality and other statistical problems that arise when estimating from few data points.

Instead of a statistical technique, in this contribution we use a Neural Network (NN) technique that is very effective for identification and control of nonlinear systems when partial or null information about systems is available [20]. It is worth to mention, that the idea to incorporate NN for identification of complex systems following a HS approach has been previously addressed. In one side, some proposals incorporate the NN identifier as a global model, losing the nature of HS [2, 15, 19]. In the other side, it is assumed that the sequence of locations is known or that it is well established by considering the discrete-time dynamics at the higher level of a hierarchical framework [12, 14]. These kinds of assumptions could not be valid because the dynamic behavior of a HS is strongly influenced by discontinuities in its system trajectories [9, 23].

In this paper an identification methodology based on Recurrent Trainable NN (RTNN) to model complex systems, in a HS approach, is presented; following a gray box retaining the characteristic behavior of HS and introducing the Hybrid RTNN (HRTNN).

The outline of the paper is as follows: In Section 2 we describe the hybrid complex systems investigated in this contribution and the identification problem is formulated. In Section 3 we present the HRTNN description. In order to show the validity of the proposed HRTNN several simulations of a commutable ideal pendulum, presenting chaos behavior, are developed in Section 4. Section 5 concludes the paper.

## 2 Modeling Framework and Problem Formulation

In this contribution, a complex system is considered as a system composed by simple subsystems; where the subsystems are active in a set of locations. Then the modeling framework for the complex system identification is based on Hybrid Dynamical Systems (HDS) structures. The HDS are characterized by a set of subsystems interconnected in a discrete manner. The applicability of this approach can be seen in the fact that several types of hybrid systems are used in chemical, bioengineering, aerospace and electronics industries, among others to model complex control systems [7, 9, 10, 17]. The Nonlinear HDS (NHDS) discussed in this paper are represented by its hybrid state equation

$$\dot{x}(t) = \sum_{i=1}^{r} \beta_{[t_{i-1},t_i)}(t) f_{q_i}\big(t,x(t),u(t)\big) \text{ a.e. on } t \in [0, t_f], \quad (1)$$

and by the hybrid output vector

$$\bar{y}(t)=\sum_{i=1}^{r}\beta_{[t_{i-1},t_i)}(t)h_{q_i}\big(t,x(t),u(t)\big) \text{ a.e. on, } t\in[0,t_f] \quad (2)$$

with available sample-data outputs y(k). $\beta_{[t_{i-1},t_i)}(\cdot)$, is the characteristic function of the interval $[t_{i-1},t_i)$ for i=1,…,r, i.e.

$$\beta_{[t_{i-1},t_i)}(t)=\begin{cases}1, & \text{if } t\in[t_{i-1},t_i),\ i=1,...,r\\ 0, & \text{otherwise}\end{cases}.$$

Here $q_i\in Q$ represents a location, Q is a finite set of discrete states (called *locations*), $x(\cdot)\in X$ is an admissible state trajectory, $X=\{X_q\}$ with $X_q\subseteq R^n$; $u(\cdot)\in U$ is an admissible input signal and $U\subseteq R^m$ is a set of admissible measurable bounded functions; $f_q\colon [0,t_f]\times X_q\times U\to R^n$ defines a family of velocity vector fields $F=\{f_q\}$; $h_q\colon [0,t_f]\times X_q\times U\to R^p$ are diffeomorphisms which define a family of vector fields $H=\{h_q\}$; and $\bar{y}(\cdot)\in Y$ is an admissible output trajectory, $Y=\{Y_q\}$ is a collection of output sets with $Y\subseteq R^p$. The interest of considering NHDS with sample-data outputs is twofold: these models can represent a wide range of systems of practical interest and sample-data outputs can be interpreted as a result of application of a quantified procedure to an original continuous model. Note that, in difference to $\bar{y}(t)$ the stepwise value y(k) is a measurable output of the system under consideration. We assume that the dynamic transitions between two subsystems are characterized by the assembly of switching pairwise disjoint hypersurfaces $M_{q,q'}:=\{x\in R^n: m_{q,q'}(x)=0\}$, where $m_{q,q'}:R^n\to R$, $q,q'\in Q$ are smooth functions with nonzero gradients. The given hypersurfaces $M_{q,q'}$ represents the *switching sets* at which a switch from location *q* to location *q'* can take place. We say that a location switching from *q* to *q'* occurs at a *switching time* $t_{sw}\in[0,t_f]$. We consider NHDS with $r\in R$ switching times: $0<t_0<t_1<\cdots<t_{r-1}<t_r=t_f$. Note that the sequence of switching times $\{t_i\}$ is not defined a priory, neither the sequence of locations: $\{q_i\}$. In order to state the problem, that we are interested on, let us introduce the following definition.

**Definition 1:** A *hybrid trajectory* of NHDS is a 3-tuple $X=\{x(\cdot),q_i,t_i\}$ such that for each i=1,…,r and every admissible input $u(\cdot)\in U$ we have

- $x(0)=x_0\notin\bigcap_{q,q'\in Q}M_{q,q'}$ and $x_i(\cdot)=x(\cdot)|_{(t_{i-1},t_i)}$ is an absolutely continuous function on $(t_{i-1},t_i)$ continuously prolongable to $[t_{i-1},t_i]$, i=1,…,r
- $x(t_i)\in M_{q,q'}$ for i=1,…,r;
- $\dot{x}(t)=f_{q_i}(t,x_i(t),u(t))$ for almost all $t\in[t_{i-1},t_i]$

Observe that given an admissible signal input $u(\cdot)$, the physical attributes of a NHDS governed by its state equation (1) are transformed by (2) into responses as system outputs. Here, we suppose that the hybrid output retains the state behavior, i.e., the transition from one location to another in the space state cause a transition in the output response. We assume that the transitions at the output are characterized by the assembly of switching pairwise disjoint hypersurfaces

$$N_{q,q'}:=\{y\in R^p: n_{q,q'}(y)=0\}, \quad (3)$$

where $n_{q,q'}:R^p \rightarrow R$, $q,q' \in Q$ are smooth functions with nonzero gradients defined as: $n_{q,q'}(y) = m_{q,q'}\left(h_{q'}^{-1}(x)\right)$. We now could formulate the identification problem as:

**Problem 1:** Assume that the NHDS (1)-(2) is unknown. The identification problem consists of obtaining a model that allow us to infer how the NHDS will respond to other inputs that we have not yet measured by approximating the output hybrid trajectory of the system NHDS. That is, for an experiment with length $t_f$, we want to determine a model with a hybrid output $\hat{Y}=\{\hat{y}(\cdot),\{\hat{q}_i\},\{t_i\}\}$ which approximate the NHDS response, visited during the experiment, by using only the observed data $\{u(t),y(k),t\in[0,t_f]\}$.

## 3 HTRNN Description

During the last decade considerable research has been devoted towards developing RNN models applied for identification and control of complex nonlinear plants [4, 5]. Under the premise of Problem 1, we follow the structure of NHDS to approach complex systems; the dynamic transitions from one location to another observed in the output response are described by the equations of mathematical physics, but the response of the subsystems is modeled by neural networks. Then, to describe the global complex system's behavior, we use an arbitrary interconnection between subsystems with discrete event, characterized by switching hypersurfaces. It means that the transition locations $\{q_i\}$ and the sequences of switching times $\{t_i\}$ are not previously defined, only the hypersurface (3) are considered. It is worth to mention, that to develop a computational identification it is necessary to take some measurements in a time interval. Then, it is pertinent to consider a discrete RTNN to performs this task. It is well known that during the sampling process it is possible to lose a location transition. However, if the direction of the trajectory is considered it is possible to detect when a hypersurface $n_{q,q'}$ has been triggered.

The RTNN topology and its associated BP learning rule are described in vector-matrix form, [4, 5, 6], as:

$$\begin{gathered}
\hat{x}(k+1) = A\hat{x}(k) + B\hat{u}(k); \\
z(k) = G[\hat{x}(k)]; \;\; v(k) = Cz(k); \;\; \hat{y}(k) = F[v(k)]; \\
w(k+1) = w(k) + \eta\Delta w(k) + \alpha\Delta w(k-1); \\
e(k) = y(k) - \hat{y}(k); \;\; F'[\hat{y}(k)] = [1-\hat{y}^2(k)]; \\
e_3(k) = G'[z(k)]e_2(k); \;\; e_2(k) = C^T(k)e_1(k); \\
G'[z(k)] = [1-z^2(k)]; \;\; \Delta B(k) = e_3(k)\hat{u}^T(k); \\
\Delta A(k) = e_3(k)\hat{x}^T(k); \;\; \Delta C(k) = e_1(k)z^T(k);
\end{gathered} \tag{4}$$

where $\hat{y}(k)$, $\hat{x}(k)$ and $\hat{u}(k)$ are output, state and input vectors of the RTNN with dimension p, N, (m+1); here $u^T = [u; u_0]$, where u is the real plant input vector with dimension m and $u_0$=-1 is a threshold entry; y is the plant output vector with dimension p, considered as a RTNN reference; A is N×N block-diagonal matrix, defined by A =

$\text{block} - \text{diag}(A_i)$; $B = [B_1; B_0]$ and $C = [C_1; C_0]$ are N×(m+1) and L×(N+1) augmented weight matrices; $B_0$ and $C_0$ are N×1 and L×1 threshold weights of the hidden and output layers; F[·] and G[·] are vector valued activation functions of type tanh(·); $F'[\cdot]$ and $G'[\cdot]$ are the derivatives of the activation functions; W is a general weight denoting each weight matrix (C, A, B) in the RTNN model, to be update; Δw (ΔC,ΔA,ΔB), is the weight correction of W (C, A, B); η,α are learning rate parameters; e, $e_1$, $e_2$, $e_3$ are error vector with appropriate dimensions, predicted by the adjoint RTNN model. It is well known that the stability of the RTNN model is assured by the activation functions (-1,1) bounds and by the local stability weight bound conditions, $|A_i| < 1$.

### 3.1 Gray-Box Approach

Following a gray-box approach we only assume that $r$ location transitions in the hybrid output can take place. These transitions are characterized by the assembly of the given switching hypersurfaces (3). In this case we propose the use of the RTNN defined by (4) together with the switching hyper surfaces (3) used like a supervisor layer. This supervisor layer defines the switching instants between the $\text{RTNN}_{q_i}$ to $\text{RTNN}_{q_j}$, i.e., when condition $\eta_{q_i,q_j}(y(k)) = 0$ is fulfilled a transition between the neural networks occurs. In Fig. 1 we introduce the HRTNN model.

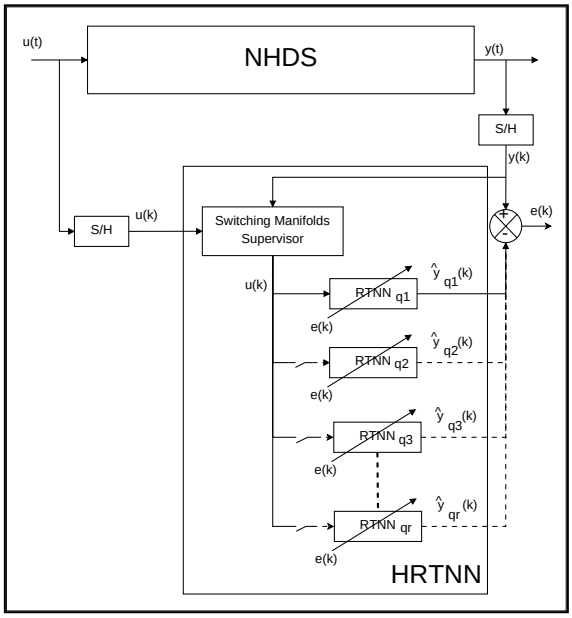


**Fig. 1** HRTNN Identifier of the Complex System: NHDS approach.

**Remark 1:** Note that in an arbitrary switching time, we are not updating the initial weights neither the initial state of the new located $\text{RTNN}_{q_i}$. Then to avoid any impulse

(error) in the updating of the weights and the state of the actual $RTNN_{q_j}$, we propose to add an Auxiliary Neural Network (ANN), showed in Fig. 2.

This ANN can be of any suitable topology. For simulation purposes we propose the use of a RTNN with the same topology as the $RTNN_{q_j}$. Observe that the convergence of this approach in a specific location is assured by the convergence of the RTNN training algorithm [4], [5], [6]. However, this convergence is subject to an enough amount of training data, and the absence of the Zeno behavior. Also note that the switching times can be computed analytically as it is shown in [11]. However, it is important to remark that the switching manifolds rule these switching times, so with the knowledge of these hypersurfaces we could know when a transition happens. The knowledge of the manifolds at the hybrid output along with an appropriated weight actualization strategy at the switching times makes possible to achieve a finite time convergence or at least a global convergence as in [12].

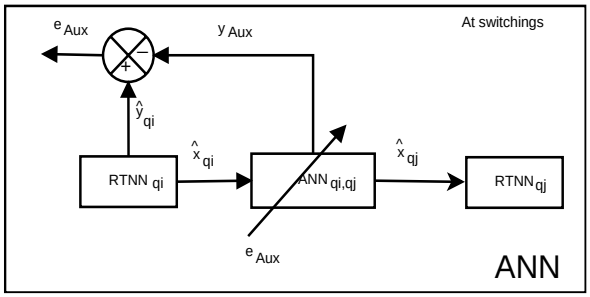


**Fig. 2** Auxiliary Neural Network Topology.

**Remark 2:** The gray-box strategy is actually a hybrid strategy, which allows us to identify the nonlinear system like a hybrid one. To complete the hybrid strategy as a black-box approach, we need structures that allow us to identify the switching manifolds (see [22] for details).

## 4 Simulation Results: Chaotic Behavior of an Ideal Commutable Pendulum

Here, the applicability of our approach is illustrated by a commutable pendulum example, taken from [21]. In an ideal form, the general mathematical model of this system is given by the following equations:

$$\Sigma = \begin{cases} \Sigma_1: \ \ddot{x} + x = 0 & x, \ddot{x} \epsilon R, \\ \Sigma_2: \ \ddot{x} + \omega^2 x = 0 & x, \ddot{x} \epsilon R, \end{cases}$$

where ω is the pendulum frequency and the switching manifolds are defined by:

$$M_{1,2}: x < 0, \quad \dot{x} = 0,$$
$$M_{2,1}: x = 0, \quad \dot{x} > 0.$$

Under some parameter conditions, the commutable pendulum presents a chaotic complex behavior, when the pendulum frequency is greater than 1[rad/s], [21]. In particular, the system commutes from a stable behavior to an unstable one. However, this chaotic nature does not mean that the whole system is unstable (see [8] for more details). With the aim to show the effectiveness of the HRTNN in the presence of some specific complex behavior, we identify the commutable pendulum with the frequency $\omega = 3.5\left(1 + x(t_i)\right)$, i=1,3,… Note that under this condition the system presents two limit cycles and it is highly unstabilizable (see the phase plane of Fig. 3). To identify the complex behavior of this specific commutable pendulum, we applied the two identification strategies, using the oscillatory input: $u(t) = \frac{1}{10}\sin\left(\frac{2\pi t}{5}\right)$.

Following the Gray box strategy without any actualization at the switching times, with the RTNN with topology (2, 4, 2), and learning parameters: $\eta$=0.6; $\alpha$=0.001, we train this network for 200 seconds with a sampling rate of 0.01, obtaining the results shown in Fig. 4, where $\frac{1}{2}e^2(t)$ is the mean square error. Note that due to the discontinuity between the states of both neural networks, there are impulses at the switching times as we have expected previously (recall Remark 1).

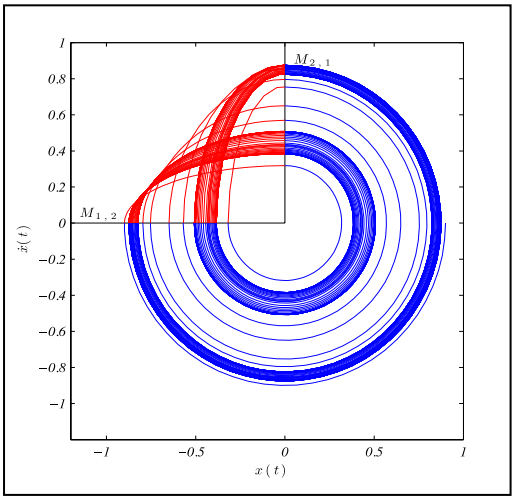


**Fig. 3** Phase Plane: $\omega = 3.5\left(1 - x(t_i)\right)$, $i mod 2 = 1$.

Finally, we follow the Gray Box Strategy with weight and state actualization at the switching times. We use the same topology and learning parameters as in the latter case. As a result, we obtain the graphics, shown in Fig. 5. Note that there are not impulses at the switching times and that the error is reduced. Observe that even when the common sense says that we can only identify stable systems; it is possible to identify unstable subsystems if the global system remains stable. The advantage of using the Gray Box Strategy is that we could identify the chaotic behavior of the system without changing the nature of the original system. If we compare these two strategies, we can see the following:

- The Gray Box Strategy without any actualization at the switching times retains the hybrid nature of the system, but it has discontinuities.
- The Gray Box Strategy with actualization, retains the hybrid nature of the system, and eliminates the discontinuities presented in the Gray Box Strategy without actualization.

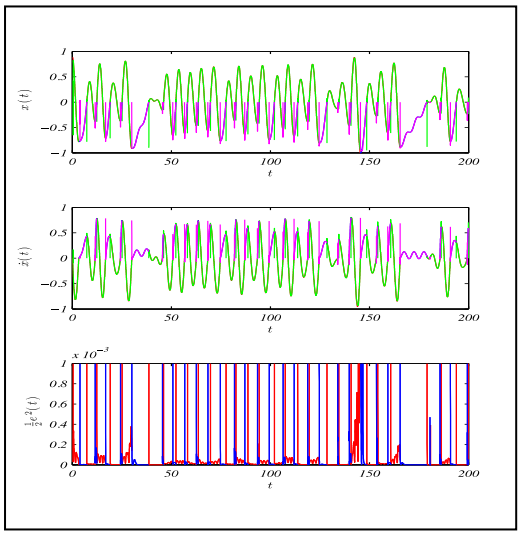

**Fig. 4** Gray Box Strategy Identification ($\sum_1$: red line, $\sum_1$ identification: green line, $\sum_2$: blue line, $\sum_2$ identification: magenta line).

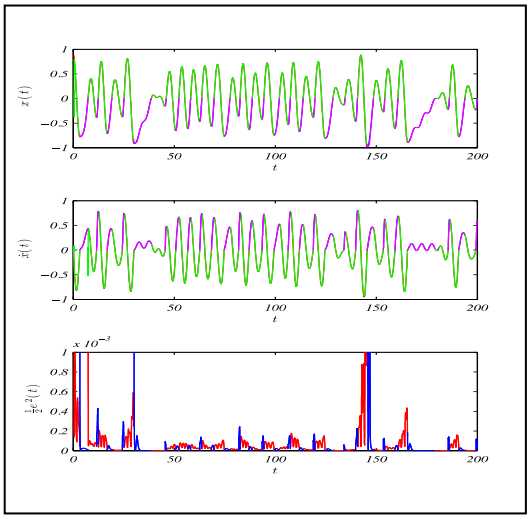

**Fig. 5** Gray Box Strategy with ANN Identification ($\sum_1$: red line, $\sum_1$ identification: green line, $\sum_2$: blue line, $\sum_2$ identification: magenta line).

## 5 Conclusion

This paper presents an intelligent approach to identify complex systems following a hybrid structure approach. We introduced the topology of the Hybrid Trainable Recurrent Neural Network. Two strategies are presented: Gray Box and Gray Box strategy with actualization of the neural network state and weights. The Gray Box strategy without actualization can identify the system into the locations and preserve the complex nature of the system, but it has several errors at the switching times. The Gray Box strategy with weight and state actualization overcomes the disadvantages of the Gray Box strategy without actualization, making it a suitable option to identify a complex system with a hybrid nature even in the presence of chaotic behavior.

## References

1. P. J. Antsaklis, X. Koutsoukos, J. Zaytoon: On Hybrid Control of Complex Systems: A Survey. Eur. J. Automat., Vol. 32, No. 9, pp. 1023–1045 (1998)
2. D. Back,T.P. Chen: Approximation of hybrid systems by neural networks. In: Proceedings of Int. Conf. on Neural Inf. Proc. and Intelligent Inf. Syst., Springer-Verlag, pp. 326–329 (1997)
3. A. Bagdasaryan: Systems Theoretic Techniques for Modeling, Control, and Decision Support in Complex Dynamic Systems. In: CoRR abs/1008.0775 (2010)
4. I. S. Baruch, C.R. Mariaca-Gaspar, J. Barrera-Cortes: Recurrent Neural Network Identification and Adaptive Neural Control of Hydrocarbon Biodegradation Processes. In: Recurrent Neural Networks, Xiaolin Hu and P. Balasubramaniam, (Eds.), Croatia: I-Tech/ARS Press, ch. 4, pp.61–88 (2008)
5. I.S. Baruch, C.R. Mariaca-Gaspar: A Levenberg-Marquardt Learning Algorithm Applied for Recurrent Neural Identification and Control of a Wastewater Treatment Bioprocess. Int. Journal of Intelligent Systems, vol. 24, pp. 1094–1114 (2009)
6. I. S. Baruch, R. Galvan-Guerra, S. M. Hernandez: Distributed Parameter Bioprocess Plant Identification and I-Term Control Using Decentralized Fuzzy-Neural Multi-Models. In Advances in Reinforcement Learning, Abdelhamid Mellouk (Ed.), Croatia: InTech, ch. 23, pp. 421–450 ( 2011)
7. M.S. Branicky, V.S Borkar, S.K. Mitter: A Unified Framework for Hybrid Control: Model and Optimal Control Theory. IEEE Trans. on Automatic Control, vol. 43, pp. 31–45 (1998)
8. M.S Branicky: Multiple Lyapunov functions and other analysis tools for switched and hybrid systems. IEEE Trans. on Automatic Control, Vol. 43, No. 4, pp. 475–482 (1998)
9. M. Buss, M. Glocker, M. Hardt, O. von Stryk, R. Bulirsh, G. Schmidt: Nonlinear Hybrid Dynamical Systems: Modeling, Optimal Control, and Applications. In: Lecture Notes in Control and Information Sciences, vol. 279, Springer-Verlag (2002)

10. C. Cassandras, D.L. Pepyne, Y. Wardi: Optimal Control of a Class of Hybrid Systems. IEEE Transaction on Automatic Control, vol. 46, pp. 398–415 (1998)
11. R. Galvan-Guerra, J.E. Velázquez-Velázquez, V. Azhmyakov: Explicit Switching Times and Location Detection for Linear Hybrid Systems. In: Proc. of the 7th Int. Conf. on Electrical Engineering, Computing Science and Automatic Control, Tuxtla Gutiérrez, Mexico, pp. 134–139 (2010)
12. A. García, I. Chairez, A. Poznyak: Hybrid DIfferential Neural Network Identifier for Partially Uncertain Hybrid Systems. In: Recent Advances in Intelligent Control Systems, Springer-Verlag (2009)
13. A. Hassibi, S. P. Boyd, J. P. How: Control of Asynchronous Dynamical Systems with Rate Constraints on Events. In: Proceedings of the IEEE Conference on Decision and Control, 2:1345–1351 (1999)
14. T. Hayakawa, W. M. Haddad, K. Y. Volyanskyy: Neural network hybrid adaptive control for nonlinear uncertain impulsive dynamical systems. Nonlinear Analysis: Hybrid Systems, vol. 2, pp. 862–874 (2008)
15. W. Holderbaum: Application of Neural Network to Hybrid Systems with Binary Inputs. IEEE Trans. on Neural Networks, vol. 18(4), pp. 1254–1261 (2005)
16. S. Kamalasadan: A Novel Multi-Agent Controller for Dynamic Systems based on Supervisory Loop Approach. Engineering Letters, EL_14_2_10 (2007)
17. A.B. Kurzhanskii, P. Varaiya: New Directions in Applications Control Theory. In: Lecture Notes Control Inform. Sci., Berlin: Springer, vol. 321, pp. 193–205 (2005)
18. L. Ljung: System Identification: Theory for the User. Prentice Hall, New Jersey, (1987)
19. N. Messai, B. Riera, J. Zaytoon: Identification of a class of hybrid dynamic systems with feed-forward neural networks: About the validity of the global model. Nonlinear Analysis: Hybrid Systems, vol. 2, pp. 773–785 (2008)
20. K.S. Narendra, K. Parthasarathy: Identification and Control of Dynamic Systems Using Neural Networks. IEEE Trans. Neural Networks, vol. 1, pp. 4–27 (2008)
21. V.R. Nosov: Complex Dynamics in an Ideal Commutable Pendulum. In: Proceedings of the 5th International Conference on Electrical Engineering, Computing Science and Automatic Control, Mexico, Mexico (2008)
22. S. Paoletti, A. Juloski, G. Ferrari-Trecate, R. Vidal: Identification of Hybrid Systems: A Tutorial. European Journal of Control, Vol. 13/2-3, pp. 242–260 (2007)
23. A. Van der Schaft, H. Schumacher: An Introduction to Hybrid Dynamical Systems. Berlin: Springer (2000)

ISSN 1870-4069

# Android App of Location Awareness Using Li-Fi

Sergio Sandoval Reyes, Victor Hugo Herver Segura

Instituto Politecnico Nacional, Centro de Investigacion en Computacion, Mexico City, Mexico

{sergio.sandoval9, vicherver }@gmail.com

**Abstract.** Li-Fi is a technology that uses visible light from a Light Emitter Diode (LED) to transmit high speed data to a photo detector, which is connected to a smartphone or tablet. Location awareness refers to devices that can passively or actively determine their location with respect to a well-known location wireless communications device. In this paper we describe a Li-Fi based application, in which a smart phone or tablet with a light sensor and within the range of a Li-Fi lamplight, immediately trigger events like displaying a picture, accessing a Web page, or playing a video.

**Keywords:** Visual light vommunications, Li-Fi lamps, Android.

## 1 Introduction

Li-Fi is a term that was coined by Harald Haas [1, 2] derived from a technology known as visible light communication (VLC). This technology uses light from light-emitting diodes (LEDs) as a medium to deliver wirelessly high-speed communication in a similar manner to Wi-Fi [3]. VLC works by switching the current to the LEDs off and on at a very high speed, too fast to be noticed by the human eye. Direct line of sight is not necessary for Li-Fi to transmit a signal; light reflected off the walls can work as well reaching rates of about 70 Mbit/s. Although both Wi-Fi and Li-Fi transmit data over the electromagnetic spectrum, Wi-Fi utilizes radio waves, whereas Li-Fi uses visible light. Furthermore, while the bandwidth with Wi-Fi is close to full capacity, Li-Fi has almost no limitations on capacity. The visible light spectrum is 10,000 times larger than the entire radio frequency spectrum [4]. Researchers have reached data rates of over 10 Gbit/s [5].

Location awareness refers to devices that can passively or actively determine their location with respect to a well-known location wireless communications device. Location awareness enables new applications for ubiquitous computing systems and mobile phones or tablets. Such applications include the automatic reconfiguration of a computing device to suit the location in which it is currently being used. Examples include publishing special offers to potential customers who are near to the retailers [6].

This paper describes a Li-Fi based application, in which a smart phone or tablet with a light sensor and within the range of a Li-Fi lamplight, immediately trigger events like displaying a picture, accessing a Web page, or playing a video. The

remainder of this paper is organized as follows: Section 2 presents a summary of works related to location-aware services. Section 3 describes the design of our location-aware application with Li-Fi lamps and Android phone or tablet with a light sensor. Section 4 shows the results of the implementation. Finally, our conclusions and future work are presented in Section 5.

## 2 Related Work

Several research works on VLC technologies have been proposed. The most important are described in the following.

### 2.1 Leds--Leads-You-Right-To-A-Discount

In [7, 8] ByteLight an English Company focused on using LEDs to provide high-speed data communications—the technology referred to as Li-Fi, felt their technology was better suited to helping people find their way around large indoor spaces. The idea was the following: imagine that you are in a department store that has replaced a number of its traditional lightbulbs with ByteLights. The lights, flickering faster than the eye can see, would emit a signal to passing smart phones. Your phone would read the signal through its camera, which would direct the smart phone (Figure 1), to pull up a deal offering a discount on a product on a nearby rack.


**Fig. 1.** A ByteLight's LED bulbs system.

### 2.2 Philips Shopping Assistant With Leds And Smart Phone

In [9] Phillips Lighting showed a LED-based indoor location detection technology. The system is similar to ByteLight, in terms of location-determination technology that relies on one-way communication between networked LED-based luminaires and customers' smartphones. In both cases the customer requires however, to download an application to utilize the technology. The communication link from luminaires to the smartphone would deliver the location data and offers. Figure 2.

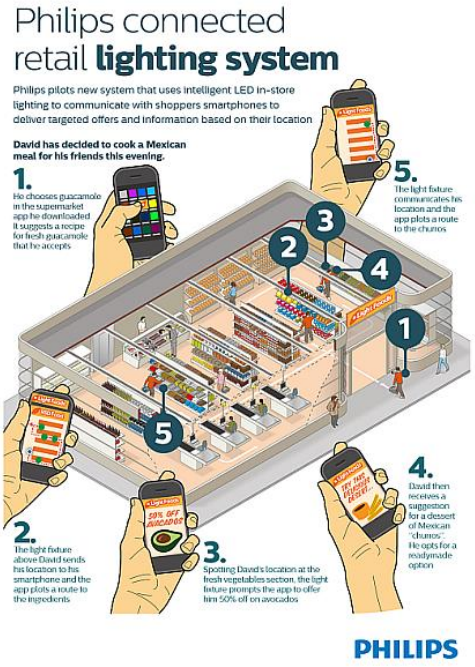


**Fig. 2.** Philips Lighting LED-based indoor location detection technology.

## 2.3 Oledcomm Li-Fi

Oledcomm [10] is a French Company that produces LiFi equipment in the telecom, and industrial markets, see Figure 3. It also sells kits to experiment with the Li-Fi technology.


**Fig. 3.** Oledcomm Li-Fi.

## 3 A Location-Aware Li-Fi Application

In the following we develop a location-aware Li-Fi application in which when an Android phone or tablet with a light sensor, is within the range of a Li-Fi lamplight, it will immediately display a picture, or access a Web page, or play a video, depending of the ID code of the lamplight. In order to do that, we will use the Oledcomm GEOLiFi XS Kit [11]. This kit contains: a) 3 GEOLiFi LED lamps, b) 1 GEOLiFi Android Tablet with an embedded sensor light; c) 1 extra GEOLiFi Dongle to be used with a Smartphone; and d) 1 GEOLiFi SDK Library. See Figure 4.


**Fig. 4.** The Oledcomm GEOLiFi XS Kit.

### 3.1 Displaying A Picture With Lifi

The GEOLiFi SDK Library has a small tutorial of how to use the Oledcomm GEOLiFi API. We begin loading the last version of Java SDK and Android Studio. After that we create a new Android application specifying the project and packages names with (in our case), minimum SDK 3, target SDK Android 4.4.2 and compiling with SDK 20. The most important part is in the MainActivity class in the *LiFiLocation ()* method, Figure 5:

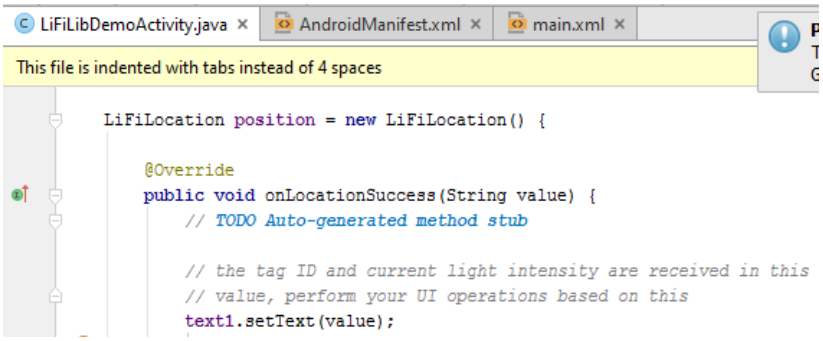


**Fig. 5.** The LiFiLocation () method.

This method is used for retrieving geolocation data for a phone or tablet from a lamp Li-Fi. When this happens the corresponding Id lamp will be available. In our case, the Id of every one of the three lamps were:

*a)* Lamp 1: 0xd5d5
*b)* Lamp 2: 0x6390
*c)* Lamp 3: 0x6e71

Having known the Ids of the three lamps, we simply use the first Id (0xd5d5) for displaying a picture in the Tablet with the following java switch code, Figure 6:

```
switch (value){
    case "0xd5d5":
        flag_nav=false;
        imagen.setVisibility(View.VISIBLE);
        imagen.setImageResource(R.drawable.cic_logo);
        video.setVisibility(View.GONE);
        web.setVisibility(View.GONE);
        break;
```

**Fig. 6.** Code for displaying a picture when the Tablet receives light from lamp1.

Of course, the *cic_logo.png* picture must be already available in the *res --> drawable directory*.

### 3.2 Displaying A Web Page With Li-Fi

The following java code allows access to a Web page when the tablet receives the light code (0x6390) from lamp 2. See Figure 7.

```
case "0x6390":

    web.setVisibility(View.VISIBLE);
    imagen.setVisibility(View.GONE);
    video.setVisibility(View.GONE);

    if (flag_nav==false)
    {/*La bandera cambia de estado para permitir que la pagina sea cargada*/
        web.loadUrl("http://www.google.com");
        flag_nav=true;
    }
    break;
```

**Fig. 7.** Accessing a Web page when a Tablet receives light code from lamp 2.

### 3.3 Displaying A Video With Li-Fi

To display a video using Li-Fi, we use the light code *0x6e71* and the following java code, Figure 8. The *video.mp4* must be already stored in this case, in the res→raw directory.

```
case "0x6e71":

    flag_nav=false;
    video.setVisibility(View.VISIBLE);
    imagen.setVisibility(View.GONE);
    web.setVisibility(View.GONE);
    Uri uri = Uri.parse("android.resource://com.example.lifilibrarydemo/"+ R.raw.video);
    video.setVideoURI(uri);
    video.start();
    break;
```

**Fig. 8.** Displaying a video with Li-Fi.

## 4 Experiments and Results

For the experiments we use as mentioned an Oledcomm GEOLiFi XS Kit with an Android OS 4.4.2 Tablet (Figure 9), thus as an Android 5.0 Smartphone Sony Xperia M4 Aqua, but with a light sensor connected into the earphone jack (Figure 10).

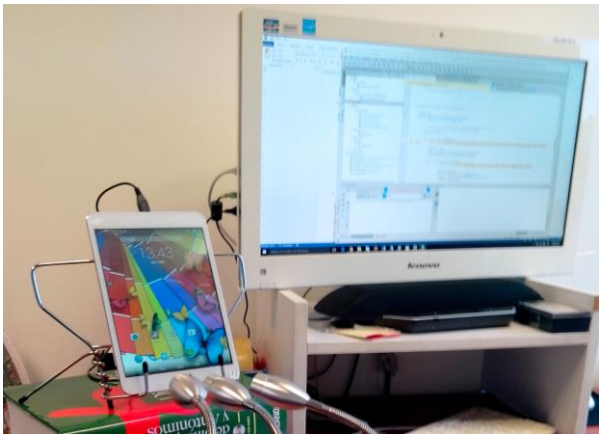

**Fig. 9.** GeoLiFi Kit Android Tablet 4.4.2 and three Li-Fi lamps.

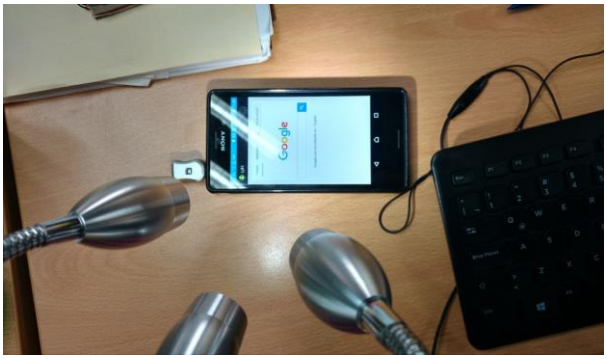

**Fig. 10.** Smartphone with attached Li-Fi sensor into the earphone jack.

Figure 11 show the corresponding picture, Web page (overlapping the picture) and the video (in the upper left corner). In this same figure it can also be noticed the embedded Li-Fi sensor (down to the right from the camera lens).

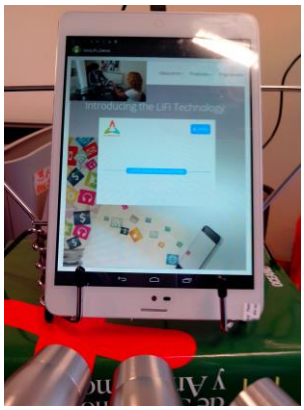


**Fig. 11.** Tablet with an embedded Li-Fi sensor.

### 4.1 Discussion of Results

Both devices worked fine with the Li-Fi lamps. However the smartphone with the attached Li-Fi sensor was less sensible to the Li-Fi light than the Oledcomm Tablet. The results obtained showed that indeed Li-Fi transmit data via the light from the lamps.

## 5 Conclusions

A location-aware Li-Fi application was developed using three Li-Fi lamps and two Android devices with a Li-Fi sensor. When the tablet or the smartphone was within the range of a Li-Fi lamplight, the light sensor read the code light from the lamp under test and triggered events like displaying a picture, accessing a Web page, or playing a video, according to the respective light code. This application may still be expanded beyond the actual state, making it more useful by developing for example, a mobile application to guide people through large indoor spaces like museums and stores.

**Acknowledgements.** This work was supported by the Instituto Politecnico Nacional Project SIP 20161439.

## References

1. Harald Haas. Harald Haas: Wireless data from every light bulb. http://www.ted.com/talks/harald_haas_wireless_data_from_every_light_bulb (2016)

2. Tsonev, Dobroslav, Videv, Stefan, Haas, Harald: Light fidelity (Li-Fi): towards all-optical networking. In: Proc. SPIE (Broadband Access Communication Technologies VIII) 9007 (2). doi:10.1117/12.2044649 (2013)
3. Sherman, Joshua: How LED Light Bulbs could replace Wi-Fi, Digital Trends. http://www.digitaltrends.com/mobile/light-bulb-li-fi-wireless-internet/ (2013)
4. Haas, Harald: High-speed wireless networking using visible light. SPIE Newsroom. doi:10.1117/2.1201304.004773; http://www.spie.org/newsroom/4773-high--speed-wireless-networking-using-visible-light (2013)
5. Vincent, James: Li-Fi revolution: internet connections using light bulbs are 250 times faster than broadband. http://www.independent.co.uk/news/science/li-fi-revolution-internet-connections-using-light-bulbs-are-250-times-faster-than-broadband-8909320.html (2016)
6. Wikipedia: Location awareness. https://en.wikipedia.org/wiki/Location_awareness (2016)
7. MIT Technology Review. LEDs Could Lead You Right to a Discount. https://www.technologyreview.com/s/426869/leds-could-lead-you-right-to-a-discount/ (2016)
8. AcuityBrands. ByteLight Services: Indoor positioning. http://www.acuitybrands.com/solutions/services/bytelight-services-indoor-positioning (2016)
9. IEEE Spectrum. Philips creates shopping assistant with LEDs and Smart Phone, February.http://spectrum.ieee.org/tech-talk/computing/networks/philips-creates-store-shopping-assistant-with-leds-and-smart-phone (2016)
10. Oledcomm Li-Fi. http://www.oledcomm.com/home/lifi (2016)
11. Oledcomm. GEOLiFI XS Kit. http://www.oledcomm.com/product/kit-lifi-xs (2016)

ISSN 1870-4069

# Clustering Techniques for Document Classification

Julio Fernández[1], Jarvin A. Antón-Vargas[1], Yenny Villuendas-Rey[1,2], José F. Cabrera-Venegas[1], Yusbel Chávez[1], Amadeo J. Argüelles-Cruz[3]

[1] Universidad de Ciego de Ávila,
Departamento de Ciencias Informáticas, Ciego de Ávila,
Cuba

[2] Instituto Politécnico Nacional,
Centro de Innovación y Desarrollo Tecnológico en Cómputo, CDMX,
Mexico

[3] Instituto Politécnico Nacional, Centro de Investigación en Computacion, CDMX,
Mexico

janton@unica.cu, yenny.villuendas@gmail.com

**Abstract.** This paper is intended to study the existing classification and information retrieval techniques in order to use an algorithm that will group the a set of documents. Therefore, the unfolding of knowledge in texts is selected as the proper methodology to be followed and the steps are explained in order to reach the unsupervised documents classification. After conducting an experiment with three of the most known methods of unsupervised documents classification and the assessment of the results with the Silhoutte index, it could be observed that the better grouping was with four groups, whose main characteristic was to deal with subjects such as: information management information, systems management, artificial intelligence, and digital image processing.

**Keywords:** Document classification, clustering, silhouette.

## 1 Introduction

Within a few years Pc´s have become a universal tool for all kinds of cultural, professional and commercial activities. Technological advancements in recent years have resulted in an exponential increase of digital information, which requires the development of specific tools for the retrieval and management of information [1]. That is the selection of a piece of information, among all the available information, for a specific user. This job is performed by the information retrieval systems [2, 3]. These systems deal with large databases composed of documents and use a model of representing information [4, 5], artificial intelligence techniques and data mining, they also process queries from users delivering the relevant documents in an appropriate range of time.

The main purpose of this kind of marketing is contacting a certain group of people to meet a specific goal (offer a service, insurance, credit card, etc.), but the problem of chose the group of costumers willing to buy the service is considered NP-hard [2]. For Due to the existence of repositories in different institutions with an increasing amount of documents in digital format [6], it has become necessary to filter all the information in order to obtain the most accurate information needed [7]. That is, discarding all that is not of interest for the users and keeping what is useful. Sometimes it is interesting to know about a particular subject, but this would result in losing precious time looking for irrelevant information. In a large database, it is unthinkable to do a manual selection of these texts, i.e. it is very difficult to precisely know what all these texts are about. Therefore, it would be very useful to be provided with an automatic tool that would properly gather and manage text documents that meet some similar criteria to the search and explore the collection throughout the clusters obtained [7].

The rest of the paper is organized as follows. Section 2 details some materials and methods used and section 3 offers a discussion about the results obtained. Finally the paper ends with some conclusions and future research suggestions.

## 2 Materials and Methods

### 2.1 Collecting and Preprocessing Texts

This is the first step of the process and consists of extracting the plain information that appears in a set of documents that have been previously grouped [8]. Since all the theses from the faculty are in PDF format, it was necessary to find a mechanism to grab text from these files.

In order to extract text from PDF files, an expert library called PDFBox was used [9]. This library offers a wide range of preprocessing tasks such as text extraction, merging multiple documents into a single one, converting plain text into a PDF file, creating PDF files from images, printing documents and others. From all these features, it was decided to work with the extraction of text from a PDF file to plain text, where it will be easier to deal with.

In addition to this library, it was used another library called FontBox [9] that contains various types of fonts to make the PDFBox library fonts compatible with the most commonly known typefaces.

### 2.2 Lexical Analysis: Segmentation

Once the text from the documents have been obtained, the first operations to be performed on the text consist on segmenting large chains into corresponding words. This process is known as the separation of lexical components [10]. These tokens (which are just the words contained in the text) are obtained using the blank space characters for segmenting the whole text into independent words.

### 2.3 Filtering and Removing Stopwords

A second step is to filter all non-alphabetical characters such as numbers and punctuation marks, since they do not provide relevant information to the classification. Then, all the text is rewritten in lowercase, this will be useful to identify the same word, regardless it is uppercase or lowercase, be identified with the same word. Afterwards, another filtering is performed to eliminate those words that do not add relevant information such as pronouns, articles and conjunctions. These words are known as stopwords [11]. A list of Spanish and English stop-words was taken form [12], in order to eliminate those words from the search.

### 2.4 Standardization: Stemming

Once the stop-words are removed from the text, lexemes of the remaining words are sought in order to remove those words derived from the same stem. Words that share the same lexeme are treated as if they were the same word, this is especially useful for words that have different number and gender because they share the same meaning [13].

In order to find the lexemes from each word, a Java-based software was used. This software is Snowball [14], which is used in several areas of information retrieval and supports multiple languages including Spanish and English. An example of its functions appears in the table 1.

**Table 1.** Conversion from word to lexeme.

| Words | Lexemes |
|---|---|
| *runs* | *run* |
| *taken* | *take* |

A direct consequence of the use of the software is that it allows us to continue filtering the text because all those words and their variations that basically mean the same are suppressed. This affects nouns, adjectives, verbs and adverbs, but not conjunctions and prepositions because they were previously filtered as stop-words.

**Table 2.** Conversion to a unique word list.

| Words | Stem |
|---|---|
| *take* | *take* |
| *taken* | |
| *runs* | *run* |
| *running* | |

Notice that the words sharing the same lexeme are considered as the same word. Otherwise, it would be more difficult to find relationships among documents because words differing in just one letter would be considered different words. This would make

it difficult to accomplish if we take into consideration the variants of a same verb in different conjugation.

### 2.5 Unique Word List

To identify the set of documents, it must be created an alphabetically sorted word list having the words from all documents, the only requirement is that the same word should not be repeated. To remove repeated words, an alphabetically sorted word list will consider repeated words, and therefore, they will be removed from the list of words. To create a unique word list, the method used is to generate a list for each document with partial single words, that is, where there is neither repeated words or two or more words with the same lexeme or stop-words- later, the word list is alphabetically arranged.

After doing this with each of the documents a unique global word list is drawn up for all documents using the previously generated lists from partial words in each document. By making an individual process for each document, it is faster to create a list of unique words because in this process there has been many filtered words that provide a lot of extra processing.

### 2.6 Feature Generation

At the end of the previous section a basis of a vector space was obtained to represent each of the documents. It would be enough to take into account the times a word appears in a given document forming a vector with an equal length to the whole word list. This concept is often called term frequency (tf). Table 3 shows the representation of a textual corpus in the vector space [15], where the frequency of a term t in a document d is the sum of the number of times it appears in the document.

**Table 3.** Vector representation of a document corpus.

| | $Term_1$ | $Term_2$ | ... | $Term_m$ |
|---|---|---|---|---|
| $Document_1$ | $tf_{d1}(t_1)$ | $tf_{d1}(t_2)$ | ... | $tf_{d1}(t_m)$ |
| $Document_2$ | $tf_{d2}(t_1)$ | $tf_{d2}(t_2)$ | ... | $tf_{d2}(t_m)$ |
| ... | ... | ... | ... | ... |
| $Document_n$ | $tf_{dn}(t_1)$ | $tf_{dn}(t_2)$ | ... | $tf_{dn}(t_m)$ |

However, not all words are equally relevant to discriminate against among the documents since there are words that are very common to all documents and thus do not serve to distinguish a document from other.

Due to the previous vector representation for each document is modified so that those words that do not serve to distinguish between documents are not taken into account. For that it is applied the TF-IDF (Term Frequency–Inverse Document Frequency) which is defined in the following formula:

$$TF - IDF(t,d) = tf_d(t) * \frac{logN}{df(t)} - 1, \quad (1)$$

where N is the total number of documents in the corpus, and df (document frequency) is the number of documents from the entire corpus in which that word appears. Thus, we see that if a word appears in all documents (such as Sp. "tener"), after this transformation its value in the table is null. The word count is performed using as a reference the unique word list that had been previously generated. An alphabetically arranged word list serves to look into each document and find the number of times each word is repeated in the text.

At the end of this text processing a matrix with a unique number associated with a corresponding associated number which will be used for further analysis and classification. This matrix is called word-documents matrix, and denoted by the letter M, it has a very large data and is based on the set of documents.

## 3 Discussion and Results

In this section the characteristics of the set of documents on which the experimentation is carried out are detailed. The experimental protocol is explained, describing the algorithms used to perform the clustering of the documents. Then is defined the evaluation metric to analyze the results of the experimentation.

### 3.1 Description of the Corpus of Documents

The FCI (Faculty of Computer Science) of UNICA (University of Ciego de Avila, Cuba) has a constantly increasing repository of theses in digital format. It has documents dating from the first graduation of computer engineering, class of 2006. These documents are in PDF format so it was sought to deal with this format.

**Table 4.** Description of the corpus used in this study.

| Scholar year | Engineering Thesis | Master Thesis | Total |
|---|---|---|---|
| 2005-2006 | 5 | 0 | 5 |
| 2006-2007 | 6 | 0 | 6 |
| 2007-2008 | 7 | 5 | 12 |
| 2008-2009 | 18 | 1 | 19 |
| 2009-2010 | 17 | 17 | 34 |
| 2010-2011 | 28 | 15 | 43 |
| 2011-2012 | 48 | 20 | 68 |
| 2012-2013 | 62 | 21 | 83 |
| 2013-2014 | 19 | 16 | 35 |
| Total | 210 | 95 | 305 |

PDF (Portable Document Format) is a document storage format developed by Adobe Systems. It is specially designed for documents that can be printed. This format is multi-platform since it can be viewed in all major operating systems (Windows, Unix \ Linux or Mac) without modifying either the appearance or the structure of the original

document. It also serves as the standard (ISO 19005-1: 2005) for electronic files containing documents intended to be preserved for a long term.

Since the academic year 2005-2006 to the 2013-2014, Computer Engineering at the FCI UNICA has stored over 235 theses, 210 are diploma papers, and 25 master theses (see Table 4).

### 3.2 Experimental Protocol

In order to find the best way to group documents diploma papers, a comparison is performed among the different algorithms for grouping documents: k-means, SOM and Hierarchical Agglomerative in its variants Single-Link, Complete-Link and Centroid.

The main disadvantage of these algorithms is that they require to set the initial number of groups to obtain in most applications, and in this particular case, there are no criteria to correctly specify this value. This is because the Corpus of Diploma Papers of Computer Engineering at UNICA is not labeled in groups.

To solve the problem of unknowing the number of groups to obtain, a necessary parameter to apply clustering algorithms. These algorithms were run in a range of 2 to a quarter of the number of documents to be grouped $\frac{N}{4}$. that is, a total of $\frac{N}{4} - 1$ runs were made for each algorithm.

Later, to determine the best grouping method, it was necessary to analyze the results with an index of internal validation. In accordance with several authors [16], one of the best performing indices in this regard is the Silhouette index.

The Silhouette index is an indicator of the ideal number of groups. A higher value of this index indicates a more desirable number of groups. Silhouette coefficient for a set is given as the average coefficient of each object silhouette sample, s(i). This index can be used for both: a group of objects (cluster) or for each object. Silhouette coefficient for an object x is:

$$s(i) = \frac{b(i) - a\,(i)}{\max\{a(i),\ b(i)\}} \tag{2}$$

Where a(i) is the average distance from the object i to all other objects in their group and b(i) is the average distance from the object i to all other objects in the nearest group. The value of s(i) can be obtained by combining the values of a(i) and b(i) as shown below:

$$s(i) = \begin{cases} 1 - \frac{a(i)}{b(i)} & if\ a(i) < b(i) \\ 0 & if\ a(i) = b(i) \\ \frac{b(i)}{a(i)} - 1 & if\ a(i) > b(i) \end{cases} \tag{3}$$

According to the value of the total silhouette groups (structures) found they can be classified into:

– 0.71-1.0, the structures are solid.

– 0.51-0.70, the structures are reasonable.

– 0.26-0.50, the structures are weak and tend to be artificial alternate methods should for data analysis.

– <0.25, no structures are found

A value of s(x) near zero indicates that the object x is on the border of two groups. On the contrary, if the value of s(x) is negative, then the object should be assigned to the nearest group. This can be observed in Figure 1 with values forming silhouette 2 (b), 3 (c) and 4 (d) groups with the set of points of (a).

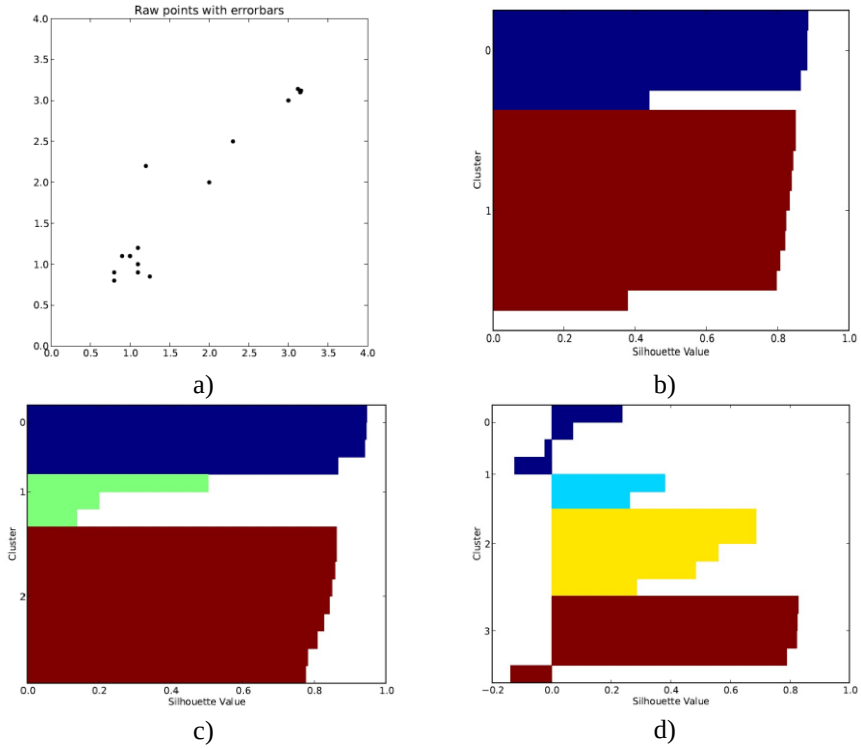


**Fig. 1.** Graphic representation of silhouette of different clusters.

As it can be seen, silhouette values are highlighted in the graphic with color values for different groups. A commonly used criterion for a better grouping is the average value of the outline of all objects in all groups. In this case, the greater Silhouette value will be chosen as the best grouping

### 3.3 Experiments and Discussion of the Results

In order to group documents in relation with their contents, the K-means, SOM and hierarchical Agglomerative algorithms are applied in combinations SingleLink, Complete-Link and Centroid on the data matrix characteristics obtained from the

Corpus of Diploma Papers. The input parameters using these algorithms are the set of data that is wanted to group. At the output of each algorithm a vector containing the labels is obtained with the group it belongs to each of the documents, as it can be seen in Figure 2.

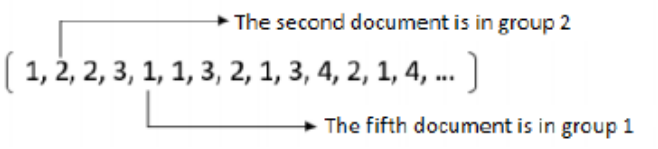


**Fig. 2.** Representation of algorithm's output vector.

The total number of documents in the Corpus is 305. It was necessary to do 76 runs for each algorithm for a range of number of groups of 2 to 77. Table 5 shows the 10 best values of Silhouette for each algorithm and the number of groups obtained in each case.

**Table 5.** Clusters with different Silhouette value for each algorithm.

| K-Means | | SOM | | Single | | Complete | | Centroid | |
|---|---|---|---|---|---|---|---|---|---|
| ***Index*** | ***Groups*** | ***Index*** | ***Groups*** | ***Index*** | ***Groups*** | ***Index*** | ***Groups*** | ***Index*** | ***Groups*** |
| 0.7681 | 4 | 0.7114 | 3 | 0.7088 | 4 | 0.5287 | 2 | 0.7281 | 4 |
| 0.7082 | 3 | 0.5658 | 4 | 0.6699 | 3 | 0.5167 | 3 | 0.5540 | 3 |
| 0.7071 | 2 | 0.4826 | 5 | 0.5014 | 2 | 0.3232 | 4 | 0.4825 | 2 |
| 0.6511 | 73 | 0.4655 | 6 | 0.3069 | 5 | 0.1364 | 77 | 0.4259 | 6 |
| 0.6292 | 74 | 0.4268 | 7 | 0.2110 | 6 | 0.1260 | 76 | 0.3709 | 5 |
| 0.6271 | 75 | 0.3814 | 8 | 0.1820 | 75 | 0.1083 | 75 | 0.3078 | 7 |
| 0.6184 | 76 | 0.2728 | 12 | 0.1807 | 76 | 0.0993 | 74 | 0.2960 | 8 |
| 0.6111 | 77 | 0.2515 | 14 | 0.1741 | 74 | 0.0735 | 73 | 0.2876 | 9 |
| 0.6085 | 71 | 0.2304 | 9 | 0.1688 | 77 | 0.0663 | 72 | 0.2782 | 10 |
| 0.6047 | 72 | 0.2201 | 10 | 0.1603 | 73 | 0.0520 | 6 | 0.2511 | 11 |

As it can be seen in the table, the K-means algorithm has the highest value of the silhouette obtained (0.7681) forming 4 groups. It was followed by the hierarchical agglomerative Centroid-Link algorithm which also obtained 4 groups but with an average value of silhouette a little lower (0.7281). Thirdly, the hierarchical agglomerative Single-Link algorithm performs a grouping of 4 groups but also with an average silhouette (0.7088).

Likewise, if we plot the three best silhouette values for each algorithm on the number of clusters obtained it shows that the formed clusters are composed of 2, 3, 4 and 5 groups. Three, out of the five algorithms used in experimentation received the best value in silhouette for a cluster consisting of four groups. K-means algorithm is the best value obtained. These results can be seen in Figure 3.

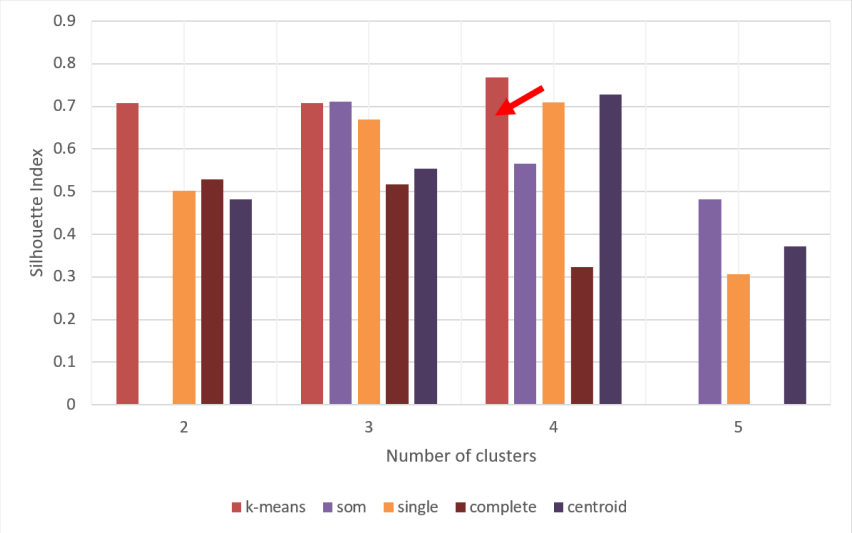


**Fig. 3.** Graphic of the three Silhouette values obtained by each algorithm with different number of clusters.

In order to understand more clearly the meaning of this Silhouette value, use Figure 4 where the silhouette of documents belonging to different groups can be seen, that is the documents belonging to the same group, appear together in a block.

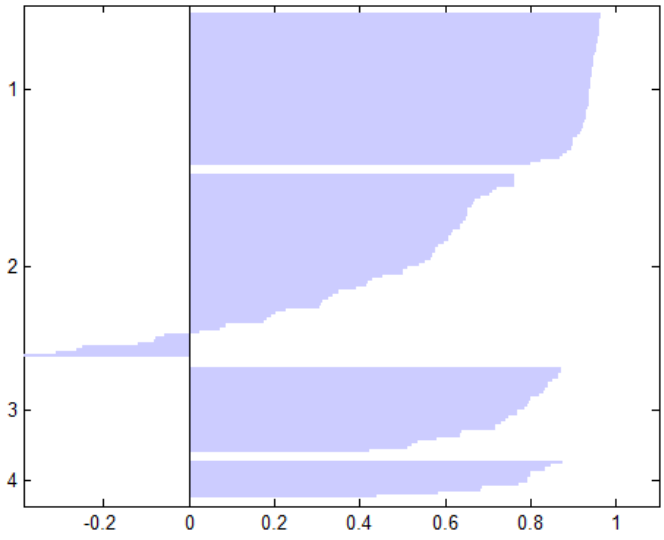


**Fig. 4.** Silhouette value of the documents by the four clusters obtained with K-means algorithm.

The silhouette value for each document is a distance that resembles how each document is similar to other documents within their own group. When compared with

the documents from other groups, taking values within a range of -1 to 1. As shown in Figure 4, the silhouette of the objects from the same group (for the four groups obtained) has close to 1 positive values and is wide which is an indicator of quality in the grouping. Only group 2 has a few objects with negative figures.

## 4 Conclusions

Clustering is amongst key text mining techniques for knowledge extraction from large collections of unlabeled documents. In this paper, we applied the Knowledge Discovery in Texts (KDT) methodology, and we use clustering to cluster a collection of thesis from the Faculty of Computer Science of the University of Ciego de Ávila in Cuba. Due to the lack of knowledge about the adequate number of desired clusters, we evaluated the different results according to an internal cluster validity index, which allow us to obtain a high-quality clustering. The best result corresponds to k-Means algorithm, with four clusters. The obtained clusters represent documents with different subjects, which are: information management systems, enterprise management systems, artificial intelligence and digital image processing.

**Acknowledgments**. The authors would like to thank the Instituto Politécnico Nacional (Secretaría Académica, Comisión de Operación y Fomento de Actividades Académicas, Secretaría de Investigación y Posgrado, Centro de Investigación en Computación, and Centro de Innovación y Desarrollo Tecnológico en Cómputo), the Consejo Nacional de Ciencia y Tecnología, and Sistema Nacional de Investigadores (SNI) for their economical support to develop this work.

## References

1. Rodríguez, E., Berrocal, J., Paniagua, C., Rodríguez, Á.: Algunas Técnicas de Clasificación Automática de Documentos. Cuadernos de documentación multimedia 15, pp. 1–2 (2004)
2. Wang, C., Song, Y., El-Kishky, A., Roth, D., Zhang, M., Han, J.: Incorporating world knowledge to document clustering via heterogeneous information networks. pp. 1215–1224 (2015)
3. Castillo, J., Fernández, J.: Methodology of Preprocessing of documents for Systems of Recovery of Information (2008)
4. Chowdhury, Gobinda: Introduction to modern information retrieval (2010)
5. Bernotas, M., Karklius, K., Laurutis, R., Slotkiene, A.: The peculiarities of the text document representation, using ontology and tagging-based clustering technique. Information Technology and Control 36(2), pp. 217–220 (2015)
6. Gamare, P., Patil, G.: Web Document Clustering using Hybrid Approach in Data Mining. International Journal of Advent Technology 3(7), pp. 92–97 (2015)
7. Hassan, M., Karim, A., Kim, J., Jeon, M.: Cdim: Document clustering by discrimination information maximization. Information Sciences 316, pp. 87–106 (2015)
8. Mu, T., Goulermas, J., Korkontzelos, I., Ananiadou, S.: Descriptive document clustering via discriminant learning in a co-embedded space of multilevel similarities. Journal of the Association for Information Science and Technology 67(1), pp. 106–133 (2016)

9. Apache PDFBox | A Java PDF Library. https://pdfbox.apache.org/ (September 2016)
10. Nalawade, Rahul, Samal, Akash, Avhad, Kiran: Improved Similarity Measure For Text Classification and Clustering. International Research Journal of Engineering and Technology (IRJET) (2016)
11. Wilbur, W., Sirotkin, K.: The automatic identification of stop words. Journal of information science 18(1), pp. 45–55 (1992)
12. Stopwords. http://www.ranks.nl/stopwords
13. Kanan, Tarek, Fox, Edward: Automated Arabic Text Classification with PStemmer, Machine Learning, and a Tailored News Article Taxonomy. J. Assoc. Inf. Sci. Technol (2016)
14. Porter, MF, Boulton, Richard: Snowball stemmer (2001)
15. Tang, Bo, He, Haibo, Baggenstoss, Paul, Kay, Steven: A Bayesian classification approach using class-specific features for text categorization. IEEE Transactions on Knowledge and Data Engineering 28(6), pp. 1602–1606 (2016)
16. Brun, Marcel, Sima, Chao, Hua, Jianping, Lowey, James, Carroll, Brent, Suh, Edward, Dougherty, Edward: Model-based evaluation of clustering validation measures. Pattern recognition 40(3), pp. 807–824 (2007)

ISSN 1870-4069

# Stochastic System Model Evaluated with First and Second Order Filters

Karen Alicia Aguilar Cruz, Romeo Urbieta Parrazales, José de Jesús Medel Juárez

Instituto Politécnico Nacional, Centro de Investigación en Computación,
Ciudad de México, Mexico

karen_ali320@hotmail.com, rurbieta700@gmail.com, jjmedelj@yahoo.com.mx

**Abstract.** This paper presents two stochastic filters considering autoregressive models of first and second order for parameter estimation and system identification. Each model is applied to a reference of the corresponding order and their recursive and non-recursive estimation results are compared; obtaining their error functional values to determine their performance. Due to the recursive methods give better approximation results, than the non-recursive ones, they are applied to describe the behaviour of the wind, which is a stochastic signal useful in the aerodynamic field, comparing the tracking results through off the functional error and the surroundings of the relative frequency histograms; including also a computational complexity graphic. To conclude, the second order filter has a better convergence performance at the expense of a higher computational cost, its pros and cons are mentioned. Nevertheless, choosing the filter order depends on its application.

**Keywords:** Estimation algorithms, recursive estimation, moment method, ARMA model, filtering techniques.

## 1 Introduction

Stochastic Systems (SS) have a great upswing in diverse scientific areas such as Biology, Physics and Chemistry [1]; where different techniques have been developed in order to give solutions to systems that can be modeled in an approximate way [2-4]. In past years, these systems have a greater relevance to deterministic models because they provide a much better characterization of the reality of the phenomena, including their uncertainty. In other areas like Administration, SS are used to determine the risk value of assets [5]; on the other hand, in Meteorology are applied to generate reliable models that allow the prediction of weather conditions with a bounded level of uncertainty [6-7].

Within the area of Control and Processing of Signals, SS look for the optimization of systems with random variables through their analysis [8-11], leading to the linear and non-linear Stochastic Filtering; being the linear Stochastic Filter with one or two delays, the model of interest for this paper.

Basic linear systems are those that can be modeled like a Black Box (BB), where only the inputs and outputs of the system can be measured, while its internal characteristics cannot be obtained directly [12-13]. The model considered in this work corresponds to a deterministic system with Gaussian noise described through an Auto-Regressive Moving Average (ARMA) model [14], leading to Gaussian linear stochastic systems, which are models that give response to BB systems through a parameter adjustment that allows the convergence to a reference system response.

Once the estimation is obtained it is necessary to determine the estimator algorithm performance by the comparison between the real and the identified responses by means of the functional error, which is a measure of how similar a signal is to a reference and how they converge to each other

Even when different filters have been designed, the question leads in which one is the best for a specific problem. For example, it will not be the same to identify the signals from a noisy turbulent wind to determine the angle variations of a flap in an airplane, than the temperature variations inside a home fridge. In some cases, the velocity of reaction is an important aspect, while in others the estimation or identification could be limited by hardware characteristics.

Within the present paper, two stochastic linear models of first and second order are presented. The Second Probability Moment (SPM) method was used [15] with finite difference equation to obtain their recursive forms for parameter estimation according to the stochastic ARMA selected model.

Then, for each different order model, their non-recursive and recursive descriptions are compared in an estimation task, determining the seconds lead to better results and these are applied to an identification example.

The example consists on determine the wind behavior, which is a practical case useful in Meteorology for obtaining weather conditions; in Aeronautic field due to the wind speed and direction are important parameters to map air routes; and in Control area, for obtaining the parameters an Unmanned Aerial Vehicle (UAV) needs for tracking trajectories tasks. Finally, the comparison of both models give as conclusion, criteria parameters for choosing one or the other in future applications.

## 2 Recursive First Order Stochastic Model

The representation of a BB system is given by (1) and (2), considering an ARMA (1, 1) stochastic model, with one input, one delay and evolution time $k \in Z_+$.

$$x_k = a_1 x_{k-1} + b w_{k-1}, \tag{1}$$

$$y_k = c x_k + d v_k, \tag{2}$$

where, for an instant of time $k$, $x_k \in R$ is the state variable, $\{y_k\} \subseteq N(\mu_{y_k}, \sigma^2{}_{y_k} < \infty)$ is the output variable, $\{w_k\} \subseteq N(\mu_{w_k}, \sigma^2{}_{w_k} < \infty)$ is a stochastic system excitation, $\{v_k\} \subseteq N(\mu_{v_k}, \sigma^2{}_{v_k} < \infty)$ is a perturbation of bounded

sequence, and $a_1, b, c, d \in R_{[-1,1]}$ are constants. According to the BB description, only $y_k$ and $w_k$ are measurable from the original system. So that, to initialize the model, not measurable variables and constants should be considered positive close to zero values, due to parameters are generally normalized acquiring values between 0 and 1 to avoid instability [16-18].

Beginning with (1) and (2) is obtained the recursive output $\hat{y}_k$ (3), having (4) as a generalized noise described by the noises that affect the system:

$$\tilde{y}_k = a_1 \tilde{y}_{k-1} + \tilde{v}_k, \tag{3}$$

$$\tilde{v}_k = -da_1 v_k + bw_{k-1} + dv_k. \tag{4}$$

Applying the second probability moment to (3), and using the expectation operator properties according to [19], it is obtained (5):

$$\tilde{a}_{1,k} = \left(E\{\tilde{y}_k \tilde{y}_{k-1}\} - dE\{\tilde{v}_{k-1}\tilde{y}_{k-1}\}\right)/\left(E\{\tilde{y}_{k-1}^2\}\right) \tag{5}$$

and the summarized description (6),

$$\tilde{a}_{1,k} = P_k / Q_k, \tag{6}$$

where $P_k = (\tilde{y}_k \tilde{y}_{k-1}) - d_k(\tilde{v}_{k-1}\tilde{y}_{k-1}) + (k-1)P_{k-1}$ and $Q_k = \tilde{y}_k^2 + (k-1)Q_{k-1}$ are the stationary functions which define the parameter (7):

$$\tilde{a}_{1,k} = \left[\tilde{y}_k \tilde{y}_{k-1} - d\tilde{v}_{k-1}\tilde{y}_{k-1} + (k-1)P_{k-1}\right]/\left[\tilde{y}_{k-1}^2 + (k-1)Q_{k-1}\right]. \tag{7}$$

Taking into account in (7) that **a)** $\tilde{a}_{1,k}$ is stationary while $P_{k-1}$ is described by $\tilde{a}_{1,k-1}Q_{k-1}$ and, **b)** the denominator is described only by $Q_k$; the estimated stochastic parameter in its recursive form is (8).

$$\tilde{a}_{1,k} = [(k-1)Q_{k-1}/kQ_k]\tilde{a}_{1,k-1} + \tilde{y}_k \tilde{y}_{k-1}/kQ_k - d\tilde{v}_{k-1}\tilde{y}_{k-1}/kQ_k. \tag{8}$$

So that, the identified output (9) could be based on the estimation (8), which includes an implicit recursion and the use of an innovation process; allowing $\tilde{v}_k$ to be approximated in distribution to a random variable $\tilde{\tilde{v}}_k$, such that $\mu(\tilde{\tilde{v}}_k) \approx \mu(\tilde{v}_k)$, $\sigma(\tilde{\tilde{v}}_k) \approx \sigma(\tilde{v}_k)$ and the distribution function $\{\tilde{\tilde{v}}_k\} \subseteq N\left(\mu_{\tilde{v}_k}, \sigma^2{}_{\tilde{v}_k} < \infty\right)$.

$$\tilde{\hat{y}}_k = \tilde{a}_{1,k}\tilde{y}_{k-1} + \tilde{\tilde{v}}_k. \tag{9}$$

The convergence error is based on the parameter estimation (8). The functional error is a recursive error measure which considers the second probability moment and allows obtaining the precision of an estimation algorithm in a probability sense. In a symbolic

way, from $\tilde{e}_k = a_1 - \tilde{a}_{1,k}$, the estimation functional error $\tilde{J}_k = E\{\tilde{e}_k \tilde{e}_k\}$ is presented recursively in (10):

$$\tilde{J}_k = (1/k)\left[\tilde{e}_k^2 + (k-1)\tilde{J}_{k-1}\right]. \tag{10}$$

## 3 Recursive Second Order Stochastic Model

The stochastic second order model, with two delays and one input (ARMA (2, 1)) is described by (11) and (12),

$$x_k = a_{1,k} x_{k-1} + a_{2,k} x_{k-2} + b w_{k-1}, \tag{11}$$

$$y_k = c x_k + d v_k, \tag{12}$$

where variables $x_k$, $y_k$, $w_k$ and $v_k$; as well as constants $a_1, b, c, d$ and now $a_2$; have the same characteristics and initializing considerations than those defining (1) and (2).

Expanding (11) and (12) is obtained the noise set (13) giving place to the recursive stochastic output (14), with two parameters to estimate ( $\tilde{a}_{1,k}$ and $\tilde{a}_{2,k}$ ).

$$\tilde{v}_k = -a_{1,k} d_k v_{k-1} - a_{2,k} d_k v_{k-2} + bcw_{k-1} + dv_k, \tag{13}$$

$$\tilde{y}_k = a_{1,k} \tilde{y}_{k-1} + a_{2,k} \tilde{y}_{k-2} + \tilde{v}_k. \tag{14}$$

Applying the second moment method to (14) and considering expressions in (15)

$$\begin{aligned} P_{k,1} &= (1/k)[(\tilde{y}_k \tilde{y}_{k-1} - \tilde{v}_k \tilde{y}_{k-1}) + (k-1)P_{k-1,1}], \\ P_{k,2} &= (1/k)[(\tilde{y}_k \tilde{y}_{k-2} - \tilde{v}_k \tilde{y}_{k-2}) + (k-1)P_{k-1,2}], \\ Q_{k,1,1} &= (1/k)[(\tilde{y}_{k-1} \tilde{y}_{k-1}) + (k-1)Q_{k-1,1,1}], \\ Q_{k,1,2} &= (1/k)[(\tilde{y}_{k-1} \tilde{y}_{k-2}) + (k-1)Q_{k-1,1,2}], \\ Q_{k,2,1} &= (1/k)[(\tilde{y}_{k-1} \tilde{y}_{k-2}) + (k-1)Q_{k-1,1,2}], \\ Q_{k,2,2} &= (1/k)[(\tilde{y}_{k-2} \tilde{y}_{k-2}) + (k-1)Q_{k-1,2,2}], \end{aligned} \tag{15}$$

we obtain the stochastic parameters (16) and (17), based on the second probability moment

$$\tilde{a}_{1,k} = P_{k,1}(Q_{k,1,1}) + P_{k,2}(Q_{k,2,1}) - d\tilde{v}_{k-1}\tilde{y}_{k-1} / kQ_{k,1,1}, \tag{16}$$

$$\tilde{a}_{2,k} = P_{k,1}(Q_{k,1,2}) + P_{k,2}(Q_{k,2,2}) - d\tilde{v}_{k-1}\tilde{y}_{k-2} / kQ_{k,2,2}. \tag{17}$$

And their recursive forms (18) and (19):

$$\tilde{a}_{1,k} = \left[(k-1)Q_{k-1,1,1}/kQ_{k,1,1}\right]\tilde{a}_{1,k-1} + \tilde{y}_k \tilde{y}_{k-1}/kQ_{k.1} - d\tilde{v}_{k-1}\tilde{y}_{k-1} / kQ_{k,1,1}, \tag{18}$$

$$\tilde{a}_{2,k} = \left[(k-1)Q_{k-1,2,2} / kQ_{k,2,2}\right]\tilde{a}_{2,k-1} + \tilde{y}_k\tilde{y}_{k-2}/kQ_{k.2,2} - d\tilde{v}_{k-1}\tilde{y}_{k-2} / kQ_{k,2,2}. \quad (19)$$

The identified output (14) is based on the estimation made by (18) and (19), with an explicit recursion and the use of an innovation process that allows it to be approximated in distribution by a random variable $\tilde{\tilde{v}}_k$, having $\mu(\tilde{\tilde{v}}_k) \approx \mu(\tilde{v}_k)$, $\sigma(\tilde{\tilde{v}}_k) \approx \sigma(\tilde{v}_k)$ and $\{\tilde{\tilde{v}}_k\} \subseteq N(\mu_{\tilde{v}_k}, \sigma^2{}_{\tilde{v}_k} < \infty)$ characteristics. Thus, the recursive stochastic output for the ARMA (2, 1) is determined by (20):

$$\tilde{\tilde{y}}_k = \tilde{a}_{1,k}\tilde{\tilde{y}}_{k-1} + \tilde{a}_{2,k}\tilde{\tilde{y}}_{k-2} + \tilde{v}_k. \quad (20)$$

On the other hand, comparing the two estimated parameters, considering the recursive errors (21) and (22),

$$\tilde{e}_{k,1} = a_1 - \tilde{a}_{1,k}, \quad (21)$$

$$\tilde{e}_{k,2} = a_2 - \tilde{a}_{2,k} \quad (22)$$

leads to the functional errors (23) and (24)

$$\tilde{J}_{k,1} = (1/k)\left[\tilde{e}^2_{k,1} + (k-1)^2\,\tilde{J}_{k-1,1}\right], \quad (23)$$

$$\tilde{J}_{k,2} = (1/k)\left[\tilde{e}^2_{k,2} + (k-1)^2\,\tilde{J}_{k-1,2}\right]. \quad (24)$$

## 4 Simulation of the First and Second Order Estimation Models

The behaviors of the presented models are analyzed through the parameters they estimate and their corresponding functional error as a criterion to measure their performance. Each different order filter is probed in their recursive and non-recursive forms to determine which of both versions is better. Parameters are normalized and then dimensionless, on the other hand, as the evolution time of the software was not measured, graphics are presented in function of number of iterations; the time in seconds will depend on the software characteristics.

To probe the first order model, it is necessary to have a first order reference signal, which in this case is created from a known constant parameter of value between 0 and 1, in this case closer to 1. Fig. 1 shows the estimated parameters compared to the reference. It is possible to see a faster convergence when using the recursive description and in both cases, it is obtained a smoothed approximation, so that, the recursive description is better. This statement also could be proved by their errors functional, which are shown in Fig. 2, where even they are similar it is possible to identify the error obtained recursively converges faster to zero.

Similarly, but now considering two reference parameters for the second order filter description; we obtain the parameter estimation from Fig. 3. In this figure, two constant parameters valued between 0 and 1, close to the bounds, are tryed to be approximated

simultaneously by using the second order recursive and non-recursive filter. The sintonization of more than one parameter is not an easy task because both parameters are related, in Fig. 3 only the second parameter is close to be approximated while the other reminds stationary to a different region but close to the reference. Fig. 4 matched with this and also helps to determine the recursive descriptions are the best.

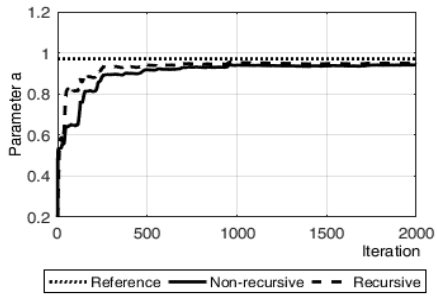


**Fig. 1.** Comparison of the normalized parameter $a$ estimated through the first order recursive and non-recursive model.

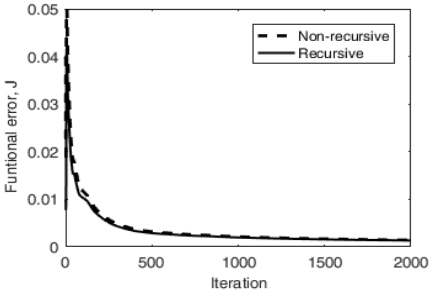


**Fig. 2.** Error functional from the parameters estimated through the recursive and non-recursive first order model.

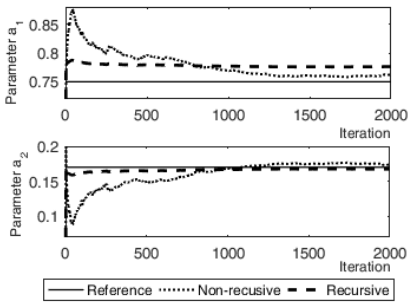


**Fig. 3.** Comparison of the normalized parameters $a_1$ and $a_2$ estimated through the second order recursive and non-recursive model.

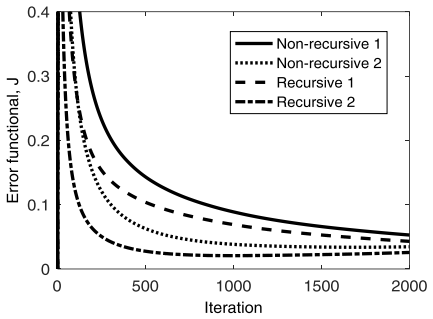


**Fig. 4.** Functional error of the parameters estimated through the recursive and non-recursive second order model.

## 5 Application Example and Results

In the area of renewable energies, models that allow the estimation of wind variations are required in order to establish design limits for a better use, and the increase of security [20]. Within the wind energy, the models described in the present paper could be applied to identify the wind speed from a specific geographic region or the power variations given by this resource [21].

To identify the real wind speed [7] shown in Fig. 5 (left), which represents the variation of its velocity in m/s, thought a timeslot of 100 s, both recursive stochastic models are used. The corresponding parameters are estimated and then applied in the identification models in order to compare their responses to the wind measured signal. The using of the recursive forms was taken because of the results obtained in Fig. 2 and Fig. 4, where the recursive parameter estimations, through the error functional, showed better performance than the non-recursive estimations.

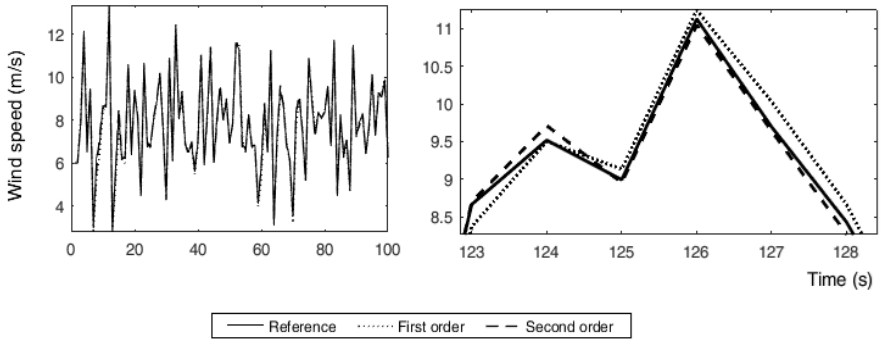


**Fig. 5.** Wind speed within an interval $t = 100s$, signal considered as a reference (left) and their estimation using first and second order methods (right).

The wind signal identifications, using both recursive models, are compared in Fig. 5 (right), where due to the large number of points defining the signal, it was considered only a smaller timeslot in order to visualize better the convergences. From Fig. 5 is possible to see the second order model has a faster convergence and better response to the shifting points in the signal; however, the first order model has visually a smoother performance, what is expected because of the model order. So that, for smooth variations a first order identification is acceptable.

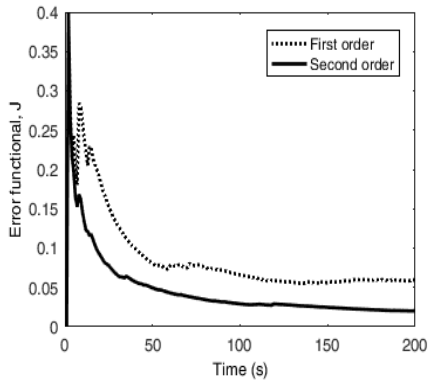


**Fig. 6.** Functional error of the output estimated signals, using the first and second order recursive methods.

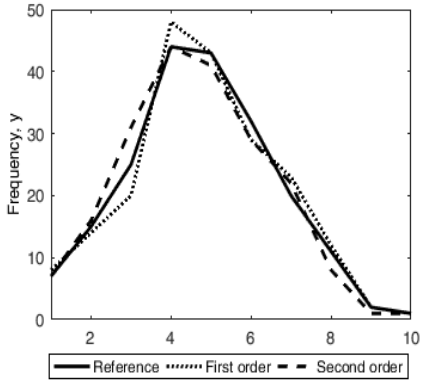


**Fig. 7.** Histogram of the output reference and the obtained estimations; using the recursive first and second order model.

A comparison between the parameter estimation and the system parameters cannot be done because the second ones are unknown, what means, it is only possible to determine the performance of the model through their identified outputs and the functional error from their output signals. Fig. 6 is the representation of the functional error obtained from the error between the output reference and the identified output signal, giving a better idea of the convergence each method has. In this figure is best seen the performance differences that was not obvious in Fig. 5.

To know if the identified output ranges corresponds to the reference range, Fig. 7 was obtained, which is the relative frequency histogram of the wind speed. From the Fig. 7 is possible to see that even with a similar distribution, the second order model produces a better envelope of the histogram.

When performing an extensive simulation of 100 repetitions of identification of the wind reference signal, using both recursive methods; and considering different initial conditions giving the stochastic sense to the system; it is observed that the obtained functional error by the identified signals cover a convergence region, as shown in Fig. 8, being this region more defined and with a faster convergence when using the second order model.

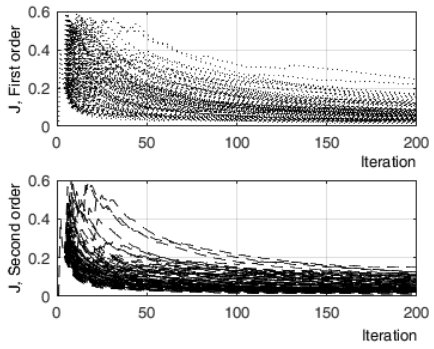


**Fig. 8.** Functional error obtained for the first and second order estimation methods; proof made with 100 different stochastic signals.

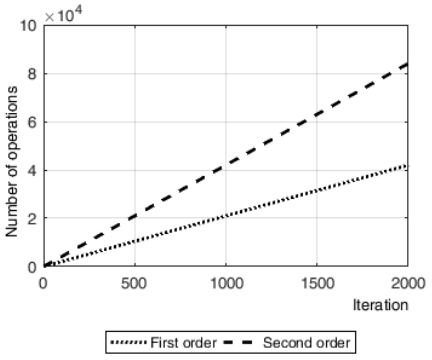


**Fig. 9.** Algorithm complexity of identifiers of first and second order.

Another characteristic which helps to compare both filters is the number of operations required to obtain an identification result. Fig. 9 displays how many the total number of operations needed are, when the iteration number increases through time.

## 6 Conclusions

The present paper describes two models with different order, first and second, to estimate stochastic parameters in a recursive and non-recursive form. According to the results, both methods have favorable characteristics, allowing the selection about which one of them is adequate for a specific system, being the recursive versions of both orders, the best.

Respect to the estimated parameters, the second order model has better approximation when not smooth variation is presented, but, it is more difficult to initialize the estimation and it was seen that only one parameter converges adequately. Nevertheless, the first order one generates more acceptable results when the parameters do not vary considerable and the approximation is easier.

Both models accomplish the objective of approximate the reference signal from the estimation of the parameters that affect the recursive model of the identifiers. However, although the second order model could be considered more accurate, its complexity is also bigger while having to tune two parameters simultaneously, instead of only one. Hence, for digital implementations, it could be more convenient the first order model.

Finally, both models analyzed have characteristics that made them useful in systems modeled as a Black-Box (BB), with stationary bounded input-output conditions; and the analysis made in this paper allows the reader to have in mind the advantages of using one or other filter order, according to its necessities.

## References

1. Britton, T., House, T., Lloyd, A. L., Mollison, D., Riley, S., Trapman, P.: Five challenges for stochastic epidemic models involving global transmission. Epidemics, 10, pp. 54–57 (2015)
2. Lecca, E. R., Puente, M. M.: Aplicaciones computacionales de las ecuaciones diferenciales estocásticas. Industrial Data, 9(1), pp. 064–075 (2006)
3. Mauricio, J. A.: Análisis de series temporales. Universidad Complutense de Madrid (2007)
4. Chernov, A., Debussche, A., Nobile, F.: Numerical methods for random and stochastic partial differential equations. Stochastics and Partial Differential Equations Analysis and Computations, 4(1), pp. 1–2 (2016)
5. Vitoriano, B.: Modelos y métodos de simulación estocástica. Aplicación en la valoración de opciones financieras.
6. Franzke, C. L., O'Kane, T. J., Berner, J., Williams, P. D., Lucarini, V.: Stochastic climate theory and modeling. Wiley Interdisciplinary Reviews: Climate Change, 6(1), pp. 63–78 (2015)
7. Emejeamara, F. C., Tomlin, A. S., Millward-Hopkins, J. T.: Urban wind: Characterisation of useful gust and energy capture. Renewable Energy, 81, pp. 162–172 (2015)
8. Ishizuka, S., Kajiwara, I.: Online adaptive PID control for MIMO systems using simultaneous perturbation stochastic approximation. Journal of Advanced Mechanical Design, Systems, and Manufacturing, 9(2), JAMDSM0015-JAMDSM0015 (2015)
9. Stojanovic, V., Nedic, N.: Robust Kalman filtering for nonlinear multivariable stochastic systems in the presence of non-Gaussian noise. International Journal of Robust and Nonlinear Control, 26(3), pp. 445–460 (2016)
10. Ramos, A., Cerisola, S.: Optimización estocástica. Pontificia Universidad COMILLAS de Madrid (2005)
11. Bartocci, E., Bortolussi, L., Nenzi, L., Sanguinetti, G. : System design of stochastic models using robustness of temporal properties. Theoretical Computer Science, 587, pp. 3–25 (2015)
12. Juárez, M., de Jesús, J., Zagaceta Álvarez, M. T., Palma Orozco, R.: Identificación con estimación para sistemas tipo caja negra. Revista Facultad de Ingeniería Universidad de Antioquia, (72), pp. 35–46 (2014)

13. Kristensen, N. R., Madsen, H., Jørgensen, S. B.: Parameter estimation in stochastic grey-box models. Automatica, 40(2), pp. 225–237 (2004)
14. Yaffee, R. A., McGee, M.: An introduction to time series analysis and forecasting: with applications of SAS® and SPSS®. Academic Press (2000)
15. Mátyás, L.: Generalized method of moment's estimation (Vol. 5). Cambridge University Press (1999)
16. Carayannis, G., Manolakis, D., Kalouptsidis, N.: A fast sequential algorithm for least-squares filtering and prediction. IEEE transactions on acoustics, speech, and signal processing, 31(6), 1394–1402 (1983)
17. Hägglund, T., Åström, K. J.: Supervision of adaptive control algorithms. Automatica, 36(8), pp. 1171–1180 (2000)
18. Meng, L., Li, L., Veres, S. M.: Aerodynamic parameter estimation of an unmanned aerial vehicle based on extended Kalman filter and its higher order approach. In: Advanced Computer Control (ICACC), 2nd International Conference, Vol.5, pp. 526–531, IEEE (2010)
19. Medel, J., Urbieta, P., García, I.: Estimación de parámetros concentrados de un proceso estocástico de segundo orden. Revista mexicana de física, 60(1), pp. 80–87 (2014)
20. Gauterin, E., Kammerer, P., Kühn, M., Schulte, H.: Effective wind speed estimation: Comparison between Kalman Filter and Takagi–Sugeno observer techniques. ISA transactions, 62, pp. 60–72 (2016)
21. Verdejo, H., Escudero, W., Kliemann, W., Awerkin, A., Becker, C.,Vargas, L.: Impact of wind power generation on a large scale power system using stochastic linear stability. Applied Mathematical Modelling (2016)

ISSN 1870-4069

# Semantic Formalism for Modelling the Group Interaction

Mario Anzures-García[1], Luz A. Sánchez-Gálvez [1], Miguel J. Hornos[2], Patricia Paderewski-Rodríguez[2]

[1] Benemérita Universidad Autónoma de Puebla, Facultad de Ciencias de la Computación, Puebla, México

[2] Universidad de Granada, Departamento de Lenguajes y Sistemas Informáticos, E.T.S.I. Informática y de Telecomunicación, Granada, Spain

{mario.anzures, sanchez.galvez}@correo.buap.mx, {mhornos,patricia}@ugr.es

**Abstract.** The process of groupware development can be founded on the conceptual modeling of group interaction, since the interaction determines how the group members communicate, collaborate, and coordinate in order to perform some tasks-in accordance with the roles; users can play-to achieve a common goal. Therefore, in this paper a formalism to model the group interaction is proposed, this approach is inspired by formalisms that have been developed within this context: an ontology of the session management policy, which establishes the group organizational structure, in terms of the roles that users (group members) will play; an Model-View-Controller architectural pattern, which establishes a set of recommendations to facilitate the process of groupware development; and a Methodology that supports the process of ontologies development, by using a set of tasks, allowing us to simplify this process. The formalism to analyze and design the interaction in a shared workspace, is composed by the following modeling: 1) Role Modeling; 2) Interaction Modeling; and 3) User Interface Modeling. Finally, a proof of concept based on a case study is presented.

**Keywords:** Semantic formalism, group interaction, ontology, methontology, model-view-controller architectural pattern.

## 1 Introduction

The group interaction is a key aspect of the groupware, which is a computer-based system that supports groups of people who are engaged in a common task (or goal), and it provides an interface to a shared environment [1]. Thus, the development of this kind of applications, must be focused on modeled group interaction. In according to Molina [2], four forms of groupware development have been established:

1. *Ad-hoc:* The application is built in a completely adapted way to the specific problem to which it is intended to support.
2. *Use of toolkits:* These provide a higher level of programming abstraction by using functions and API (Application Programming Interfaces).

3. *Use of components:* They allow the construction of groupware by using predefined building blocks.
4. *Use of conceptual modeling:* The process of collaborative environment development is based on conceptual modeling.

With regard to conceptual modeling, some proposals have been made, such as: Coordination Theory [3] supplies a theoretical framework for analyzing coordination; Conceptual Model [4] characterizes the groupware from users' view point with three complementary model: ontological, coordination, and user interface; AMENITIES [5] is based on models of tasks and provides dynamic aspects, using an extension of UML notations called COMO-UML; TOUCHE [6] manages the interaction among the users through UML notations; CIAM [7] supports the user interface design of groupware enabling integration with software processes through UML notation (that it has called CIAN); and Interaction Modeling [8] proposes a framework for analyzing and designing virtual spaces oriented to collaborative work. However, these cannot be considered formal, since they lack the necessary expressivity and formality to specify the group work interaction. On the other hand, several authors [2, 9, 10, 11] have established limitations about conceptual modeling of the work group:

1. Lacking of theoretical and computational models that allow to adequately specify the group activities mediated by information technology.
2. Difficulties for addressing the integral modeling of interactive aspects among individuals and task aspects of group work.
3. Lacking of adequate conceptual specification artifacts for modeling collaborative tasks which have to be mediated by CSCW systems.

Therefore, in this work, a semantic formalism to model group interaction is proposed, which is based on: 1) An ontological model [12, 13, 14] for group organizational structure (which supplies a formal and explicit specification of this structure); 2) A Model-View-Controller (MVC) architectural model [15, 16] to develop groupware (which offers a set of templates that serves as a guideline to analyze, design, and implement groupwork); and 3) Methontology [17, 18] for building ontologies (which uses a set of intermediate representations, based on tabular and graphical notations). This formalism is composed of the specification of: 1) the division of labor in accordance with the established roles (Role Modeling); 2) the group interaction with respect to the defined task type (Interaction Modeling); and 3) the presented Information, the Participant and/or Context views regarding the collaboration carried out by users performing a role (User Interface Modeling).

The paper is organized as follows: The models supporting the formalism are described in Section 2. The background of this conceptual formalism is explained in Section 3. The formalism development is detailed in Section 4. The case study is defined in Section 5. Finally, conclusions and future works are presented in Section 6.

## 2 Models Supporting the Proposed Formalism

Three are the models aiding the suggested formalism: ontological model, MVC architectural pattern, and methontology.

### 2.1 Ontological Model

An ontology is presented as an organization's resource and knowledge representation through an abstract model. This representation model provides a common vocabulary of a domain and defines the meaning of the terms and the relations among them. The ontology supplies a set of *concepts* or classes, *relations*, *axioms*, and *instances* to describe a domain in a formal and explicit way [19]. In the groupware domain, the ontologies have mainly been used to model tasks or sessions, by defining concepts and terms, such as group, role, actor, task, etc.. Moreover, semiformal methods (e.g. UML class diagrams, use cases, activity graphs, transition graphs, etc.) and formal ones (such as algebraic expressions) have also been applied to model the sessions.

The ontologies can be implemented in various kinds of languages [20]. Some based on First-order (predicate) logic, other Frames-based languages with more expressive power but less inference capability; others based on descriptive logic [21] that are more robust in the power of reasoning as OWL [22, 23]. On the other hand, the Description Logic provides readily available reasoners such as Pellet [24] and HermiT [25]. OWL ontologies can also be combined with rules using the new W3C Rule Interchange Format (RIF) standard [26]. For developing ontologies are used tools, which provide graphical interfaces that facilitate the knowledge representation and reasoning. This article focuses on Protégé [27], which is an engineering tool open source ontology and a knowledge-based framework. Ontologies in Protégé can be developed in a variety of formats, including OWL, RDF (S), and XML Schema.

### 2.2 MVC Architectural Pattern

An architectural pattern captures the essence of a successful solution to commonly occurring problems in software design. Thus, a pattern can be seen as a clear and generic set of instructions, ensuring to use a solution that has been proven in countless software design problems with excellent results, allowing customize the pattern to solve specific problems. The importance in the architectural pattern approach is its potential to bridge the gap between high-level requirements and design.

MVC improves modularity by encapsulating volatile implementation details behind stable interfaces that reduce the effort required to understand and maintain existing software. In such way, it reduces the cost and improves the quality of software. The Model characterizes unique forms of data in an application; it will notify to its Views that a change has occurred in the Model, so that they may react suitably. View is a (visual) representation of its model. A view typically has associated a model and is notified when the model (or a part of it) changes, allowing the view to update itself accordingly. All these notifications must be in the model terminology. Users are able to interact with views, and this includes the capacity to access and modify the model. Controller is the link between a user and the application. It provides the user with input by arranging for relevant views to present themselves in suitable places on the screen. It receives user output, translates it into the appropriate messages and passes these messages to one or more views. In groupware, MVC has been used to manage the interaction among user's groups [17, 18, 19, 20, 21].

### 2.3 Methontology

Methontology is a methodology that supports the ontology construction process, from scratch or the reuse of existing ontologies. It defines common and structured guidelines that establish a set of principles, design criteria and phases for building the ontology. This methodology organizes and converts an informally perceived view of a domain into a semi-formal specification using a set of intermediate representations based on tabular and graphical notations that can be understood by domain experts and ontology developers. All this provides the necessary flexibility and simplicity in the ontology construction process. Methontology includes a set of eleven tasks for structuring knowledge within the conceptualization activity [17]: 1) to build the glossary of terms; 2) to build concept taxonomies; 3) to build ad hoc binary relation diagrams; 4) to build the concept dictionary; 5) to define ad hoc binary relations in detail; 6) to define instance attributes in detail; 7) to define class attributes in detail; 8) to define constants in detail; 9) to define formal axioms; 10) to define rules; and 11) to define instances.

## 3 Background of the Semantic Formalism

The proposed formalism is derived from created models to manage group interaction: Group Organizational Structure Ontology, and customized MVC Architectural Pattern.

### 3.1 Ontology- Based Group Organizational Structure

This ontology (see Fig. 1) establishes the *Group Organizational Structure* (GOS) [12, 13, 14] that is governed by a specific *policy*, which determines how the group is organized. This structure is made up of users. *Policy* (Pol) defines a configuration of the group organizational structure accord to each role established. *Users* can be people, either individuals or groups, although they may also refer to systems playing one or more roles. *Role* (R) is responsible for the tasks that users can perform, and provides one status as well as one right/obligation in the application. *Status* (S) describes the role hierarchy. *Rigth/obligation* (R/O) constrains the user actions in the shared workspace. *Task (*T) is made up of one or more activities, allowing users to achieve a given goal in a certain moment.

An *Event* (E) triggers a task. *Activities* (A) are actions that allow a role to execute a set of operations by using resources; which represent the resources used to carry out the activities. *Tasks-Precedence (*TP*)* indicates the order that tasks may have. A Task cab be *Sequential, Parallel, Partially-Concurrent,* and *Fully-Concurrent* kind. *Sequential-Task* (ST) specifies one activity follows the other.

*Parallel-Task* (PT) happens at the same time, but they use different objects, and no interference between them can occur. *Partially-Concurrent-Task* (PCT) refers to tasks that can be active at the same time but there is no simultaneous modification of any object.

*Fully-Concurrent-Task* (FCT) occurs when two or more simultaneous tasks to modify rights to same set of objects. Stage (g) reflects each of the collaboration

moments and is composed by a set of Tasks. Stage-*Precedence* (SP) indicates the execution order of the stage.

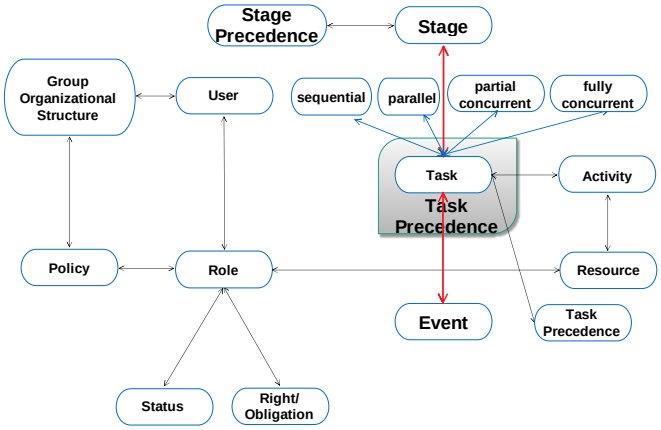


**Fig. 1.** Group Organizational Struture Ontology [12].

### 3.2 Customized MVC Architectural Model

The MVC architectural pattern [15, 16] offers a way to simplify the groupware development; providing the necessary flexibility and responsiveness to adjust to the changing needs within the group. This model is customized for characterizing and developing groupware (see Fig. 2).

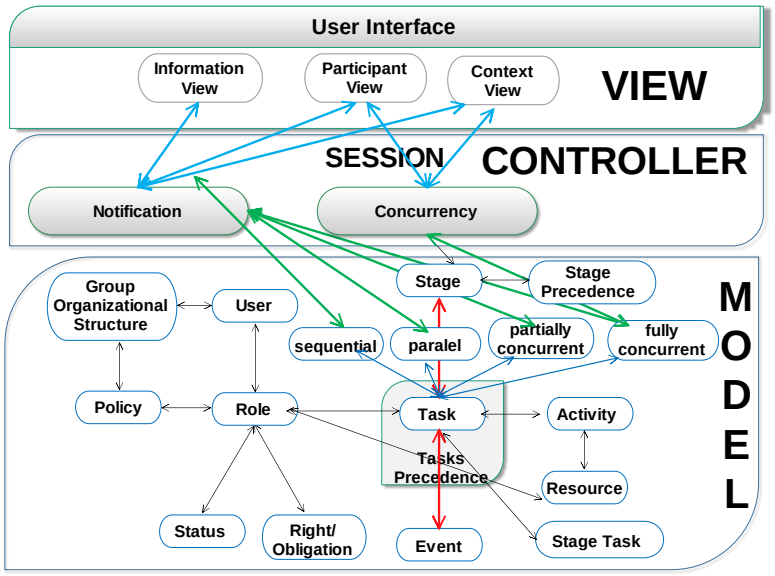


**Fig. 2.** Layered architectural pattern for building groupware [15].

In the which: the Model is group organizational structure ontology described in the section 3.1. The View is user interface, which is symbolized by the Information View (that provides all the information that helps the user to interact with the application), the Participant View (that allows to each user to be aware of what other's users are doing), and the Context View (that represents workspace where all information of shared resources is shown; which is named memory or history group).

The Controller establishes the notification and concurrency to manage and control appropriately group interaction.

## 4 The semantic Formalism Development

Group organizational structure ontology is considered the principal base for defining the three models that constituent the semantic formalism. Furthermore, some entities of the Interaction and User Interface Modeling are added by using MVC architectural pattern. The usage of rules, and tabular notation is taken from methontology.

### 4.1 Role Modeling

The group organizational structure ontology stipulates the entities, relations, and rules that determine the division of labor, for the roles to perform the group work in an appropriate manner. So, the Role Modelling can be specified by defining at what moment each task is executed, and by whom. Consequently, this model must define the Stages (g) in which the group work will be carried out, the order (Precedence Stage - SP) in which they will be made, the Tasks (T) and its order will be executed in each Stage, and the role that will perform them.

### 4.2 Interaction Modeling

The way in which users interact depends on the type of task they perform according to the role they play. Since: A sequential task establishes that a role should expect to be notified that another finishes his task so he can start his.

A parallel task determines that two or more roles can perform tasks that are different, at the same time; notifying to the roles and entities corresponding the carried-out modifications. A partial concurrent task stipulates that two or more roles perform the same task at the same time but modify different resources, therefore, it should only notify to the appropriate roles and entities the made adjustments. A complete concurrent task indicates that two or more roles perform the same task at the same time using the same resources, therefore, the notification and concurrence should be implemented.

Consequently, in all tasks, the communication (Cm) and collaboration (Cb) between users are used, only in the last task the coordination (Cr) is done. In such a way that the template (see Table 2) correspondent to the Interaction Modelling should contain the Role with the Tasks carried out by he/she, the Task Type (TT), and used mechanism (Notification-N-and Concurrency-C). The elements of this modeling are based on the analyzed ontology and MVC. The columns and rules are founded on methontology.

### 4.3 User Interface Modeling

In accordance with the customized MVC architectural pattern to develop groupware, the user interface is structured with respect to presented views, which can be: information view, participant view, and/or context view. The view shown depends on the task type performed. The view content be subject to used resources to execute the task. The information view is displayed when any task type has occurred. The participant view or context view are exhibited when a Partial Concurrent or Fully Concurrent has happened. On the other hand, the information view implicates individual actions, while the other views represent collaborative work. The participant view generates the group awareness. The context view produces the group memory. Therefore, the template of the User interface modeling (see Table 3) presents User Interface (UI), the three view types and the task type that produces them. The three views allow the communication; while the participants and the context view facilitate collaboration and coordination.

## 5 Proof Conceptual of the Semantic Formalism

The case study is an Academic Virtual Space (AVS), which provides a shared workspace to simplify student's access through the Internet to the course material imparted by the teachers. AVS presents a simple stage called Academic Collaboration (AcC), so that the column of the stage, and stage precedence are omitted in the paper rest. It includes two roles: Teacher (Tc), and Student (St). The Table 1 presents the AVS description.

**Table 1.** Description of the application AVS.

| R | E | T | TP | A | R |
|---|---|---|---|---|---|
| Tc | Access to AVS | Registering | 1 | Enter data | labels, box text, bottom |
| Tc | Starting Session | Login | 2 | Enter data | labels, box text, bottom |
| Tc | Logged | Creating Profile | 3 | Enter data | labels, box text, bottom |
| Tc | Logged | Creating Course | 4 | Enter data | labels, box text, bottom |
| Tc | Access to Course | Publishing HomeWork | 5 | Enter data | labels, box text, bottom, file |
| Tc | Homework | Creating deadline | 6 | Enter data | labels, box text, bottom |
| Tc | Creating deadline | Download St HW | 10 | Enter data | labels, box text, bottom, file |
| Tc | Download HW | Upload Reviews | 11 | Enter data | labels, box text, bottom, file |
| Tc | | Send Messages (Mss) | | Write Mss | labels, box text, bottom |
| St | Access to AVS | Registering | 1 | Enter data | labels, box text, bottom |
| St | Starting Session | Login | 2 | Enter data | labels, box text, bottom |
| St | Logged | Creating Profile | 3 | Enter data | labels, box text, bottom |
| St | Created Course | Registering Course | 7 | Enter data | labels, box text, bottom |
| St | Register Course | Download Tc HW | 8 | Enter data | labels, box text, bottom, file |
| St | Download HW | Upload HW | 9 | Enter data | labels, box text, bottom, file |
| St | | Send Messages (Mss) | | Write Mss | labels, box text, bottom |

The Template of the Role Modeling (see Table 2) is gotten in accordance with the explicated in the section 4.1. In this template is possible to see the role that participates and in what moment does this. Furthermore, the task called "Send Messages" can be performed when the role (Teacher or Student) requires it.

The Template of the Interaction Modeling (see Table 3) is developed with respect to the explained in the section 4.2. In this template, the group interaction is visualized through the performed task type, which determine the required aspect (communication, collaboration, or coordination) to support the group interaction. In addition, a set of rules is added for establishing and controlling the users' participation in this interaction.

The Template of the User Interface Modeling (see Table 4) is acquired regarding with the clarified in the section 4.3. This template presents the views' resultants from task and synchronization type used. In addition, a set of rules to determine the displayed view type is presented in the template.

**Table 2.** Template of the Role Modeling.

| Role | Event | Task | TP |
|---|---|---|---|
| Tc | Access to AVS | Registering | 1 |
| Tc | Starting Session | Login | 2 |
| Tc | Logged | Creating Profile | 3 |
| St | Access to AVS | Registering | 1 |
| St | Starting Session | Login | 2 |
| St | Logged | Creating Profile | 3 |
| Tc | Logged | Creating Course | 4 |
| Tc | Access to Course | Publishing HomeWork | 5 |
| Tc | Homework | Creating deadline | 6 |
| St | Created Course | Registering Course | 7 |
| St | Register Course | Download Tc HW | 8 |
| St | Download HW | Upload HW | 9 |
| Tc | Creating deadline | Download St HW | 10 |
| Tc | Download HW | Upload Reviews | 11 |
| Tc | | Send Messages (Mss) | |
| St | | Send Messages (Mss) | |

**Table 3.** Template of the Interaction Modeling.

| R | Task | PT | TT | N | C | Aspect | Rule |
|---|---|---|---|---|---|---|---|
| Tc | Registering | 1 | ST, PT | X | | Cm | if [[Tsk](?X) & |
| Tc | Login | 2 | ST, PT | X | | Cm | [Act](?Y)](?X,?Y)] then |
| Tc | Creating Profile | 3 | ST, PT | X | | Cm | [composited Act] (?X,?Y) |
| St | Registering | 1 | ST, PT | X | | Cm | if [[A](?X) and |
| St | Login | 2 | ST, PT | X | | Cm | [R](?Y)](?X,?Y)] then [has R] |
| St | Creating Profile | 3 | ST, PT | X | | Cm | (?X,?Y) |
| Tc | Creating Course | 4 | ST | X | | Cm, Cb | if [[T](?X) and |
| Tc | Publishing HomeWork | 5 | ST | X | | Cm, Cb | [PCT](?Y)](?X,?Y)] then is_a |
| Tc | Creating deadline | 6 | ST | X | | Cm, Cb | PCT] (?X,?Y) |
| St | Registering Course | 7 | ST | X | | Cm, Cb | if [[T](?X) and [PCT](?Y)] and |
| St | Download Tc HW | 8 | PCT | X | X | Cm, Cb | [N](?Z)] (?X,?Y, ?Z)] then |
| St | Upload HW | 9 | PCT | X | X | Cm, Cb | actives N] (?X,?Y, ?Z) |
| Tc | Download St HW | 10 | PCT | X | X | Cm, Cb | if [[T](?X) and [FCT](?Y)] and |
| Tc | Upload Reviews | 11 | ST | X | | Cm, Cb | [N](?Z)] and [C](?W) |
| Tc | Send Messages (Mss) | | FCT | X | X | Cm, Cb, Cr | (?X,?Y,?Z,?W)] then actives N |
| St | Send Messages (Mss) | | FCT | X | X | Cm, Cb, Cr | and C] (?X,?Y,?Z,?W) |

## 6 Conclusions and Future Work

In this paper, a semantic formalism for modeling the group interaction in groupware has been established. As a result, this approach is constituted by three models: role

modeling (the roles are the actives participants of the interaction), interaction modeling (the task type determines how the users will interact), and user interface modeling (the interaction is performed in the shared workspace, which is presented in the user interfaces). This formalism is based on the group organizational structure ontology; customized MVC architectural model, and methontology, which supply a set of elements to model the interaction of group through representations based on tabular notations.

The future work is orientated to specify a methodology to develop groupware, which is founded in the formalism here proposed.

**Table 4.** Template of the User Interface Modeling.

| R | Task | TT | N | C | IV | PV | CV | Aspect |
|---|---|---|---|---|---|---|---|---|
| Tc | Registering | ST, PT | X | | X | | | if [[T](?X) and [N](?Y)] and |
| Tc | Login | ST, PT | X | | X | | | [IV] (?Z)(?X,?Y,?Z)] then |
| Tc | Creating Profile | ST, PT | X | | X | | | actives IV] (?X,?Y, ?Z) |
| St | Registering | ST, PT | X | | X | | | if [[T](?X) and [PCT](?Y)] and |
| St | Login | ST, PT | X | | X | | | [PV](?Z)] and [CV](?W) |
| St | Creating Profile | ST, PT | X | | X | | | (?X,?Y,?Z,?W)] then actives PV |
| Tc | Creating Course | ST | X | | X | | | and CV] (?X,?Y,?Z,?W) |
| Tc | Publishing HomeWork | ST | X | | X | | | if [[T](?X) and [FCT](?Y)] and |
| Tc | Creating deadline | ST | X | | X | | | [PV](?Z)] and [CV](?W) |
| St | Registering Course | ST | X | | X | | | (?X,?Y,?Z,?W)] then actives PV |
| St | Download Tc HW | PCT | X | X | X | X | X | and CV] (?X,?Y,?Z,?W) |
| St | Upload HW | PCT | X | X | X | X | X | |
| Tc | Download St HW | PCT | X | X | X | X | X | |
| Tc | Upload Reviews | ST | X | | X | | | |
| Tc | Send Messages (Mss) | FCT | X | X | X | X | X | |
| St | Send Messages (Mss) | FCT | X | X | X | X | X | |

## References


1. Ellis, C.A., Gibas, S.J., Rein, G.L.: Groupware: Some Issues and Experiences. Communications of the ACM, Vol. 34-1, pp. 39–58 (1991)
2. Molina, A., Redondo, M., Ortega. M.: A Review of Notations for Conceptual Modeling of Groupware Systems. In New Trends on Human-Computer Interaction (Eds. J. Macías, A. Granollers, P. Latorre). pp. 1–12 (2009)
3. Crowston, K., Rubleske J., Howison J.: Coordination theory: A ten-year retrospective. Human-Comput. Interaction in Management Information Systems. M. E. Sharpe, Inc. (2006)
4. Ellis, C., Wainer, J.: A conceptual model of groupware. Proceedings of the 1994 ACM Conference on CSCW, pp. 79–88 (1994)
5. Garrido, J. L., Gea, M., Padilla, N., Canas, J.J., Waern Y.: AMENITIES: Modelo de entornos cooperativos. Actas del III Congreso Internacional Interacción Persona-Ordenador, pp. 97–104 (2003)
6. Ruiz Penichet., V.M.: Task-Oriented and User-Centred Process Model for Developing Interfaces for Human-Computer-Human Environments. Ph.D. dissertation, Universidad de Castilla-La Mancha (2007)
7. Molina, A.I., Redondo, M.A., Ortega, M., Hope, U.: ClAM. A methodology for the development of groupware user interfaces, Journal of Universal Computer Science, vol. 14-9, pp. 1435–1446 (2008)

8. Rodríguez, D., García-Martínez, R.: Modeling the Interactions in Virtual Spaces Oriented to Collaborative Work. Chapter 10, Carlos Mario Zapata, Guillermo González, Roberto Manjarrés, Fabio Alberto Vargas, and Wiliam Arévalo (Eds.), Software Engineering: Methods, modeling, and Teaching, Vol. 1, Lima, Perú (2012)
9. Rodríguez, D., García-Martínez, R.: Modeling the Interactions in Virtual Spaces Oriented to Collaborative Work. Chapter 10, Carlos Mario Zapata, Guillermo González, Roberto Manjarrés, Fabio Alberto Vargas, and Wiliam Arévalo (Eds.), Software Engineering: Methods, modeling, and Teaching, Vol. 1, Lima, Perú (2012)
10. Sosa, M., Zarco, R., Postiglioni, A.: Modelando Aspectos de Grupo en Entornos Colaborativos para Proyectos de Investigación. Revista de Informática Educativa y Medios Audiovisuales Vol. 3, pp. 22–31 (2006)
11. Giraldo, W., Molina, A., Collazos, C., Ortega, M., Redondo, M.: Taxonomy for Integrating Models in the Development of Interactive Groupware Systems. Journal of Universal Computer Science, Vol. 14-19, pp. 3142–3159 (2008)
12. Anzures-Garcia, M., Sanchez-Galvez, L.A., Hornos, M.J., P. Paderewski: A Knowledge Base for the Development of Collaborative Applications. Engineering Letters, vol. 23-2, International Association of Engineers, Hong Kong, pp. 65–71 (2015)
13. Anzures-García, M., Sánchez-Gálvez L.A.: Policy-based group organizational structure management using an ontological approach. In Proc. International Conference on Availability, Reliability and Security (ARES), pp. 807–812 (2008)
14. Anzures-García, M., Sánchez-Gálvez, L.A., Hornos, M.J., Paderewski-Rodríguez, P.: Ontology-Based Modeling of Session Management Policies for Groupware Applications. Lecture Notes in Computer Science, Vol. 4739, pp. 57–64, Springer, Heidelberg (2007)
15. Anzures-García, M., Sánchez-Gálvez, L.A., Hornos, M.J., Paderewski, P.: Facilitating the development of Collaborative Applications with the MVC Architectural Pattern. Chapter 19. Software Engineering: Methods, Modeling, and Teaching, Vol. 4, In press (2016)
16. Anzures-García, M., Sánchez-Gálvez, L.A., Hornos, M.J., Paderewski-Rodríguez, P.: A software architecture for defining a methodologic approach to develop Collaborative Applications. Research in Computing Science: Advances in Computer Science and Engineering, Vol. 105, pp. 9–20 (2015)
17. Fernández-López, M., Gómez-Pérez, A., Juristo, N.: Methontology: From Ontological Art towards Ontological Engineering. In: Spring Symposium on Ontological Engineering of AAAI. Stanford University, California, pp. 33–40 (1997)
18. Fernández-López, M., Gómez-Pérez, A., Pazos, A., Pazos, J.: Building a Chemical Ontology Using Methontology and the Ontology Design Environment. IEEE Intelligent Systems & their Applications. Vol. 4-1, pp. 37–46 (1999)
19. Gómez-Pérez, A., Fernández-López, M., and Corcho, O.: Ontological Engineering with Examples from the Areas of Knowledge Management, e-Commerce and the Semantic Web. Springer (2004)
20. Uschold, M., Grüninger, M.: Ontologies: Principles, Methods and Applications. Knowledge Engineering Review 11(2), pp. 93–155 (1996)
21. Baader, F., Calvanese, D., McGuinness, D., Nardi, D., Patel-Schneider, P. F. editors: The Description Logic Handbook: Theory, Implementation and Applications. Cambridge University Press (2003)
22. Patel-Schneider, P.F., Hayes, P., Horrocks, I.: OWL Web Ontology Language semantics and abstract syntax. W3C Recommendation, 10 February (2004)
23. Horrocks, I., Patel-Schneider, P.F., van Harmelen, F.: From SHIQ and RDF to OWL: The making of a web ontology language. J. of Web Semantics, Vol. 1-1, pp. 7–26 (2003)
24. Pellet OWL reasoner. Maryland Information and Network Dynamics Lab. http://www.mindswap.org/2003/pellet/index.shtml (2003)

25. Motik, B., Shearer, R., Horrocks, I.: Optimized reasoning in description logics using hypertableaux. In Proc. of the 21st Int. Conf. on Automated Deduction (CADE-21), volume 4603 of Lecture Notes in Artificial Intelligence, Springer pp. 67–83 (2007)
26. RIF RDF and OWL Compatibility. W3C Recommendation, Available at http://www.w3.org/TR/rif-rdf-owl/ (2010)
27. Protégé Ontology Editor and Knowledge Acquisition System, http://protege.stanford.edu

ISSN 1870-4069

# Analysis of Performance for a Chairs Classifier through Deep Learning

Javier Maldonado Romo, Mauricio Olguín-Carbajal, Israel Rivera-Zárate, Raul Galvan

Instituto Politécnico Nacional, Mexico City, Mexico

javier.mr.21@gmail.com, molguinc@ipn.mx, irivera@ipn.mx, raulgalvan92@outlook.com

**Abstract.** Deep learning is a branch of machine learning and this technique allows us to create classifiers. We must find the best dataset size for a classifier process to permit using less time and give good accuracy. In this paper we will propose models with different deep layers and size dimensions for detecting the best model to solve a task that needs quick time processing.

**Keywords:** Artificial intelligence, deep learning, convolutional neural network, classifier.

## 1 Introduction

In this topic of investigation about artificial intelligence there are many techniques for processing and classifying the information. Each technique performs in different situations. Recently, there has been an interest in topics regarding artificial intelligence that is deep learning. Deep learning is a topic that is not new but has one feature that allows it to be a good technique to detect patrons in photos, audios and linguistics. Deep learning is a popular technique, but it still needs graphic card units to improve performance. GPU helps to improve processing times but it is still necessary to use deep learning because the GPU has many computer process units that work in parallel to solve the problem faster.

There are web sites which contains several datasets concerning different subjects. One dataset that is famous from deep learning is the CIFAR-10 dataset. This dataset is found on the Kaggle web site. It is a competition where there are ten classes that contain one thousand images by class; the images are in red, blue and green channel colors. Also it has the dimensions of thirty two in width and height. In 2009 one research team achieved an accuracy of 92% using deep learning. Many research teams around the world use deep learning for processing data using GPU. The time is less compared with CPU and cheaper than CPU cluster.

To apply deep learning we can use the following tips: the first aim is that dataset has much information, the different classes have many images that represents a split and the system could process the information because dataset has much data that

helps to identify the features of each class. If dataset does not have much data that represents the class information it might not be useful to apply deep learning. This step is the most important before selecting deep learning. The second step is to select the image dimensions because Kaggle competition has 32 pixels, but it is possible to use this dimensions for all datasets. The last step is the number of deep layers; this aim is important because it depends on the performance system.

This work shows behavior in different situations. If the size dimensions are shorter it could reduce the processing time and hold the accuracy or increment size dimensions. To develop this paper we used Torch7 which is a tool for deep learning developed by Toronto University. This tool has a great performance when used in CPU and GPU. There are many papers that measure the performance between CPU and GPU. The result is that using GPU is better, and it is not necessary to check the performance with different hardware; we will only make the test on GPU. The test with CPU is not important because we know that the GPU is quicker in this case. Our classifier has four classes where three classes are different type chairs and the last class is the nothing class or anything that is not a chair.

Alex Krizhevsky has several paper which show that using GPU on deep learning achieved better performance than using CPU. In his paper called Convolutional Deep Belief Networks on CIFAR-10, he mentions how to solve the CIFAR-10 model with convolutional neural networks and how these layers help improve the accuracy with dataset that contain a large number of samples, where the CIFAR-10 model has 10 classes and each class has 1000 images for the classifier. Alex Krizhevsky proposes his architecture with CUDA in the paper Convolutional Neural Networks for Object Classification in CUDA. This contribution shows that convolutional networks benefit to obtain many features with different kernels to classify any object. The last important contribution is the development where the dataset is not only 32 pixels, it is for a data set with large dimensions using other types of layer and techniques such as dropout which helps to reduce the operations between layers.

## 2 Experiment Description

This experiment consists in creating a fork from model CIFAR-10; in our case we have four classes and the dataset is different. The first goal is to launch the model CIFAR-10 to verify that all the tools execute correctly. We found the CIFAR-10 model for Torch7 is in its official web site. This example is just for CPU, but if we want to achieve a better performance it is necessary to makes the changes to execute on GPU. For this experiment the GPU is Nvidia GTX860M; it has 640 CUDA cores and 2 GBytes in memory RAM. The CUDA is the technology to execute parallel tasks on Nvidia GPU. Torch7 is optimized for using CUDA. Torch7 is only available in Ubuntu 14.04 and later versions. There are no supports to operate other systems, but it is possible to execute Torch7 on MacOS which only needs to have Nvidia GPU to achieve a good performance.

Torch7 uses Lua language that is a C++ extension. Lua is released for parallel tasks such as Multicore process using OpenMP. The experiment is separated in five

sections that are the following: load data, model, loss function, train and test. The load data has to read all images when the images have 32 pixel size dimensions in width and height. This section exchanges our dataset with four classes. The model file contains the number layers of the original model; it contain three layers. The first layer is spatial convolution with transfer function Tanh and Maxpooling. The second layer also is spatial convolution with same function transfer Tanh and its respective Maxpooling. The last layer is classified lineal to determine which is the best result. The following figure shows some images for each class that represents our experiment.

**Fig. 1.** Dataset for training 32 pixels in which appear two samples for each respective class.

The figure above shows the four classes: the first couple shows office chair color blue; the next couple is normal chair color black, after office chair color black and the last can be anything. Each class is represented by 180 images. The training is supervised and each image has a label indicating its class.

The most important in this experiment is measuring the different times that finished the training. We are going to change the size dimensions. The first is to execute the normal dimensions that are 32 pixels, then change dimensions to 16 pixels, after 8 pixels, and also change the size up to 64,128 and 256 pixels, remembering that the change in size is in width and height. Our target is to check which model finished first and also measure the epoch's number that is necessary to obtain a good accuracy. The epochs are the number the times it requires the training to obtain our value of accuracy.

The figure below shows the images with 16 pixels by side dimensions.

**Fig. 2.** Dataset for training 16 pixels showing two samples for each respective class.

Dataset 16 pixels model for us is the same image but it lost data, and the information that was lost is important when the system does not train. If the dimensions are changed in an upper value, and the dataset has more data, could we get better results? In this paper we try to prove this theory.

## 3 Test and Result

We have described the experiment features, now let us try the different model with respect to dataset. Before changing the dataset it is important to launch our CIFAR-10 fork model to measure the time.

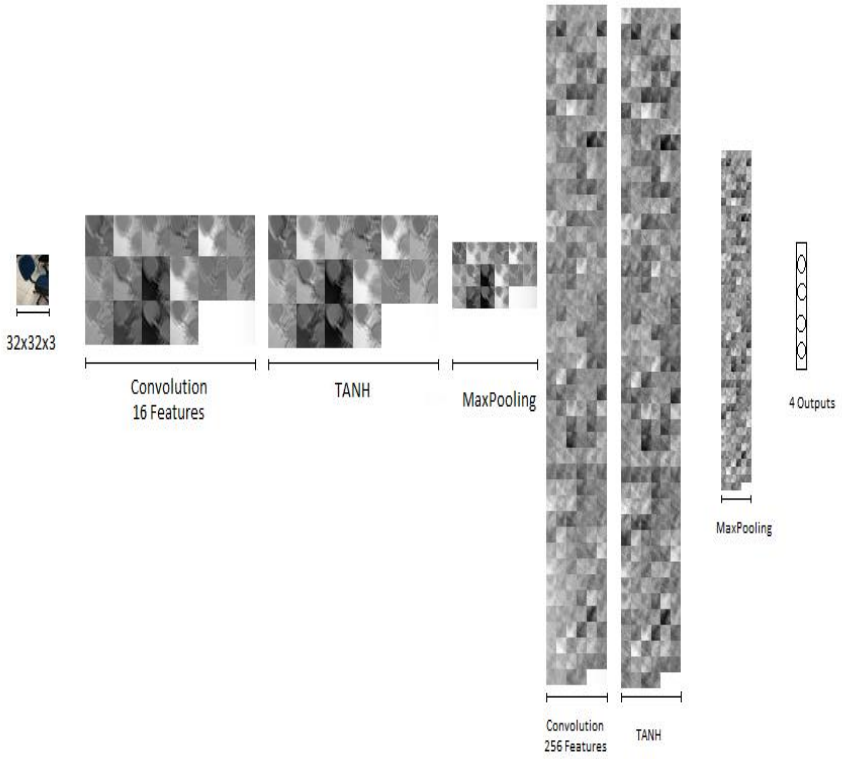


**Fig. 3.** Graphic description model 32, modifications in each layer is observed.

Figure 3 above shows the model behavior when processing a sample of 32 pixels. Inputs are 32 pixels side by side with red, green and blue channels; the image enters in the model and applies three layers. The first layer consists of a spatial convolution layer with 16 features of size three kernel. Figure 3 shows the image result, following the model passing into its transfer Tanh function and gives the result and last entry Maxpooling with size two kernel.

The Maxpooling result now is the input for the next layer that also has spatial convolution, but now has 256 features with size three kernel continuing with its Tanh and Maxpooling result. Before entering the last layer it is necessary to reshape the input because at this point the input is a matrix. To classify the input it needs to be a vector and reshape the matrix in 256*5*5 that is equal to 6400 samples that makes a vector. This vector is the input for the last layer that lineal classifies the output in four where each output represent a class. It is necessary to apply these steps for each model and measure the times.

The table below specifies the different features about different models. In models with 16 pixels the layers are less than with models of 32 pixels, and more layers in the 64, 128 and 256 pixels.

**Table 1.** Details for each model which shows their respective features.

| Layer | Feature | Model 8 | Model 16 | Model 32 | Model 64 | Model 128 | Model 256 |
|---|---|---|---|---|---|---|---|
| 1 | Network | Conv. | Conv. | Conv. | Conv. | Conv. | Conv. |
| | Output | 16 feat. | 16 feat. | 16 feat. | 32 feat. | 64 feat. | 128 feat. |
| | Kernel / classifier | 5x5 | 5x5 | 5x5 | 5x5 | 5x5 | 5x5 |
| | Function | Tanh | Tanh | Tanh | Tanh | Tanh | Tanh |
| | Out layer | Max pool 2x2 | Max Pool 2x2 | Max pool 2x2 | Max pool 2x2 | Max pool 2x2 | Max pool 2x2 |
| 2 | Network | reshape | Conv. | Conv. | Conv. | Conv. | Conv. |
| | Output | 16x2x2 | 256 | 256 | 512 | 1024 | 2048 |
| | Kernel / classifier | Linear 128 | 5x5 | 5x5 | 5x5 | 5x5 | 5x5 |
| | Function | Tanh | Tanh | Tanh | Tanh | Tanh | Tanh |
| | Out layer | Linear 4 | Max Pool 2x2 | Max Pool 2x2 | Max Pool 2x2 | Max Pool 2x2 | Max Pool 2x2 |
| 3 | Network | | Reshape | Reshape | Conv. | Conv. | Conv. |
| | Output | | 256x5x5 | 256x5x5 | 256 | 512 | 1024 |
| | Kernel / classifier | | Linear 128 | Linear 128 | 5x5 | 5x5 | 5x5 |
| | Function | | Tanh | Tanh | Tanh | Tanh | Tanh |
| | Out layer | | Linear 4 | Linear 4 | Max Pool 2x2 | Max Pool 2x2 | Max Pool 2x2 |
| 4 | Network | | | | Reshape | Conv. | Conv. |
| | Output | | | | 256x4x4 | 256 | 512 |
| | Kernel / classifier | | | | Linear 128 | 5x5 | 5x5 |
| | Function | | | | Tanh | Tanh | Tanh |
| | Out layer | | | | Linear 4 | Max Pool 2x2 | Max Pool 2x2 |
| 5 | Network | | | | | Reshape | Conv. |
| | Output | | | | | 256x5x5 | 256 |
| | Kernel / classifier | | | | | Linear 128 | 5x5 |
| | Function | | | | | Tanh | Tanh |

| | | | | | | | |
|---|---|---|---|---|---|---|---|
| | Out layer | | | | | Linear 4 | Max Pool 2x2 |
| 6 | Network | | | | | | Reshape |
| | Output | | | | | | 256x5x5 |
| | Kernel / classifier | | | | | | Linear 128 |
| | Function | | | | | | Tanh |
| | Out layer | | | | | | Linear 4 |

The following graphics show the behavior of each model until obtaining an accuracy of 100%. The 256 pixel model results are not important as 256 pixels have much data; it is slow compared with other models because it has had 46 minutes in three epochs. The result is not important because the time is longer and it is not the best performance. This dataset has much data but when is has much data the operations are bigger and require more resources and computer power. There are other techniques that reduce the data and operations, but this technique could be in another experiment. Therefore, the 256 pixels model is discarded.

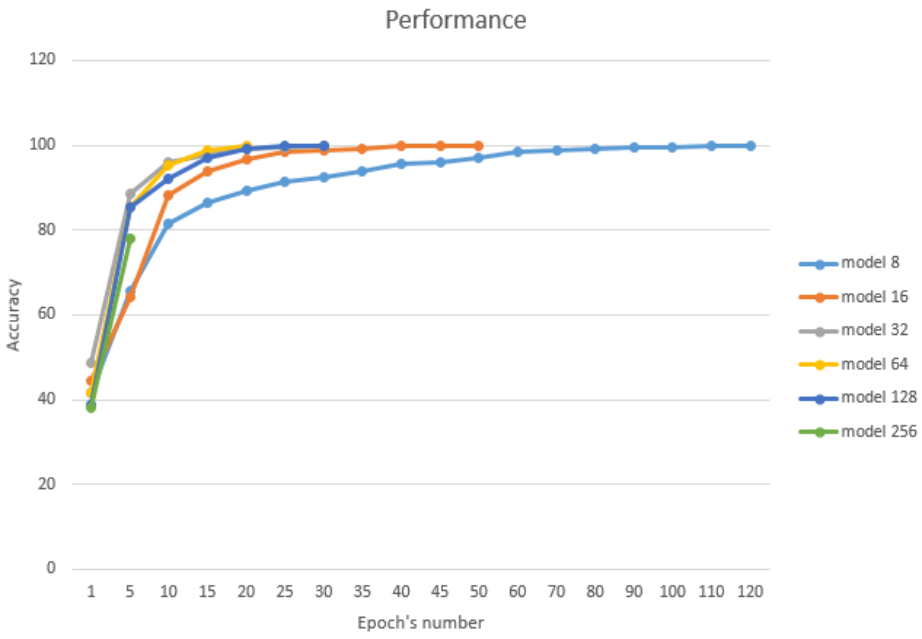


**Fig. 4.** Accuracy obtained in each 5 epochs.

The table below shows the principal features in our experiment. The 32 pixels model shows our threshold in parameters such as epoch number and seconds to get 100% accuracy. There are others features that demand on GPU. Other GPU's with more CUDA cores could be more powerful.

**Table 2.** Details about behavior and performance for every model

| Feature | Model 8 | Model 16 | Model 32 | Model 64 | Model 128 | Model 256 |
|---|---|---|---|---|---|---|
| Epoch | 117 | 41 | 30 | 17 | 23 | 3 |
| Memory RAM GPU (MB) | 440 | 434 | 445 | 488 | 651 | 730 |
| GPU USES (%) | 43 | 34 | 83 | 91 | 99 | 99 |
| Time in Seconds | 56 | 30 | 40 | 165 | 1800 | 2700+ |

The table indicating the 32 pixels model is the best option with least number of epochs and time. Another important point is the low power in GPU and fast response time. The 16 pixels model is excellent but this model needs more epochs using less time and demand in GPU. This point is relevant for embedded systems that cannot use much energy such as mobile devices. The mobile device requires Nvidia GPU and there are not many devices with these GPU on the market, or systems in real time, and it is good idea to use this model.

The model 8 requires many epochs and much time. Otherwise, it is not recommended to use very small images because there is not much information and might have a high error. When changing the dimensions upper to 64 pixels the data grows and so does the information. In the table we show that it is necessary for 17 epochs to obtain 100% accuracy, because there is more data. However, the time is not good compared with model 32 in applications where the response time and accuracy are not important. Our last observation is that models 128 and 256 are not recommendable to use this dataset with these models because the data and operations grow. This deep layer requires more power and more time; the number of epochs is not less than the 64 pixels model and the required time is longer. There are other techniques that could help to improve the performance and try to prove what happened with each model and its respective dataset.

## 4 Conclusions

This paper describes behavior and features of different models applying them to classify four classes. The most important are the follow two points: the first is about the model with less dimensions such as 8 and 16 pixels; these models have low information compared with 32 pixel models. The 8 pixels model is not recommendable because it has low information and could produce many errors. The 16 pixels model is excellent; both models are great for applications in real time because their response time is fast and accuracy. The second point is for the model

with bigger dimensions of 64, 128 and 256 pixels. The 64 pixels model for processing information is the best because it has much information but requires 5 minutes to train. If there is an application where the time is not important this model is perfect. The 128 and 256 models are not advisable to use. Both models have much information that decreases the performance but does not reduce the epoch number. Our future work is to approve other deep layers such as the RELU and DROPOUT technique that are special for models with big images.

## References

1. Alex Krizhevsky: Convolutional Deep Belief Networks on CIFAR-10 (2009)
2. Alex Krizhevsky: Convolutional Neural Networks for Object Classification in CUDA (2009)
3. Alex Krizhevsky, Ilya Sutskever: ImageNet Classification with Deep Convolutional Neural Networks (2011)
4. Torch7. www.torch.ch
5. Kaggle Competitions. www.kaggle.com/competitions
6. Cifar10 Model. www.cs.toronto.edu/~kriz/cifar.html
7. Nvidia GTX860M Specification. www.geforce.com/hardware/notebook-gpus/geforce-gtx-860m

ISSN 1870-4069

# Telemarketing Success: Evaluation of Supervised Classifiers

Yosimar O. Serrano-Silva[1], Yenny Villuendas-Rey[2], Cornelio Yáñez-Márquez[1]

[1] Instituto Politécnico Nacional, Centro de Investigación en Computación, CDMX, México

[2] Instituto Politécnico Nacional, Centro de Innovación y Desarrollo Tecnológico en Cómputo, CDMX, México

oswaldo17@live.com.mx, yenny.villuendas@gmail.com, coryanez@gmail.com.

**Abstract.** Nowadays telemarketing constitutes a way in which goods and services companies can access to possible potential customers through phone calls. Telemarketing campaigns are focused on offer to potential customers or users, contracting or buying a good or service. Ascertain a priori which phone calls will be successful is a competitive advantage to the companies due to this allow them to reduce costs and focus on most likely groups of potential customers which would contract or buy the goods or services offered. For this task it is necessary to classify the phone calls in successful and unsuccessful calls, which is possible using supervised classifier. In this paper, we tested some supervised classification algorithms and compare their performance, based on the Area under the ROC Curve, over different well-known telemarketing datasets.

**Keywords:** Telemarketing classification, supervised classification, unbalanced data.

## 1 Introduction

Nowadays telemarketing is an important strategy to increase the level of sales, looking for potential clients using different communication channels like phone calls, internet, etc. In fact financial institutions like banks and insurance companies are the most benefited of this kind of campaigns using different techniques like speech dictation systems [1] to checking incomplete sales where the telemarketer fails providing sales information to a certain client.

The main purpose of this kind of marketing is contacting a certain group of people to meet a specific goal (offer a service, insurance, credit card, etc.), but the problem of choosing the group of costumers willing to buy the service is considered NP-hard [2]. For this reason some approaches has been proposed to predict the success of telemarketing calls [3], where applying a decision support system using some techniques of data mining, automatically can predict the result of phone calls used to sell long term deposits.

In the literature we can find more examples of works about prediction in telemarketing environment using a different approach. Customer lifetime value is a variable considered as the value of a costumer in terms of expected benefits based on future interactions with the customer and in [4] is used for predicting future behavior of that costumers and in this way, improve the return-on investment.

Nevertheless, working with data sets from telemarketing environment has the disadvantage that, in most of the cases, have unbalanced classes and mixed attribute types [5], for which is very important to choose the classification models in accordance with this situation.

A situation like unbalanced classes is present in a dataset when one of the classes has more elements than the others. This situation represents a problem at the moment of work with this kind of datasets due to the fact that unbalanced classes, in general, creates biased learning. The consequences of this are reflected during the testing phase because the biased learning causes that the classifiers just recognize appropriately the elements of the ruling class and therefore, give us inaccuracy results.

In this article is presented an experimental work using different supervised classifiers with telemarketing datasets with the purpose to know which one has the best performance under the circumstances described above.

The rest of the paper is organized as follows. Section 2 details some aspects of the classifiers used in this comparison and section 3 offers a discussion about the results obtained. Finally, the paper ends with some conclusions and future research suggestions.

## 2 Sampling and Error Measurement

One of the most common method applied to validate the classifier performance in multiple jobs within the literature is stratified cross-validation (SCV). This method is based on partitioning the data set into two complementary subsets. This couple of subsets is used for training and testing the classifier and the main purpose of this technique is keep the same class distribution in both subsets.

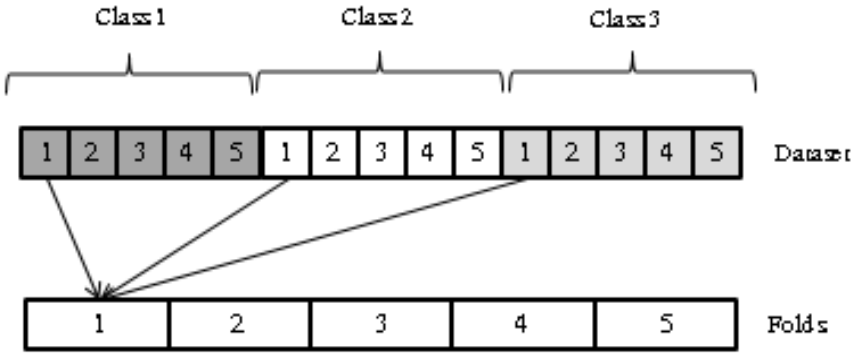


**Fig. 1.** Process to divide the dataset into k=5 subsets following the SCV technique.

To carry out this partition, as it shown in the Figure 1, it is necessary divide every class of the original dataset into k different partitions with the same number of patterns as possible. After that to form each fold, a partition of every class is taken.

Then one of these folds is use as testing data and the remaining k-1 folds are use as training data. Worth mentioning that this process is repeated k times and each fold is use as testing data exactly once.

The most popular value of k is 10, but in the case of unbalanced classes is most common use k equal to 5, in order to increase the performance of the algorithms, and to diminish the negative impact of unbalanced classes in the classification process. In addition, it is necessary to use a correct error measurement that can handle the problem of unbalanced classes and avoid inaccuracy results. The Area under the ROC curve (AUC) is a metric that comply with this requirement. This is a popular classification metric which exhibits the benefit of being independent of the class distribution (see Table 1):

**Table 1.** Confusion matrix.

| | Predicted as Positive | Predicted as negative |
|---|---|---|
| Positive instances | TP | FP |
| Negative instances | FN | TN |

$$AUC = (TPR + TNR) / 2, \quad (1)$$

$$TPR = TP / (TP + TN), \quad (2)$$

$$TNR = TN / (TN + TP). \quad (3)$$

The results obtained with this measurement can be interpreted as ideal classification model if the value of the AUC is 1.0 and as random classifier if the value is 0.5. Moreover this measurement has been demonstrated that can be calculated as the average of the True negative Rate (TNR) and True Positive Rate (TPR) for discrete classifiers by Sokolova et al. [6].

This measurement has been used in different works e.g. to quantify the performance of imbalance learning ensembles [7] or to measure if there is a performance improvement as in [8] working with unbalanced classes.

## 3 Results and Discussion

### 3.1 Datasets

To accomplish the different experiments, four datasets that belong to telemarketing environments were used, with the characteristic of unbalanced classes. As you can see in Table 2 the unbalanced ratio is higher than 1.5 which means that in the four cases there is present the problem of unbalanced classes. This problem is important to consider because can produce a biased learning and inaccurate results using an inappropriate error measurement as mentioned earlier.

On the other hand, these datasets were taken from the Machine Learning repository of the University of California [9]. It is worth mentioning that the dataset were donated by S. Moro, P. Cortez and P. Rita [3] who obtained them from real bank data.

The Bank-full data corresponds to the original version of the dataset called Bank Marketing which has 45211 records with17 attributes (7 numerical and 9 categorical) and do not have missing values. This dataset consist of information obtained from a direct marketing campaign of a Portuguese banking institution which was based on phones calls. Often, more than one contact was required to the same client in order to know if a bank term deposit would be or not subscribed. On the other hand, the Bank data is a sample of 10% from the Bank-full dataset randomly selected. This small dataset was made with the aim to test more computationally demanding machine learning algorithms.

**Table 2.** Caracteristics of the datasets used in this work.

| *Data set* | *Instances* | *Attributes* | *Classes* | *Missing values* | *Unbalance Ratio* |
|---|---|---|---|---|---|
| Bank | 4521 | 17 | 2 | No | 7.677 |
| Bank-full | 45211 | 17 | 2 | No | 7.548 |
| Bank-additional | 4119 | 21 | 2 | No | 7.956 |
| Bank-additional-full | 41188 | 21 | 2 | No | 7.876 |

The Bank-additional-full dataset is also based on the Bank marketing data, but this different version is enriched by the addition of new social and economic attributes. This dataset has 41188 instances with 21 attributes (10 numerical and 10 categorical). Also the Bank-additional dataset is a short version of the previous one, with 10% of the examples randomly selected from the Bank-additional-full data.

### 3.2 Algorithms to Compare

The following subsection provides a brief introduction of the most common classification models which were chosen for comparison of results in the next part of this work.

**Nearest Neighbor (1-NN)**

Nearest Neighbor model [10] follows the structure of a learning technique called instance-based learning. This classifier use a dissimilarity measure to carry out the classification of a pattern, using the closest instances of the training set, according to the measure selected, to give to each pattern from the testing set a class label. This model is based on the idea that every pattern from a dataset share some similar characteristics and properties with some individuals around.

The most popular similarity measure used when the dataset just has numerical attributes is the Euclidean distance (equation 4), and because of the use of a distance measure, this kind of model are called minimum distance classifiers.

$$d(y,x) = \sqrt{\sum_{j=1}^{n}(y_j - x_j)^2}. \quad (4)$$

**C4.5**

C4.5 is an algorithm that builds decision trees from a dataset based on information entropy concept [11]. This model chooses one of the attributes of the pattern that divide effectively it set of samples into better subsets. This process is repeater for each node and the criterion of splitting the subsets is the difference in entropy known as normalized information gain. In this way, the attribute with the highest normalize information gain value is selected to make the decision. By last this model has some base cases. The first case is when an instance of previously-unseen class is encountered, in this case the algorithm makes a decision node higher up the tree using the expected value. The second case is when none of the attributes provide any information gain. When this case occurs, once more the algorithm makes a decision node higher up the tree using the expected value. Finally, if the tree has made a decision node higher up the tree using the expected value, this model creates a leaf node for the decision tree indicating to choose the class.

**Repeated Incremental Pruning to produce Error Reduction (RIPPER)**

Repeated Incremental Pruning to produce Error Reduction is a this classification model proposed in 1995 by William W Cohen [12]. This algorithm is based on the association rules with reduced error pruning (REP) and in fact is an optimized version of the IREP classifier.

In this kind of algorithms, the training data is splint into other two sets: a growing set and a pruning set. Then a rule set is formed using some heuristic method to increase this set. This final rule set us simplified using one of the pruning operators and this would delete any single condition or any single rule; this process is repeated several times. At each stage of simplification, the preselected pruning operator is which return the greatest reduction of error on the pruning set. This process ends when any pruning operator produce an increment in the error on the pruning set.

**Multilayer Perceptron (MLP)**

The Artificial Neural Network is a learning paradigm based on biological neural networks, in particular the human brain. Anatomically this system is composed for networks of biological neurons interconnected, which are able to process and conduct electrical impulses to produce an output. In 1943 it was proposed an abstract and simple model of an artificial neuron as a binary device [13]. This model has an operating threshold below which this neuron is inactive. Also, it has excitatory and inhibitory inputs, and depending on if there is any of these inputs the neuron is active.

This model is very simple, if there is not an inhibitory input, the resultant of the excitatory inputs is determined and if this is greater than the threshold, the output is 1 otherwise is 0.

Based on the work of McCulloch and Pitts, in 1957 it was proposed the perceptron[14]. One of the most interesting characteristics of this model was its ability

of learning to recognize and classify objects. The perceptron was constituted by a set of input sensors which receives the patterns to recognize or classify and am output neuron to do the classification task. Nevertheless, this model was not capable to converge on good solutions in problems with classes linearly non-separable [15].

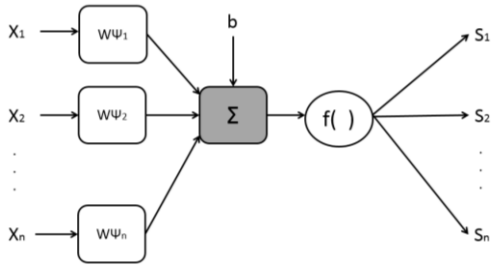


**Fig. 2.** Artificial neuron scheme.

Finally in 1986 the Multilayer Perceptron (MLP) [16] was proposed to solve the limitations of the perceptron. This network consists of multiple layers of artificial neurons; the most common architecture of a simple MLP network has 3 layers: an input and an output layer with one hidden layer however, the general model allows use an unlimited number of hidden layers.

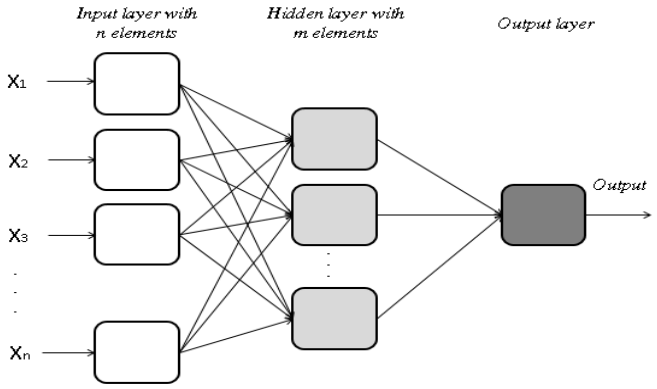


**Fig. 3.** General model of a MLP network with one hidden layer.

Finally, the supervised training stage is one of the most popular algorithms called back-propagation. The bases of this algorithm are in the error-correction learning rule [16].

### Sequential Minimal Optimization Algorithm for Training a Support Vector Classifier (SMO)

Sequential Minimal Optimization (SMO) [17] is an algorithm for training Support Vector Machines [18] and was proposed to solve the problem of the very large quadratic programming optimization problem that implies this kind of training.

Considering a classification problem with a dataset ($x_1$, $y_1$), …, ($x_n$, $y_n$) where $x_i$ is an input vector and $y_i$ is a binary label corresponding to it. A soft-margin support vector machine is trained by solving a quadratic programming problem, which is expressed in the dual form as follows:

$$\underset{\infty}{\text{Max}} \sum_{i=1}^{n} \alpha_i - \frac{1}{2} \sum_{i=1}^{n} \sum_{j=1}^{n} y_i y_j K(x_i, x_j) \alpha_i \alpha_j, \tag{5}$$

subject to:

$$0 \leq \alpha_i \leq C, \quad for\ i = 1, 2, \ldots, n, \tag{6}$$

$$\sum_{i=1}^{n} y_i \alpha_i = 0, \tag{7}$$

where C is an SVM hyperparameter and K($x_i$, $x_j$) is the kernel function, both supplied by the user; and the variables $\alpha_i$ are Lagrange multipliers.

This is an iterative algorithm to solve the optimization problem. SMO converts this problem into a set of smallest possible sub-problems, which are then solved analytically. Due to the fact of the linear equality constraint involving the Lagrange multipliers $\alpha_i$, the smallest possible problem involves two such multipliers. Then, for any two multipliers $\alpha_1$ and $\alpha_2$ the constraints are reduced to:

$$0 \leq \alpha_1, \alpha_2 \leq C, \tag{8}$$

$$y_1 \alpha_1 + y_2 \alpha_2 = k. \tag{9}$$

And this reduced problem can be solved analytically. The algorithm proceeds as follows [18]:

- Find a Lagrange multiplier $\alpha_1$ that violates the Karush–Kuhn–Tucker (KKT) conditions for the optimization problem.
- Pick a second multiplier $\alpha_2$ and optimize the pair ($\alpha_1$, $\alpha_2$).
- Repeat steps 1 and 2 until convergence.

When all the Lagrange multipliers satisfy the KKT conditions (within a user-defined tolerance), the problem has been solved.

**Naive Bayes (NB)**

Naïve Bayes algorithm [19] assumes, for an instance x that its attributes {$x_1$, $x_2$, …, $x_n$} have a conditional independence due to its class. For this reason, the conditional likelihood of every attribute can be expressed as follows:

$$p(x|\omega_i) = \prod_{j=1}^{n} p(x_j|\omega_i). \tag{10}$$

Using the Bayes theorem, the posteriori likelihood is:

$$p(\omega_i|x) = \mathrm{p}(\omega_i) \prod_{j=1}^{n} p(x_j|\omega_i). \tag{11}$$

Finally, for every pattern of the testing set is given a class as is describe in the following equation:

$$\omega^* = argmax_{\omega j} \mathrm{p}(\omega_i) \prod_{j=1}^{n} p(x_i|\omega_j). \quad (12)$$

Each was tested with the different datasets in Waikato Environment for Knowledge Analysis (WEKA) software [20] in its version number 3.6.13. The adequate parameter values for the algorithms were found by trial and error.

### 3.3 Discussion

The results obtained with the different models to every dataset, using the Stratified Cross Validation with k=5 as model validation technique, are shown in Table 3. We use the Area under Roc curve (AUC) [7] as performance measure.

**Table 3.** Area under the curve ROC.

| *Classifiers* | *Bank* | *Bank-full* | *Bank-additional* | *Bank-additional-full* |
|---|---|---|---|---|
| 1-NN | 68.5500 | 64.5137 | 60.0203 | 64.5302 |
| C4.5 | 65.9709 | 72.4634 | 69.6285 | 74.6412 |
| RIPPER | 69.1389 | 67.1002 | **76.6134** | **75.6068** |
| MLP | 67.4566 | 70.0040 | 66.6038 | 70.2377 |
| SMO | 57.3892 | 58.5780 | 63.8087 | 63.9084 |
| Naive Bayes | **70.7500** | **72.5500** | 75.6500 | 75.5500 |

As you can see in the Table 3, Naive Bayes was the model which obtain the best performance in two of the datasets and on the other hand, SMO was the worst algorithm in three of the four datasets. As well, the RIPPER model was the best working with the Bank-additional-full dataset and Bank-additional. Another aspect to highlight is that the distance used by the NN classifier could not have been the correct due to its results were not competitive as usual. The performance of the C4.5 is a special case because was very competitive in the full version of the datasets, but it was affected by the sampling of 10% of the other two datasets. Finally, it can be seen that the problem of unbalanced classes affect the performance of all the classifiers because, even when these are some of the most important models in the literature, they could not even reach an 80% of accuracy. In addition, it is worth mentioning that most of the classifiers got better results using the default parameters from WEKA, just in some cases like RIPPER or C4.5 there was an improvement modifying some values.

## 4 Conclusions and Future Work

In the telemarketing environment, there are some datasets that can be considered important to test automated decision-making systems, but in most of the cases, these datasets have some characteristics that make more complicated this task. In this work we compared six different classification techniques in credit environment: Nearest Neighbor, C4.5, Repeated Incremental Pruning to produce Error Reduction, Multilayer

Perceptron, and Sequential Minimal Optimization Algorithm for training a Support Vector classifier and Naive Bayes.

These algorithms were compared using the Area under the curve ROC due to the problem of the unbalanced classes present in telemarketing datasets. Our studies showed that Naïve Bayes Simple model turned out to be best classifier with the RIPPER model both getting the best performance in two datasets and on the other hand the SMO classifier got the worst performance in this comparative, even using different kernels.

**Acknowledgments.** The authors would like to thank the Instituto Politécnico Nacional (Secretaría Académica, Comisión de Operación y Fomento de Actividades Académicas, Secretaría de Investigación y Posgrado, Centro de Investigación en Computación, and Centro de Innovación y Desarrollo Tecnológico en Cómputo), the Consejo Nacional de Ciencia y Tecnología, and Sistema Nacional de Investigadores for their economical support to develop this work.

## References

1. Jung, D., Bae, M.-K., Choi, M.Y., Lee, E.C., Joung, J.: Speaker diarization method of telemarketer and client for improving speech dictation performance. J. Supercomput. 72, pp. 1757–1769 (2016)
2. Talla Nobibon, F., Leus, R., Spieksma, F.C.R.: Optimization models for targeted offers in direct marketing: Exact and heuristic algorithms. Eur. J. Oper. Res. 210, pp. 670–683 (2011)
3. Moro, S., Cortez, P., Rita, P.: A data-driven approach to predict the success of bank telemarketing. Decis. Support Syst. 62, pp. 22–31 (2014)
4. Moro, S., Cortez, P., Rita, P.: Using customer lifetime value and neural networks to improve the prediction of bank deposit subscription in telemarketing campaigns. Neural Comput. Appl. 26, pp. 131–139 (2014)
5. Abdi, L., Hashemi, S.: To combat multi-class imbalanced problems by means of over-sampling and boosting techniques. Soft Comput. 19, pp. 3369–3385 (2015)
6. Sokolova, M., Japkowicz, N., Szpakowicz, S.: Beyond Accuracy, F-Score and ROC: A Family of Discriminant Measures for Performance Evaluation. In: Sattar, A. and Kang, B. (eds.) AI 2006: Advances in Artificial Intelligence: 19th Australian Joint Conference on Artificial Intelligence, Hobart, Australia, December 4-8, 2006. Proceedings. pp. 1015–1021. Springer Berlin Heidelberg, Berlin, Heidelberg (2006)
7. Díez-Pastor, J.F., Rodríguez, J.J., García-Osorio, C.I., Kuncheva, L.I.: Diversity techniques improve the performance of the best imbalance learning ensembles. Inf. Sci. (Ny). pp. 325, 98–117 (2015)
8. Frank, E., Bouckaert, R.R.: Naive Bayes for text classification with unbalanced classes. In: Furnkranz, J and Scheffer, T and Spiliopoulou, M. (ed.) Knowledge discovery in databases: PKDD 2006, proceedings. pp. 503–510. Springer-Verlag Berlin, Heidelberg Platz 3, D-14197 Berlin, Germany (2006)
9. Lichman, M.: UCI Machine Learning Repository, http://archive.ics.uci.edu/ml.
10. Aha, D.W., Kibler, D., Albert, M.K.: Instance-based learning algorithms. Mach. Learn. 6, pp. 37–66 (1991)
11. Quinlan, J.R.: C4.5: Programs for Machine Learning. Morgan Kaufmann Publishers (1993).
12. Cohen, W.: Fast effective rule induction. Twelfth Int. Conf. Mach. Learn. 115–123 (1995).

13. McCulloch, W.S., Pitts, W.: A logical calculus of the ideas immanent in nervous activity. Bull. Math. Biophys. 5, pp. 115–133 (1943)
14. Rosenblatt, F.: The perceptron, a perceiving and recognizing automaton Project Para. Cornell Aeronautical Laboratory (1957)
15. Minsky, M.L., A. Papert, S.: Perceptrons. MIT Press (1969)
16. Rumelhart, D.E., Hinton, G.E., Williams, R.J.: Learning representations by backpropagation error. Nature. 323, pp. 533–536 (1986).
17. Platt, J.C.: Fast Training of Support Vector Machines using Sequential Minimal Optimization. In: Schölkopf, B., Burges, C.J.C., and Smola, A.J. (eds.) Advances in Kernel Methods: Support Vector Learning (1998)
18. Cortes, C., Vapnik, V.: Support-Vector Networks. Mach. Learn. 20, pp. 273–297 (1995)
19. Duda, R., Hart, P.: Pattern Classification and Scene Analysis. Willey, New York (1973)
20. Hall, M., Frank, E., Holmes, G., Pfahringer, B., Reutemann, P., Witten, I.H.: The WEKA data mining software: an update. SIGKDD Explor. 11, pp. 10–18 (2009)

Impreso en los Talleres Gráficos
de la Dirección de Publicaciones
del Instituto Politécnico Nacional
Tresguerras 27, Centro Histórico, México, D.F.
noviembre de 2016
Printing 500 / Edición 500 ejemplares